

**DEVELOPMENT OF LASER-INDUCED BREAKDOWN
SPECTROSCOPY TECHNIQUE FOR THE ANALYSIS OF FISH
SAMPLES FROM THE ARABIAN GULF**

BY

Lutfi Mulyadi Surachman

A Thesis Presented to the
DEANSHIP OF GRADUATE STUDIES

KING FAHD UNIVERSITY OF PETROLEUM & MINERALS

DHAHRAN, SAUDI ARABIA

In Partial Fulfillment of the
Requirements for the Degree of

MASTER OF SCIENCE

In

PHYSICS

MAY 2018

KING FAHD UNIVERSITY OF PETROLEUM & MINERALS
DHAHRAN - 31261, SAUDI ARABIA
DEANSHIP OF GRADUATE STUDIES

This thesis, written by **Lutfi Mulyadi Surachman** under the direction of his thesis advisor and approved by his thesis committee, has been presented and accepted by the Dean of Graduate Studies, in partial fulfillment of the requirements for the degree of **MASTER OF SCIENCE IN PHYSICS** .



Dr. Abdullah A. Al-Sunaidi
Department Chairman



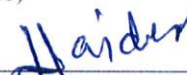
Prof. Salam A. Zummo
Dean of Graduate Studies

29/8/18

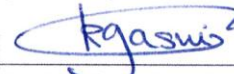
Date



Prof. Mohammed A. Gondal
(Advisor)



Dr. Muhammad B. Haidar
(Member)



Dr. Khaled Gasm
(Member)

© Lutfi Mulyadi Surachman
2018

| I would like to dedicate this thesis to my mother |

ACKNOWLEDGMENTS

||

I express my heartfelt and sincerest gratitude to Professor Gondal who supervised my research work, offered guidance, and devoted substantial amounts of time to ensure the success of my research endeavour. I would like to thank all group member of the Laser physics, KFUPM for any given supports and warm friendship during my research. May Allah give special rewards in this world and hereafter to all lecturers, giving huge learning motivation to get the Master of Science in Physics at KFUPM.

Additionally, the next acknowledgment is for the Centre of Research Excellence in Nanotechnology (CENT-RI) for providing monthly research funding for the duration of this thesis work. Furthermore, I express my special and heartfelt thanks to Prof. Fida F. Al-Adel, along with Mr. Dastageer helping me in my experiments and corrections, and the committee members of my thesis, Dr. Muhammad Baseer Haider, and Dr. Khaled Gasmil for the assistance and guidance provided in the course of this thesis work. May Allah give special rewards to all personnel who helped me during the completion of my master's degree. Finally, my special acknowledgment goes to my mother, family and Indonesian friends, lecturers, staff and community for moral support and motivation to continuously strive towards the best achievement in life.

TABLE OF CONTENTS

ACKNOWLEDGMENTS	V
TABLE OF CONTENTS.....	VI
LIST OF TABLES	IX
LIST OF FIGURES	X
LIST OF ABBREVIATIONS.....	XIII
ABSTRACT.....	XIV
ملخص الرسالة	XVI
CHAPTER 1 INTRODUCTION.....	1
1.1 Overview.....	1
1.2 Theoretical Background of LIBS	3
1.2.1 Introduction	3
1.2.2 LIBS Principle.....	3
1.2.3 Analytical Technique using LIBS.....	4
1.2.4 Factors that Influence the Plasma Parameters	4
1.2.5 Setup Geometry	8
1.2.6 Observation of Time window.....	9
1.2.7 The Effect of Binder	9
1.2.8 Mechanical Failure on surface of solid	10

1.2.9 Laser Ablation	11
1.2.10 Qualitative Analysis	11
1.2.11 The Study of Plasma as a Process of Ionization (Opacity of Plasma)	12
1.2.12 LTE Condition and Optically Thin Plasma	15
1.2.13 Detection Limit	18
1.3 Motivation	18
1.4 Objectives	19
CHAPTER 2 LITERATURE REVIEW	20
CHAPTER 3 EXPERIMENTAL METHOD	27
3.1 Configuration of the LIBS System	27
3.2 ICCD Camera	28
3.3 Spectrometer	29
3.4 The LIBS Emission Collecting System.....	30
3.5 Energy meter	31
3.6 Oven.....	32
3.7 Focusing Lens.....	33
3.8 Target Holder.....	33
3.9 Inductively Coupled Plasma – Mass Spectrometry (ICP-MS).....	33
3.10 Fish Sample Preparation	35
3.11 Preparation of fish samples for ICP (Inductively coupled plasma) analysis	36
3.12 Precautions taken during experiment.....	38
3.13 LIBS Data Accumulation and Analysis	38

CHAPTER 4 LIBS ANALYSIS OF ARABIAN FISH SAMPLES	39
4.1 Introduction	39
4.2 LIBS Signal Intensity Optimization.....	40
4.3 The Plasma Parameter Analysis	42
4.4 Elemental Detection and calibration curves.....	45
4.5 Quantitative Analysis and Risk Assessment	76
CHAPTER 5 CONCLUSION	85
REFERENCES	87
VITAE.....	100

LIST OF TABLES

Table 3.1 ICCD Camera Specifications.....	29
Table 3.2 The spectrograph specifications.....	30
Table 4.1 selected wavelengths for characteristic atomic transition lines of calcium and other parameter for Boltzman plot.....	43
Table 4.2 The common elements in the fish samples	76
Table 4.3 the elemental concentration detected in the fish samples using	77
Table 4.4 Estimated Daily Intake of Fe (mg/kg body-weight /day)	78
Table 4.5 Iron Risk Criteria	79
Table 4.6 Iron Risk Consumption.....	79
Table 4.7 Estimated Daily Intake of Mn (mg/kg body-weight /day).....	80
Table 4.8 Manganese Risk Criteria.....	80
Table 4.9 Manganese Risk Consumption	80
Table 4.10 Estimated Daily Intake of Ba (mg/kg body-weight /day).....	81
Table 4.11 Barium Risk Criteria.....	81
Table 4.12 Barium Risk Consumption.....	81
Table 4.13 Target Hazard Quotient (THQ) of Fe	83
Table 4.14 Target Hazard Quotient (THQ) of Mn.....	83
Table 4.15 Target Hazard Quotient (THQ) of Ba.....	83
Table 4.16 Hazardous Index	84

LIST OF FIGURES

Figure 1.1 Population in the energy level	15
Figure 3.1 Schematic diagram of the LIBS set-up.....	27
Figure 3.2 The LIBS System Set-Up [61]	28
Figure 3.3 The LIBS emission collecting system	31
Figure 3.4 Ophir Energy Meter [61]	32
Figure 3.5 Oven	32
Figure 3.6 The ICPMS Set-Up.....	34
Figure 3.7 Pelletized fish samples, from the right to the left, the sample names are Sarah, Bagoh, Bory, Hered, Bulfusyan.....	35
Figure 3.8 The grinder of the LIBS Samples	38
Figure 4.1 Dependence of the LIBS intensity on time delay	41
Figure 4.2 LIBS Intensity dependence on energy.....	41
Figure 4.3 LIBS spectra of Calcium lines selected for Boltzman plot for calculation of Plasma Temperature	43
Figure 4.4 Boltzman plot to calculate the plasma temperature.....	44
Figure 4.5 Stark broadening profile of Ca I 732.61 for estimation of electron density....	44
Figure 4.6 Typical LIBS Spectrum indicating persistent Mg line in 260-290 nm region for (a) Bulfusyan fish at 280.27 nm	46
Figure 4.7 Typical LIBS Spectrum indicating persistent Mg line in 260-290 nm region for (a) Sarah fish and (b) Bagoh fish at 280.27 nm	47
Figure 4.8 Typical LIBS Spectrum indicating persistent Mg line in 260-290 nm region for (a) Bory fish and (b) Hered fish at 280.27 nm	48
Figure 4.9 Calibration curve for detection of Magnesium.....	49
Figure 4.10 Typical LIBS Spectrum indicating persistent Ca line in 290-330 nm region for (a) Bulfusyan fish at 315.8 nm	50
Figure 4.11 Typical LIBS Spectrum indicating persistent Ca line in 290-330 nm region for (a) Sarah fish and (b) Bagoh fish at 315.8 nm.....	51
Figure 4.12 Typical LIBS Spectrum indicating persistent Ca line in 290-330 nm region for (a) Bory fish and (b) Hered fish at 315.8 nm.....	52

Figure 4.13 Calibration curve for detection of Calcium	53
Figure 4.14 Typical LIBS Spectrum indicating persistent Fe line in 350-380 nm region for (a) Bulfusyan fish at 358.12 nm	54
Figure 4.15 Typical LIBS Spectrum indicating persistent Fe line in 350-380 nm region for (a) Sarah fish and (b) Bagoh Fish at 358.12 nm	55
Figure 4.16 Typical LIBS Spectrum indicating persistent Fe line in 350-380 nm region for (a) Bory fish and (b) Hered Fish at 358.12 nm.....	56
Figure 4.17 Calibration curve for detection of Iron	57
Figure 4.18 Typical LIBS Spectrum indicating strong Mn line in 400-410 nm region for (a) Bulfusyan fish at 407.94 nm	58
Figure 4.19 Typical LIBS Spectrum indicating strong Mn line in 400-410 nm region for (a) Sarah fish and (b) Bagoh fish at 407.94 nm.....	59
Figure 4.20 Typical LIBS Spectrum indicating strong Mn line in 400-410 nm region for (a) Bory fish and (b) Hered fish at 407.94 nm.....	60
Figure 4.21 Calibration curve for detection of Manganese	61
Figure 4.22 Typical LIBS Spectrum indicating strong Ba line in 760-790 nm region for (a) Bulfusyan fish at 778.04 nm	62
Figure 4.23 Typical LIBS Spectrum indicating strong Ba line in 760-790 nm region for (a) Sarah fish and (b) Bagoh fish at 778.04 nm.....	63
Figure 4.24 Typical LIBS Spectrum indicating strong Ba line in 760-790 nm region for (a) Bory fish and (b) Hered fish at 778.04 nm.....	64
Figure 4.25 Calibration curve for detection of Barium.....	65
Figure 4.26 LIBS spectra of sample 1 Sarah fish at (a) 450nm and (b) 585 nm central wavelengths	66
Figure 4.27 LIBS spectra of sample 1 Sarah fish at (a) 720 nm and (b) 810 nm central wavelength.....	67
Figure 4.28 LIBS spectra of sample 2 Bagoh fish at (a) 450nm and (b) 585 nm central wavelength.....	68
Figure 4.29 LIBS spectra of sample 2 Bagoh fish at (a) 720 nm and (b) 810 nm central wavelength.....	69

Figure 4.30 LIBS spectra of sample 3 Bory fish at (a) 450nm and (b) 585 nm central wavelength.....	70
Figure 4.31 LIBS spectra of sample 3 Bory fish at (a) 720 nm and (b) 810 nm central wavelength.....	71
Figure 4.32 LIBS spectra of sample 4 Hered fish at (a) 450nm and (b) 585 nm central wavelength.....	72
Figure 4.33 LIBS spectra of sample 4 Hered fish at (a) 720 nm and (b) 810 nm central wavelength.....	73
Figure 4.34 LIBS spectra of sample 5 Bulfusyan fish at (a) 450nm and (b) 585 nm central wavelength.....	74
Figure 4.35 LIBS spectra of sample 5 Bulfusyan fish at (a) 720 nm and (b) 810 nm central wavelength.....	75

LIST OF ABBREVIATIONS

LIBS	: Laser-Induced Breakdown Spectroscopy
LTE	: Local Thermodynamic Equilibrium
ICP	: Inductively Coupled Plasma
ICP-MS	: Inductively Coupled Plasma Mass Spectroscopy
ICP-OES	: Inductively Coupled Plasma Optical Emission Spectroscopy
TRLIBS	: Time Resolve Laser-Induced Breakdown Spectroscopy
LAS	: Laser Ablation Spectroscopy
LSS	: Laser Spark Spectroscopy
UV	: Ultra - Violet
Nd-YAG	: Neodymium Yttrium Aluminum Garnet
KBr	: Potassium Bromide
EDI	: Estimated Daily Intake
THQ	: Target Hazard Quotient
HI	: Hazardous Index

ABSTRACT

Full Name : [Lutfi Mulyadi Surachman]
Thesis Title : [The Development Of Laser-Induced Breakdown Spectroscopy
Techniques For The Analysis Of Fish Samples From The Arabian Gulf
]
Major Field : [Physics]
Date of Degree : [May 2018]

A Laser Induced Breakdown Spectroscopy set-up was used to detect and analyze different elements in a variety of fish samples purchased from the local market. Toxic elements may be present in the fish from environmental contaminations, such as those arising from industrial discharges, oil spills and agricultural pollution. The fish samples were completely dried, ground into fine powder and subsequently pelletized using the pressing machine with a pressure of 6 bars for dry samples, 2 bars for wet samples, and 4 bars for medium condition. Signal intensity optimization, especially the optimum time delay, was first investigated. By using fish samples with the same dimension and maximum incident laser energy, the optimum time delay was approximately 100-125 ns. The study of local thermodynamic equilibrium and optically thin plasma conditions, along with estimating the electron number density and electron temperature, were conducted to make sure the Mc-Whirter criterion holds for the plasma. This is to ensure that the laser – induced plasma generated for our analysis is thin enough to overcome the self-absorption problem, which would yield an accurate system capable of detecting the elemental concentrations with better accuracy and improved limit of detection. Once the system was optimized, it was applied for detecting the presence of a variety of elements in the fish samples. It is worth mentioning that we successfully detected nutrients like Calcium, Magnesium, and

Potassium, some heavy elements like Iron, Barium and Manganese and toxic element like Mercury inside the fish samples. The electron temperature and electron density generated by the laser-induced plasma was estimated to be $T = 14137.55 \pm 3448.29$ K and $4.2764 \times 10^{16} \text{cm}^{-3}$ respectively. To evaluate the human health risk assessments for the fish consumption, estimated daily intake, target hazard quotient and hazardous index were calculated based on average body weight, fish consumption rate and life expectancy of people (male and female) in Saudi Arabia.

|

ملخص الرسالة

الاسم الكامل : لطفي مليادي سرشمان

عنوان الرسالة : تطوير تقنيات التحليل الطيفي بالليزر لتحليل عينات الأسماك من الخليج العربي

التخصص : علوم فيزيائية

تاريخ الدرجة العلمية : مايو 2018

تم تطبيق إعداد الليزر التي يسببها انهيار الطيفي للكشف عن العناصر المختلفة وتحليلها في مجموعة متنوعة من عينات الأسماك التي تم جمعها من السوق المحلية. قد تكون السموم الموجودة في الأسماك موجودة بسبب التلوث البيئي، مثل النفايات الصناعية وانسكاب النفط والملوثات الأخرى. تم طحن العينات إلى مسحوق ناعم ثم تحريكها بعد ذلك باستخدام آلة الضغط بضغط 6 بار للعينات الجافة، وبارين للعينات الرطبة، و 4 أشربة لحالة متوسطة. تم التحقيق لأول مرة في تحسين كثافة إشارة، خاصة التأخير الزمني الأمثل. باستخدام نفس البعد لعناية السمك بحجم العملة وطاقت الليزر القصوى، كان التأطيم الزمني المثالي حوالي 100-125 نانوثانية. تم إجراء دراسة للتوازن الديناميكي الحراري المحلي وحالة البلازما الرقيقة بصرياً، وخصوصاً حساب كثافة عدد الإلكترونات ودرجة حرارة الإلكترونات، للتأكد من أن معيار Mc-Whirter يحمل لبلازما. من المهم التأكد من أن البلازما التي يسببها الليزر في دراسة رقيقة بما يكفي للتغلب على مشكلة امتصاص الذات وأن يكون لديها نظام دقيق للكشف عن تركيز العناصر بدقة أفضل وحدود محسنة للكشف. بمجرد أن يتم تحسين نظام، ثم تم تطبيقه لكشف العناصر في مجموعة متنوعة من عينات الأسماك. ومن الجدير بالذكر أننا نجحنا في الكشف عن المغذيات المقاسة مثل الكالسيوم والمغنيسيوم والبوتاسيوم، حديد وغيرها وبعض السموم مثل الباريوم والمنغنيز والزنك داخل عينات الأسماك. تم تقدير درجة حرارة الإلكترون وكثافة الإلكترون الناتجة عن البلازما التي يسببها الليزر $T = 14137.55 \pm 3448.29$ و $4.2764 \times 10^{16} \text{ cm}^{-3}$ على التوالي. لتقييم تقديرات المخاطر الصحية لاستهلاك الأسماك، تم حساب المقدار المقدر اليومي، وقيمة المخاطر المستهدفة والمؤشر الخطير على أساس متوسط وزن الجسم ومعدل استهلاك الأسماك ومتوسط العمر المتوقع للناس (الذكور والإناث) في المملكة العربية السعودية.

CHAPTER 1

INTRODUCTION

1.1 Overview

A laser (Light Amplification by Stimulated Emission of Radiation) source emits light by the stimulated emission of electromagnetic radiation [56], and it has several extraordinary properties over conventional light sources: it has very low beam divergence, a high intensity $I = \frac{P}{A}$, temporal and spatial coherence, and it is monochromatic. More details of the laser properties are separately explained in the next subsection, in relation with the factors that influence the plasma parameters. A laser has three main parts: the pumping source (the flash lamp), the active lasing medium (Nd: YAG crystal, for this work) and the optical resonator. The LIBS technique ranks highly amongst the various analytical spectroscopy techniques in terms of detecting the various chemical species present in a test sample. It can analyze – both qualitatively and quantitatively – materials in all physical states – solid, liquid or gas. LIBS has some unique properties over other spectroscopic techniques, such as the target not needing to exhibit fluorescence, Raman or IR activity. The LIBS technique involves simply irradiating any target with a pulsed laser beam and measuring the resultant spectrum [56].

The working principle underlying the LIBS technique is as follows: the output of a pulsed laser is incident on the target surface, due to which plasma sparks are generated, and its emission spectra is acquired with a detector. The wavelength of emitted lines and

intensities emitted by the plasma are compared with a reference and calibrated using samples of known concentration to quantitatively and qualitatively estimate the composition of the unknown sample [83].

The main principle of the LIBS can be described as follows [83]: a focused laser pulses strikes the sample, thus vaporizing, atomizing and exciting it. The light emitted from the plasma plume is collected, dispersed and analyzed, to determine the spectral lines of the elements present within the sample. Compared to other available analytical techniques like atomic absorption spectroscopy, Inductively Coupled Plasma Mass Spectrometry (ICP-MS) and Inductively Coupled Plasma Optical Emission Spectroscopy (ICP-OES), LIBS has lower analytical performance capabilities. However, the ICP and atomic spectroscopy require sample digestion that involves hazardous chemical usage and disposal. This process creates serious environmental and health-related problems to the environment. Therefore, LIBS has often remained preferable spectroscopic technique for qualitative and quantitative analysis due to its smaller environmental footprint. It has many applications in diverse areas such as Industry [13][19], medicine [27][63], Forensic sciences [100][108], Space exploration [71] and environmental monitoring [47] - [48]

1.2 Theoretical Background of LIBS

1.2.1 Introduction

The acronym LIBS (Laser-Induced Breakdown Spectroscopy) can be abbreviated in several ways: (LIPS) Laser-Induced Plasma Spectroscopy, (TRLIBS) Time-Resolved LIBS, (LAS) Laser Ablation Spectroscopy, and (LSS) Laser Spark Spectroscopy [26][93]. LIBS principle is based on Atomic Emission Spectroscopy (AES): due to discrete energy levels, the excited atoms undergo de-excitation, resulting in emission of radiation with certain frequencies and intensities.

The intensity data is used to calculate the concentration of radiating atoms, whereas from the frequency data, we obtain information about the radiating transition and thus the radiating species present.

The 3 primary AES components are: detector, wavelength selector, and excitation source. The excitation source is used to excite the target atoms. A detector records specific wavelengths, based on the wavelength analyzer. Subsequently, at a specific frequency, pre-determined by wavelength analyzer, the detector evaluates the intensity of radiating atoms.

1.2.2 LIBS Principle

In LIBS system, a UV pulsed laser strikes the sample surface. Through the collisional and multi-photon processes, the laser beam will temporarily create multi-colored plasma with temperature up to 25 kilo Kelvin. The plasma temperature will decrease due to plasma cooling down on the sample surface [21] - [72]. A monochromator (spectrograph) captures the signals to disperse the light wavelength from the plasma emission into its constituent wavelength. Furthermore, the spectrograph identifies the

chemical elements present in the sample based on unique wavelengths of transition lines. Detection time after excitation of the laser is an important parameter to be factored in. After a few microseconds, the plasma components re-absorb electron and become excited neutral atoms. Subsequently, by releasing unique wavelengths, which are the elemental fingerprint present in the sample, these neutral atoms de-excite from the excited to the ground state [99]. Additionally, if delay time is at an earlier time then the emission of singly ionized atomic species is detectable. The time of detection, or the gate time delay is adjusted by tuning the delay time between detector and laser.

1.2.3 Analytical Technique using LIBS

Development and study of the LIBS have been very intensive research activity over the past three decades [77]. This owes to the LIBS unique capabilities, allowing material analysis under such conditions wherein other analytical techniques may fail to offer meaningful result. Firstly, due to high laser intensities required to start the plasma emission, the laser pulse is able to excite the sample in a single step. Secondly, since the spot size is very small, due to the excellent collimation properties of a laser beam, the actual space for the spectral analysis can be well defined, thus allowing for spatial mapping of the present elements. Thirdly, the LIBS analysis can be conducted on physically-remote samples using fiber optic.

1.2.4 Factors that Influence the Plasma Parameters

Laser-solid interaction is a phenomenon that depends on several coupled parameters such as properties of laser, ambient conditions (pressure) and target material properties.

1.2.4.1 Properties of Laser

1.2.4.1.1 Monochromaticity

Unlike conventional light sources, emitting over a wide wavelength range, a laser source emits highly monochromatic radiation, which means that it has an effectively single wavelength or frequency. The plasma production itself is not contingent upon this monochromatic property. The power per unit area (or intensity) highly influences the plasma production, rather than the monochromatic nature of the beam. This monochromatic property of light is very useful to probe the plasma using atomic species resonance excitation in some special cases [29].

1.2.4.1.2 Directionality

Laser beam directionality means that the laser utilized in LIBS experiments has a very small beam divergence angle, in the order of milliradians. Beam directionality ensures that the laser beam is strongly focused to a very small spot size and strikes precisely at the point of interest. Directionality and coherence are inter-related parameters. Spatial coherence is indirectly-correlated with a small beam divergence and thus the capability of the laser to generate high irradiance. Nonetheless, we observed that in our LIBS experimental set-up, temporal and spatial coherence was not required, since the irradiance was considerably constant, and the plasma formation was not affected by the laser beam coherence. [30]

1.2.4.1.3 High laser intensity (Irradiance)

The laser irradiance intensity is defined as the power per unit area $\left(\frac{W}{cm^2}\right)$. The irradiance also describes the laser peak power per cross section of the beam output. A very large LIBS signal intensity, approaching billions or even trillions of watts per unit area is attainable since the laser can generate ultra-short pulses, in the order of femto- or nanoseconds. In the LIBS experiment, having a laser with high powers per unit area is very important. This process depends on the optical system utilized to produce the laser beam. [16][30]

1.2.4.2 Ambient Conditions

The plasma size and shape rely on the surrounding conditions, like the ambient gas and pressure composition. The plasma emission intensity increases with increasing pressure. This increasing intensity is the result of plasma confinement, generating a denser and hotter plasma. Under medium pressure, the hot plasma is surrounded by an ever-increasing concentration of the absorbing species. This increasing concentration makes the hot plasma thinner and thus it expands more rapidly. Hence, the emission intensity decreases and the effects of absorption become more significant under moderately high pressure conditions. Using a pressure range of $50 < P < 500$ torr in the air, adsorption effects can be minimized [70].

1.2.4.3 The Laser Induced Plasma and target material property relationship

The aspect of materials, that influence the plasma plume shape and size, are its mechanical, thermal and physical properties. Not only does the ablated target mass rely on the intensity of laser but it also relies on the sample material properties. The heat conduction and ablated mass relationship satisfies the following formula [61]:

$$m(t) = B(AI)^2\tau^{\frac{3}{2}} + A(alt) \quad (1)$$

Note that I is Intensity of laser, τ is the laser pulse time, B, A are proportional to thermal properties of the sample, a is the factor for energy coupling, t is duration of the laser pulse.

For nanosecond laser pulses, The laser fluency must exceed the threshold value (in order of $\frac{J}{cm^2}$) to form the laser induced plasma.

The plasma formation process commences with vaporization of the target material. Vaporization occurs if the energy of laser incident on the surface of the sample exceeds the vaporization latent heat (L_v) of the target material. This implies that no vaporization occurs if the laser fluency is below the threshold value. The threshold fluency F_{th} for the evaporation satisfies the following relation,

$$F_{th} = \rho l_v a^{1/2} w^{1/2}; a = \frac{K}{\rho C_p} \quad (2)$$

Note that K is the thermal conductivity, C_p is the specific heat per unit mass, w stands for the width of the laser pulse, a is the thermal diffusivity, L_v is the vaporization latent heat of the sample, ρ is the sample density.

Thermal properties of materials, like boiling and melting temperature and thermal conductivity, affect the threshold intensity value. This implies that the thermal effects influence the laser ablation [18]. The crater dimensions, plasma shape and size are

influenced by the mechanical and physical properties of the material. In more detail, the laser energy fraction coupled to target material surface is determined by sample reflectivity. Due to material undergoing phase change under high temperatures and high laser intensities, materials with a reflecting surface can effectively absorb the laser energy. [94]

The crater shape and size, affected by surface reflectivity, boiling temperature, specific heat and density can be written as, [8]

$$D = \frac{A(1 - R)}{\rho C_p T_b} \quad (3)$$

Note that R stands for the surface reflectivity, A is the constant of proportionality, T_b stands for the boiling temperature, and D is the crater diameter.

1.2.5 Set-up Geometry

The plasma geometry and intensity profile of spatial emission strongly depend on the power density of laser, alignment of the optical system to focus the laser, and the plasma plume emission for spectrum data acquisition. For these reasons, it is essential to comprehend the effect of light collection (for spectrum recording) and that of optical alignment on the LIBS signal intensity. To enhance precision, cylindrical lenses are preferable to spherical ones [34]. During the analysis of liquid samples, the lens must be protected from liquid back-splashes due to the shock waves; hence, we focus the laser beam slightly off the normal plane of the sample surface. For solid target analysis, the focused beam of laser is targeted directly normal to the target surface. Before focusing on the target surface, the laser leads to breakdown in the surrounding air; this phenomenon, especially in the presence of dust clouds, affects the laser intensity incident on the target surface.

To obtain stabilized disintegration while optimizing the space of interaction [12][107], the distance between the target surface and focusing lens should be marginally shorter than the focal length. Because of its simplicity and reproducibility, the plasma emission collection is performed axially perpendicular to the target surface.

1.2.6 Observation of Time window

The plasma temperature is initially very high. However, the temperature progressively decreases as the plasma expands further away from the target surface. By observation, a continuum radiation controls the beginning of the plasma evolution. After the plasma expansion, which is accompanied by decreasing temperature, the evolution of the line intensities is observable. The emission lines are superimposed on the continuum emission. During LIBS analysis for material composition, only the emission line is important. Usually the continuum emission decays faster compared to the emission line. Hence, using LIBS involves setting appropriate time delay such that the difference between the line emission and the background noise is clearly visible [107].

1.2.7 The Effect of Binder

In LIBS sample preparation, binding materials play important roles. To prevent sample disintegration during laser irradiation, the prepared samples must be strongly bonded prior to the LIBS experimental analysis. To obtain a homogenous sample, we first grind the samples until an extremely fine powder with unconsolidated particles is obtained. Subsequently, the samples are pelleted using a binding material [26]. If the powder sample has intrinsic binding strength, it obviates the need for binding materials. Appropriate binding materials should be selected to achieve LIBS analysis with higher precision and sensitivity. The finely-ground powder is usually mixed with the following suitable binding

materials: poly (vinyl) alcohol, starch, Ag, Al, or KBr. Next, the powder is placed in a special die and pressed hydraulically. Previous studies have reported that to find the best binder, different LIBS signal intensity of various magnesium lines (279.5, 517.2, 383.8 and 518.3 nm) can be used. The magnesium spectra were acquired from known varying pellet concentration using available binders. To understand the process of the laser ablation, the ablated crater images were captured using the Optical Scanning Microscopy. For this work, The relatively measured LIBS signal intensities of the 518.3 nm Magnesium line were recorded as 130, 227, 387, 538 and 735 using Aluminum, Silver, poly (vinyl alcohol), starch and Potassium Bromide respectively as binder materials. From the aforementioned results, we conclude that for the analysis of LIBS sample powder, the best binder material is potassium bromide.

1.2.8 Mechanical Failure on surface of solid

The pulse leading edge quickly heats, melts and vaporizes into a layer. This edge is above the surface of the target provided the illumination of the laser is sufficient to generate the plasma plume. Subsequent laser pulses heat the already evaporated materials. When weak plasma ionization occurs, a portion of the laser energy goes into the surface while the plasma absorb the remaining portion of the laser energy. Sufficiently-high energies render the plasma opaque to the laser beam, resulting in the surface being shielded from the beam. At the same time, the front shape of the plasma plume grows toward the laser. This process happens when the frequency of the plasma exceeds the frequency of the laser.

1.2.9 Laser Ablation

The properties of the laser beam and sample material highly influence the laser ablation process. Micro to milijoules laser fluencies can affect atomic and ionic removal without inducing defects in the sample surface. Subsequent laser pulses strike the material under melting and condensation conditions. The surface reflectivity changes and a crater appears. The elements present in the previous sample may possibly evaporate partially in such a way that the newly deposited target material does not show the same composition.

Some important physical consideration in the laser ablation are the longer or shorter pulsed length effects, minimum threshold laser intensity for initiation of vaporization, the ablation rate and the need to maintain the sample composition in the plasma state after ablation. To produce vaporization, the minimum laser power density must satisfy the following relation. [84]

$$I_{min} = \left[\frac{L_v \rho \kappa^{1/2}}{\Delta t^{1/2}} \right] \frac{W}{cm^2} \quad (4)$$

Note that $t^{1/2}$ is laser pulsed length [67],[24], κ is the sample thermal diffusivity, ρ is the target density, and L_v is the vaporization latent heat.

1.2.10 Qualitative Analysis

The strong and persistent lines of the LIBS spectra are the first to identify the most common and higher concentration in the test samples. The elements with high intensity are likely to be nutritious elements such as Potassium, Calcium, Sodium and Magnesium. On the other hand, the elements exhibiting low intensity are plausibly toxins such as Mercury, Arsenic, Chromium, etc or heavy elements such as Iron, Manganese, copper etc. The LIBS wavelengths are usually compared to the available wavelength database of NIST (National Institute of Standards and Technology). Identification of strong lines requires wavelength

difference resolution of 0.03 to 0.2 nm along with verification of the presence of three strong to moderate lines of intensity at least [26].

1.2.11 The Study of Plasma as a Process of Ionization (Opacity of Plasma)

A plasma is a local assembly of overly electrically neutral ions, electron and atoms. There are several parameters associated with plasma formation, of which the most fundamental is its ionization degree. Plasmas tend to have a certain life times, possessing three stages. The First stage is the process of plasma ignition. This process includes bond breaking and shielding of plasma during the laser pulse process, depending on type of illumination and duration of the pulsed laser. During the cooling process, the plasma effects atomic emission. The second stage is the LIBS spectra collection optimization. After the ignition stage, the plasma keeps cooling and expanding. Simultaneously, the electron temperature and its number density change. For LIBS spectral assignments, the last stage of the plasma life times is not preferential.

The main purpose of the LIBS experiment is to generate plasma in Local thermodynamic equilibrium and optically thin condition. When the emitted light escapes and traverses without being affected by effective scattering or absorption, the plasma becomes optically thin.

The plasma radiation intensity satisfies the following equation,

$$I(\lambda) = \left(\frac{\varepsilon(\lambda)}{\alpha(\lambda)} \right) (1 - \exp(1 - L\alpha(\lambda))) \quad (5)$$

Note that $\alpha(\lambda)$ is the coefficient of absorption (cm^{-1}), L stands for the length of plasma along the observer line sight, and $\varepsilon(\lambda)$ is the emissivity.

If the self-absorption does not occur then the value of $\alpha(\lambda)$ will be very small and equation (5) can be approximated to be:

$$I(\lambda) = \left(\frac{\varepsilon(\lambda)}{\alpha(\lambda)} \right) (\alpha(\lambda)L)\varepsilon(\lambda)L \quad (6)$$

To ensure a plasma is in LTE condition, different tests has been developed of which the easiest way involves determining the relative intensities of emission lines of closely spaced upper level in the same multiplet. It confirms the prediction from the fundamental theory of Kuhn in 1963. However, the disadvantages of the method are neighboring line interferences and self-absorption. The other famous method to prove the LTE condition is the Mc-Whirter criterion. The formulation of this method is based on the premise that the density of electron in the observed plasma must be sufficiently high to have the collisional processes dominate the population in the energy levels. The Mc-Whirter criterion satisfies the following inequality:

$$n_e \geq 1.6 \times 10^{12} T^{\frac{1}{2}} (\Delta E)^3 cm^{-3} \quad (7)$$

Note that The units of T , n_e and ΔE (the highest energy differences) are $^{\circ}K$, cm^{-3} , and eV respectively.

Different quantity distribution like population of energy levels or stages of ions and speeds of electron, depend on temperature as a quantity of single plasma provided the existence of LTE condition proves experimentally correct.

The Classical Maxwell distribution for the velocity F_m satisfies the following equation,

$$f_m(v)dv = \left(\frac{m}{2\pi kT_e} \right)^{\frac{3}{2}} \exp \left[-\frac{mv^2}{2kT_e} \right] 4\pi v^2 dv \quad (8)$$

Note that v and m are the electron velocity and mass.

The relative population of energy levels, whether molecular or atomic in origin, can be explained by the distribution of Boltzman equation:

$$\frac{N_j}{N_o} = \left(\frac{g_j}{Z} \right) \exp \left[-\frac{E_j}{KT} \right] \quad (9)$$

$$\frac{N_j}{N_i} = \left(\frac{g_j}{g_i} \right) \exp \left[-\frac{(E_j - E_i)}{KT} \right] \quad (10)$$

Note that J is the total angular momentum, g_{ij} is the statistical weights of the levels $(2J_{ij} + 1)$, N_{ij} is the population of energy level E_{ij} , N_o is population of the total species, Z is the partition function, j and i refer to the two energy levels.

1.2.12 LTE Condition and Optically Thin Plasma

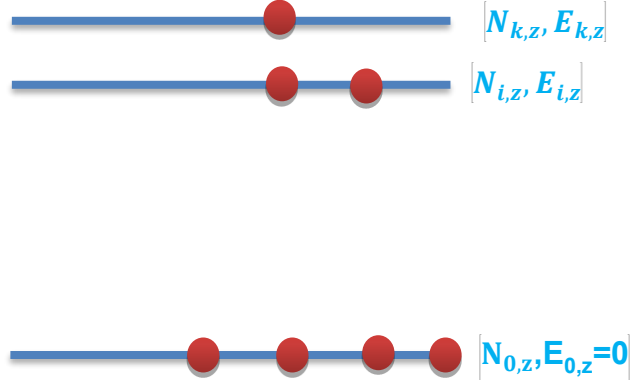


Figure 1.1 Population in the energy level

In the prevailing conditions, the electron population in the energy levels can be explained by the Boltzmann distribution:

$$\frac{N_{k,z}}{N_0} = \left(\frac{g_{k,z}}{p} \right) \exp \left[- \frac{E_{k,z}}{K_b T} \right] \quad (11)$$

Note that K_b is the Boltzmann constant, p_z is the partition function, T is the temperature of electron, N_z is the species number density in an ionization stage z , $N_{k,z}$, $E_{k,z}$ and $g_{k,z}$ are population, energy and the upper energy level (k^{th}) degeneracy in an ionization stage z .

In an optically thin plasma condition, The integrated intensity I_z of the lines of the atomic emissions, that occur between the lower energy level I and the upper energy level K, with ionization stage z , satisfies the following equation,

$$I_z = \frac{hc}{4\pi\lambda_{ki,z}} A_{ki,z} N_{k,z} L \quad (12)$$

Note that h is plank's constant, c is the speed of light, L is the characteristic length of the plasma, $A_{ki,z}$ is the transition probability, $\lambda_{ki,z}$ is the spectral line wavelength.

By substitution of equation (11) into equation (12), we get the following relation:

$$I_z = \frac{hc}{4\pi\lambda_{ki,z}} A_{ki,z} L \left(\frac{N_0 g_{k,z}}{P_z} \right) \exp \left[-\frac{E_{k,z}}{K_b T} \right] \quad (13)$$

Taking the natural logarithm of both side of equation (13) gives the following result :

$$\ln \left[\frac{\lambda_{ki,z} I_z}{A_{ki} g_{KZ}} \right] = -\frac{E_{kz}}{K_b T} - \ln \left[\frac{4\pi Z}{hc L N_0} \right] \quad (14)$$

Note I_z is the integrated signal intensity, K_b is the Boltzmann constant, T is temperature of the plasma, $A_{ki,z}$ is the probability of transition, $\lambda_{ki,z}$ is the wavelength of the transition line, $g_{k,z}$ is the upper level (k^{th}) degeneracy, P_z is the ionization z partition function, L is the plasma characteristic length, N_0 is the total population in the ground state, Other symbols have their own usual definitions [64].

In the ideal case, we obtain a straight line when the left side of the previous formula is plotted against the upper level energy, which gives $-\frac{1}{KT}$ gives the slope. To obtain a straight line, some parameters, such as well spaced energy level, accurate line intensities, and accurate transition probabilities. [109][22][98], must be measured accurately

Lines of transition originally have zero line width, however, due to some other processes (Doppler, Instrumental, Natural and Stark broadening [98][60][74]), the lines get broadened to some extent. Regarding the produced electric field due to the collision of ions and electrons, The Stark broadening is the most influential process. It causes discrete energy levels to broaden, resulting in the wavelength shifts.

The full width at half maximum (FWHM) $\Delta\lambda_{1/2}$ of a stark-broadened profile using a Lorentzian fitting satisfies the following relation,

$$\Delta\lambda_{1/2} = 2w \left[\frac{N_e}{10^{16}} \right] + 3.5 \left[\frac{N_e}{10^{16}} \right]^{5/4} \left[1 - \frac{3}{4} N_D^{-\frac{1}{3}} \right] w \left[\frac{N_e}{10^{16}} \right] A^0 \quad (15)$$

Note that w is the impact factor of electron, N_e is the density of electron, A is the broadening parameter of ion, N_D is the total particle in the Debye sphere. [60][74]

The first term on the right side of equation (15) explains the electronic broadening and the second term explains the ionic contributions to the broadening. For non-hydrogen ions, the stark broadening is primary due to the impact of electrons, since the ionic perturbation is negligible compared to the electronic perturbation, so, reduction of equation (15) satisfies the following formula,

$$\Delta\lambda_{1/2} = 2w \left[\frac{N_e}{10^{16}} \right] \quad (16)$$

Note:

1. ω is an impact factor of electron. This factor depends on temperature. Over the temperature range of (10000 – 80000)K, it only changes by a factor of two.

The Stark broadening profile is a great tool to determine the density of electron within an acceptable range of error.

1.2.13 Detection Limit

It is the sensitivity of the LIBS technique to detect the lowest concentration of analyte in the LIBS sample. The calculation can be performed by the following equation,

$$LOD = \left[\frac{3\sigma}{S} \right] \quad (17)$$

Note that σ is the standard error of the experimental calibration data, S is the sensitivity, which is the ratio between intensity and concentration (the slope of calibration curve).

1.3 Motivation

The existence of toxins and heavy elements in biological samples like fish and other biological tissues can be investigated using LIBS to determine whether it is in compliance with the regulatory requirements legislated by food authorities. We have analyzed a few biological samples because dietary consumption is the primary source of exposure to the elements for people who are not occupationally exposed. A vast spectrum of chronic ailments afflicting patients in the Kingdom of Saudi Arabic such as liver, renal and kidney failures are often associated with the intake of the toxins and heavy elements. Hence, by analyzing the presence of the elements present in consumables, and comparing it with the corresponding elements present in the bodies of patients, we can develop a prognostic marker for studying the correlation between a toxic and/or heavy element and a specific diseases. For example, fish tends to be rich in Mn; by studying the incidence of Mn poisoning in patients and correlating it to their fish consumption, a relationship can be built between health risk parameters (the EDI, THQ, and HI) of fish samples and Mn-related

diseases. A similar strategy can be applied for other toxins or heavy elements present in food and their corresponding diseases.

1.4 Objectives

- To develop a method using LIBS for application of biological sample analysis.
- To analyze and identify the LIBS spectra using atomic and ionic transitions.
- To study the LIBS signal intensity, which depends on various parameters (Energy of laser, elemental concentration, time delay, etc)
- To study the plasma parameter.
- To find the concentration of each element especially toxic ones present in the samples.
- To evaluate the human health risk assessment for the fish consumption.

CHAPTER 2

LITERATURE REVIEW

In the early 1960s, Laser Induced Breakdown Spectroscopy (LIBS) technique was first introduced for application of solid material analysis. The sparks from the electric discharge induce the excitation of the ablated materials [25]. For the analysis of multi-elements, LIBS ranks amongst the best analytical technique. Because of the reliability and relatively cheapness for the research and laboratory analysis, groundbreaking achievement and progress in the technology of both detector and laser has been performed since 1980s. Therefore, for the qualitative and quantitative analytical investigation of an impressive variety of samples, LIBS is a renowned analytical techniques. [35] [41] [65] [51] [7] [90] [89] [53]

Due to its unique characteristics such as fast online monitoring response, sensitive detection for multi-elemental analysis, relatively easy sample preparation, ability to perform remote-sensing detections, and high resolution for the mapping of surface, enhancement of the LIBS technique has undergone manifold enhancement over several decades [83]. These unique LIBS characteristics stimulates its application in an impressive myriad of applications, including food [75][42][82][39][81][97], environmental monitoring [46][59][92][40][54], geological samples [58][95] [96], industrial samples [28][80][69][55][45][52] [44], space exploration [14][101][103], agriculture [88][37][102], archeology [87][73][86], and identification of biomedical samples [15][32][9].

LIBS is an advanced analytical technique for analyzing the elemental composition of a wide range of samples, like rocks, explosives, cosmetics, metals, biocompatible samples etc regardless their states - solid, gas or liquid [30]. It has also been used for biomedical samples, such as tissues, teeth, body stones, nails, teeth, blood, etc [49]. Due to its need for little sample preparation and its ability to deliver results rapidly for biomedical sample analysis, LIBS has evolved into a well-established diagnostic techniques.

In this thesis, we analyze biocompatible samples. LIBS has been used by Josef Kaiser et al for recognizing trace elements in the matrix of microbiological samples. This technique is not commonly used to analyze bacterial and animal samples. It has been historically utilized to differentiate between healthy and cancerous tumor cells from a histological section of a dog, through which it was deduced that the concentration of elements present in the healthy and tumor cells is different. To achieve optimum results, the analysis was performed under pressure and the samples were frozen to -196°C . Some of the detected elements were Ca, Al, Fe, Cu, K, Na, and Mg. In conclusion, this research study has demonstrated the ability of LIBS to identify elements present in microbiological samples and thus act as a prognostic marker for various diseases.

Vincent Juve et al [38] used UV (LIBS) to identify elements present in fresh vegetables. They used consumable root, stem and fruit vegetable obtained commercially. In this research, an Nd: YAG laser was utilized, lasing at 266 nm, having 10 mJ energy and 10 Hz rate of repetition. The strong transmission between 200 and 850 nm is shown by the used fiber. Root spectra were recorded for a few elements from the internal to the external part, while the spectra of the stem were recorded at the different height of the plant from its lower to upper one. Good spectra of lines were identified using an NIST database,

yielding 422 lines, among which 391 spectral lines were emitted by atomic and ionic species, 9 lines were emitted by molecules C₂, and CNs, and 22 lines were emitted by unknown lines. Therefore, the LIBS technique has demonstrated its ability to detect trace elements including organic, metallic and nonmetallic ones in newly-harvested vegetables and thus can also be used for the other biological samples like fish etc.

LIBS also has been applied for the analysis of cancerous human cells. The pathogenesis of different kinds of cancers is a result of heavy metal distribution. However, colon cancer data and exposure to heavy metals lack correlational data. One of the few studies by Emre et al., compares blood samples of healthy people to those having metastatic colon cancer. The study was done by measuring heavy metal levels and noting that higher levels are linked with the presence of cancer [33]. Colorectal cancer [CRC] is presumed to involve a complex array of inherited susceptibility and environmental DNA genotoxic exposure, yet mostly no genetic predisposition is found and etiology continues to remain elusive. New observation suggests a strong relation between dietary intake and life style especially red meat, saturated fats, food, and alcoholic consumption. Also, sedentary lifestyle is a possible contributor to the CRC development. In spite of numerous challenges involved, [110] for the first time, they were able to employ the highly accurate LIBS technique to directly measure the levels of heavy metals in CRC tissues.

Xiong Wan and Peng Wang studied heavy metals in organism, including different part of the fish's body, using their optimized LIBS set-up. The qualitative study uses LIBS signal analysis whereas the quantitative study uses an internal standard-based quantitative analysis (ISQA) algorithm. In this study, they found that the heavy metals are densely distributed in liver and gills rather than homogenously distributed throughout the entire body of the fish [106].

F.C Alvira et al [11] developed a novel LIBS set-up, based on a low-cost, small and ultra-compact excitation source. The emitted light is in the multi-pulse regime, giving a maximum energy of 300 mJ. The developed LIBS system can detect copper and lead contaminations in the examined fish samples. The generated spectra were those of skin, scales and muscle of both frozen and fresh fish. Using their developed LIBS set-up, they obtained an improved limit of detection of 0.2 ppm and 0.25 ppm for copper and lead respectively.

L.V. Ponce et al developed a LIBS system to monitor the accumulated copper and lead contamination in the edible fish species, namely (*Oreochromis Niloticus*) tilapia del nilo. The developed LIBS system was compared with results from the atomic absorption spectroscopy. The improved limits of detection of the utilized LIBS set-up are 100 ppm and 25 ppm for copper and lead respectively. Those concentrations are less than the maximum limit, imposed by relevant health agencies. The developed LIBS system is useful for governmental use to monitor the edible fish contamination online.

In the Persian Gulf, Homira Agahat et al [5] studied the trace metal accumulation in the liver and muscle tissues of five different varieties of the fish samples obtained from the Persian Gulf. After digesting the fish samples using nitric acid and hydrogen peroxide

inside a microwave oven, the samples are ready for ICP-MS analysis. They found the present of the following elements in the fish samples: As, Cd, Co, Fe, Mn, Ni, Tl, Zn, Al, Be, Cr, Cu, Pb, Mo, Sb, V. In brief, this research proved the fact that the metals present were mainly found in greasy grouper, younger flathead, and tiger-tooth fishes. Of the examined fish species, the grunt fish shows strongly accumulated elements in the older fish samples. Positive and strong correlations between the present elements like Al, Ti, Pb, Co, Al and Fe were significantly noticed in the three or more species. This study concluded the fact that the liver and muscle tissues can perform the role of bio-indicators for identifying the presence of toxins in fishes living in metal-contaminated coastal area. This research also concluded that the elemental concentrations found in the fish samples are lower than the safety permissible limit, which means that there is no negative impact on public health with the exception of Arsenic.

Mehjbeen Javed and Nazura Usmani reported detection of six heavy metals, (Fe, Ni, Zn, Co, Cu, Mn) in the muscles of *Mastacembulus Armatus* using atomic absorption spectrometer. The concentration of the detected heavy elements are Mn (9.03 ppm), Cu (41.36 ppm), Co (9.06 ppm), Zn (186.19 ppm), Fe (213.29 ppm) and Ni (58.59 ppm). In this study, the estimated mean daily consumption rate of the heavy metals by fish consumption is 19.5×10^{-3} kg/day, factoring in the amount of fish that adults (female and male) consume. For Nickel and Cobalt, the examined fish samples show risks of carcinogens since the target hazard quotient (THQ) exceeds one. This study reported high Hazardous Index (HI). At conclusion, it was indicated that the consumers of the examined fish were at risk of toxicity from Nickel and Cobalt.

Amani S Alturiqi [10] used atomic absorption spectroscopy to evaluate some heavy metals detected in the fish samples from the Saudi Arabian markets in the four major urban and industrial cities in the kingdom (Jazan, Riyadh, Dammam and Tabouk). The elements present in the fish samples are Mn, Zn, Cd, Cu, Pb, Hg and Fe. The concentrations of the elements in the sausage are 18.51, 0.125, 242.44, and $15.43 \frac{\mu g}{g}$ for Cu, Hg, Fe and Pb respectively. For the luncheon fish, the concentration of the elements are 73.94, 4.08 and $32.67 \frac{\mu g}{g}$ for Zn, Cd and Mn respectively.

The elemental composition of Arabian fish was studied by Sabry Mohammed El-bahr and Ahmed Abdel Ghany. In this study, the heavy metals (Cd and Pb) and The trace elements (Fe, Cu, Mn and Zn) were detected for three different fish species, namely Spangled Emperor (shieri), Red striped seabream (Andak) and Black Seabream (Spondyliosma cantharus). After digesting the fish samples, 20 samples of each fish were examined using the atomic absorption spectrometry. In this study, it was reported that the quantity of trace elements and detected heavy metals were as follows: Fe > Zn > Cu > Mn > Pb > Cd. In this study, the authors found metal content variations in the muscles of the three fish. The highest measured concentration was that of Zinc, manganese and copper in the S. Santharus. The P. Major muscles accumulated the highest concentration of Iron, and in the three varieties of the fish muscles, Lead and Cadmium concentration levels are comparable. For Zn, Mn, Pb, Cd, Fe and Cu, the maximum daily intake were 0.0009, 0.0001, 0.0000, 0.0000, 0.0035, 0,0003 respectively. In conclusion, the less heavy metals found in the fish muscles is a positive indication that consuming fish does not influence it's consumer's health [31].

Shahid Mahboob, HF Alhakim Al-Balawi, F Almisned, Al-Quraishi and Z Ahmad conducted research on the distribution of metal in fish tissue, including the risk assessment for the very important fish species of Saudi Arabia. In this research, the detected elements are Cadmium (Cd), Nickel (Ni), Zinc (Zn), Arsenic (As), Chromium (Cr), Lead (Pb), Copper (Cu), Manganese (Mn) and Iron (Fe). They found these elements in the muscle tissues of four different samples, namely *Clarias Gariepinus*, *Aphanius Dispar Dispar*, *Poecillia Latipinia*, and *Oreochromis Niloticus*). The samples were collected from Wadi Hanifah over two different seasons. The heavy metal concentrations, with the exception of Pb, Cu, Ni, and Cd in *P. Latipina* and *A.d. Dispar* were below the safe permissible limit set by the relevant authorities. This also indicates the extent of heavy metal pollution. In the tissues of the fish muscles, the present study explains that the least and most accumulated metals are Chromium and Zinc respectively. This study concluded that from the human health viewpoint, the current consumption rate of *P. Latipina* and *A.d. Dispar* species in Saudi Arabia possibly correlates with the health risks for the fish consumer. [79]

CHAPTER 3

EXPERIMENTAL METHOD

3.1 Configuration of the LIBS System

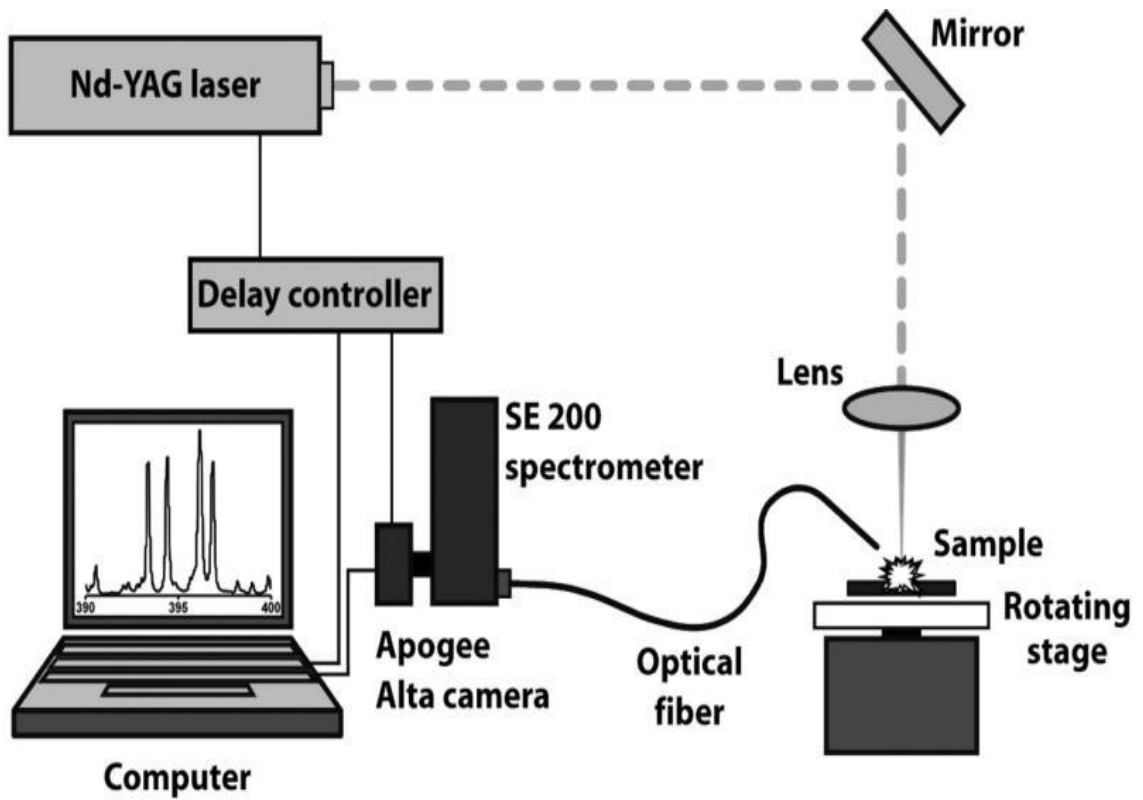


Figure 3.1 Schematic diagram of the LIBS set-up

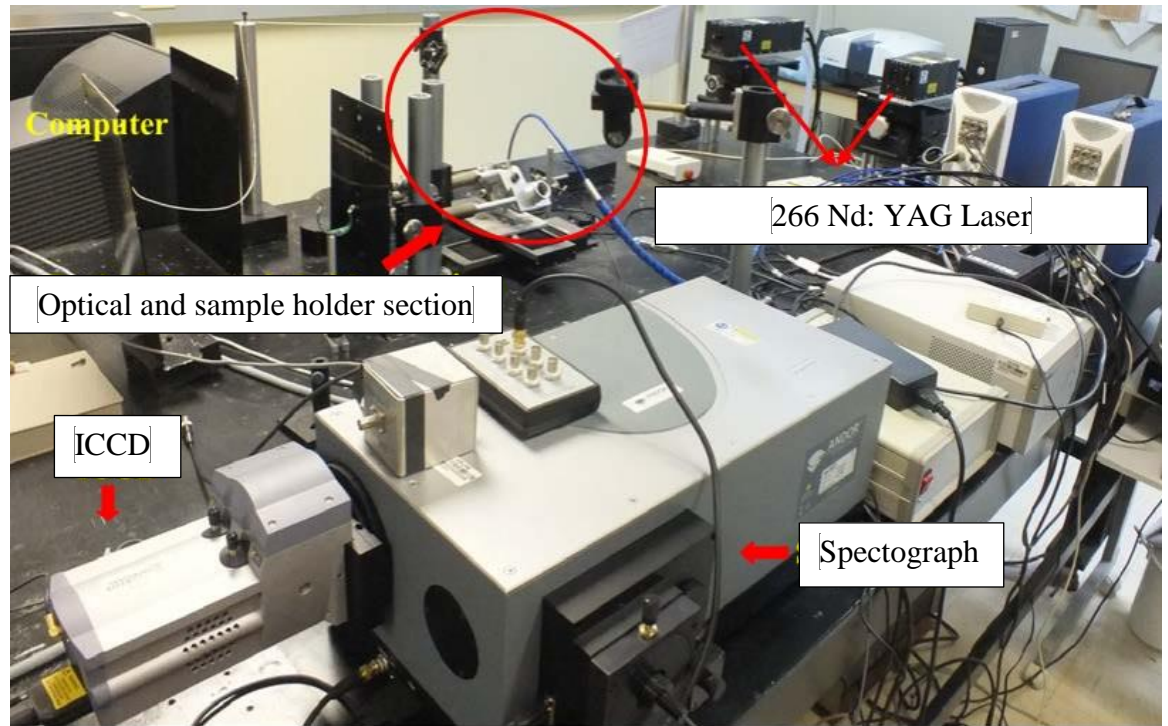


Figure 3.2 The LIBS System Set-Up [78] [50] [85]

3.2 ICCD Camera

To acquire the desired signal from the light of plasma, our LIBS set-up utilizes a specified Integrated Charge Coupled Device (ICCD) camera (Table 3.1). Highly sensitive imaging can be performed using this camera. This camera can even capture the lightening action even though the incoming of the light beam is highly intense. By adjusting time gate delay, the camera can increase the signal to noise ratio So as to yield a strong signal. The time gate delay measures the time elapsed between the firing of the laser pulse and the opening of the ICCD camera window. It is after how long the window of the ICCD camera start to opening. The other time-associated parameter is the gate width, which is the time interval during which the window remains open. In this LIBS experiment, we keep the gate width to its default value as pre-defined by the software, and the time gate delay as mostly set at 100 ns.

Table 3.1 ICCD Camera Specifications

I Star 332	
Aperture	F/6.5
Focal length	500 mm
Pixel matrix	1024 x 1024
Pixel size	13 μm

3.3 Spectrometer

Spectrometer is an electronic tool utilized in the LIBS set-up to measure the spectra of a sample. The wavelength interval of typical LIBS Spectra ranges from vacuum ultraviolet to the near infrared, which is a considerably complex and wide interval. To cover such a wide range for LIBS analysis, a good spectrometer should have the following characteristics:

- a. To resolve the closely spaced lines of spectra, the spectrometer should have a readout time and short data acquisition.
- b. The spectrometer should have high resolution and wide range of spectra.
- c. It should have large dynamic range and give high quantum efficiency over a whole recorded spectrum.

To obtain the generated LIBS signal from the fiber optics, a highly resolved spectrograph, specified in Table 3.2, was utilized. Using the second grating (groove density = 1200 lines/mm), the spectrometer generates clearly visible and well-resolved spectra in the range of 200-900 nm. The wavelength obtained by our LIBS analysis has remarkable accuracy, exhibiting very small differences, compared to the wavelength values on the NIST database.

Table 3.2 The spectrograph specifications

SR-500 (General)	
Type	Czerny-Turner arrangement with imaging toroidal optics
Focal Length	500mm
Aperture	f/6.5
Reciprocal Dispersion	1.7nm/mm (nominal)
Wavelength Range	190nm to 10 μ m (detector dependent)
Wavelength Resolution	0.05nm (< 0.1 nm with 25 μ m pixel CCD detector)
Wavelength Reproducibility	\pm 0.05nm
Wavelength Accuracy	\pm 0.2nm
Focal Plane Size	28mm wide x 14mm high
Time to switch gratings	< 10 secs
Stray Light	1.5×10^{-4} (measured at 20nm from 633nm laser line)

3.4 The LIBS Emission Collecting System

The light gathering system consists of lenses and optical fiber. To collect, converge and direct the light into the optical fiber, the set-up utilizes the miniature convex lens. To obtain optimum signal acquisition conditions, the fiber optic was oriented at angle of 45⁰ with respect to the plane perpendicular to the sample surface. The fiber optic guides the light signal to the ICCD camera. For easy lens alignment, to gather the spark maximum signal, the light gathering system can be translated in two dimension. [66]

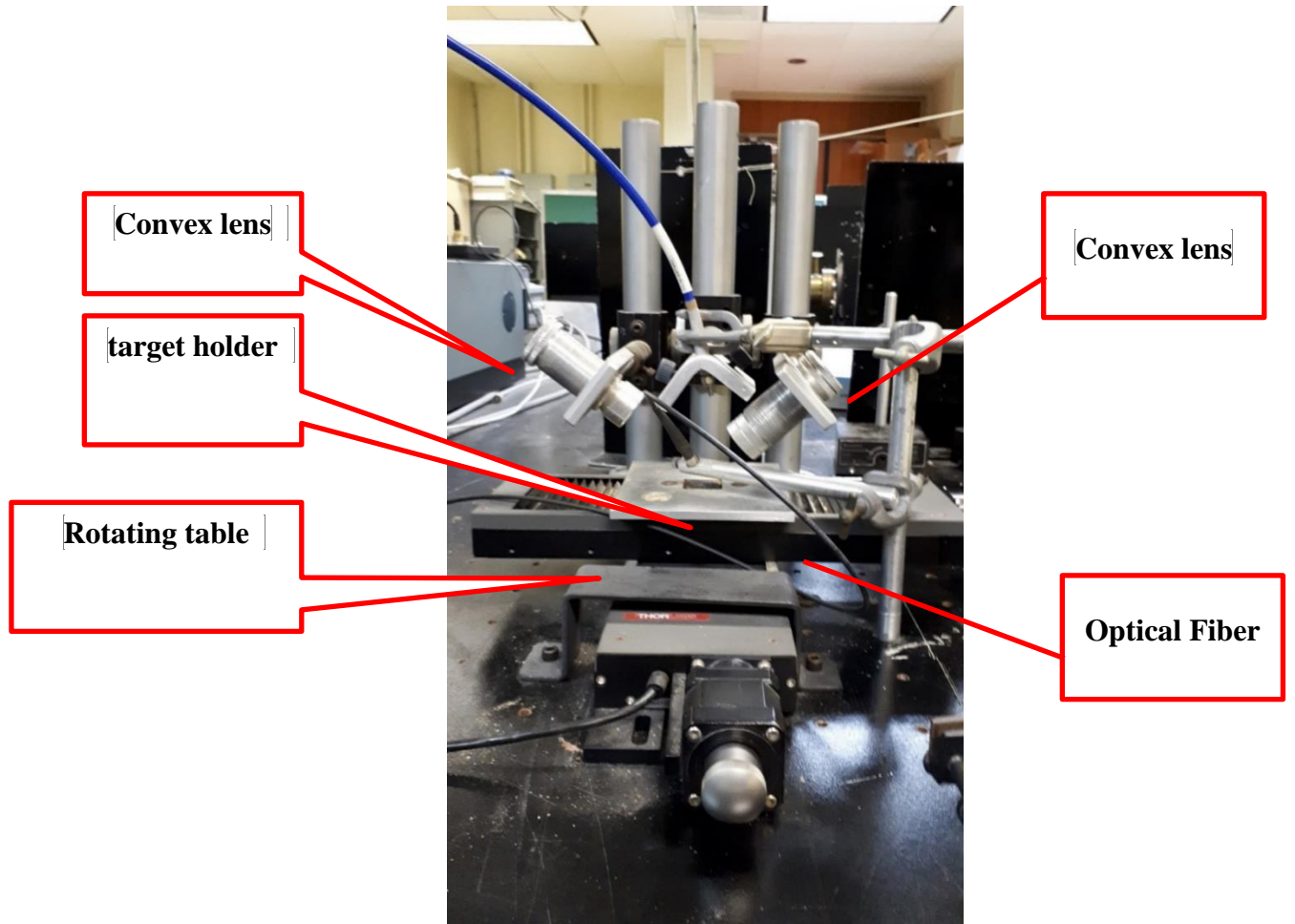


Figure 3.3 The LIBS emission collecting system

3.5 Energy meter

LIBS signal optimization requires energy measurement, to determine the energy per pulse that yields optimum signal. In this research, we utilize Ophir model 300 radiometer to measure the optimum energy. The laser energy within the range of 30 - 50 mJ was used to study the dependence of LIBS signal of a chosen marker wavelength of an element on the incident laser energy.

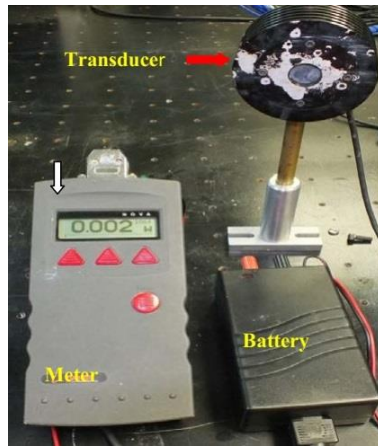


Figure 3.4 Ophir Energy Meter [78]

3.6 Oven

Prior to the LIBS Spectral analysis, the samples were prepared as follows. Fish meat was dried using an oven so that it can be ground easily. After grinding the meat, the samples were prepared by the pelleting process.



Figure 3.5 Oven

3.7 Focusing Lens

The LIBS experiment utilizes a quartz lens (diameter = 8 mm, focal length = 30 mm), as quartz material has maximum transmission at the wavelength of interest. The applied lens is a double convex lens, to minimize spherical aberration, so that maximum energy is directed to the sample surface.

3.8 Target Holder

The sample holder is an important part of the LIBS system. Figure 3.3 shows the pictorial view of the sample holder for our system. It is a 2 dimensional tool to translate the sample along the X and Y coordinates in a horizontal plane. To ensure the sample is clearly visible, the holder was made of an eye protective polymer. This holder is important to ensure that the laser is incident on the smooth sample surface. Under such conditions, visible signals will be generated on the LIBS computer.

3.9 Inductively Coupled Plasma – Mass Spectrometry (ICP-MS)

(ICP-MS) is an analytical tool to determine trace element of different kinds of samples. The main components of an ICP-MS set-up are a detector, interface, spray chamber, plasma torch, and nebulizer. Figure 3.6 shows the set-up of the ICP-MS device. The ICP-MS system works based on the spontaneous photon emission from ions and atoms in the discharge of a radio frequency signal. Gas and liquids are injected into the system directly. Solid sample are digested using nitric acid to form a solution prior to analysis, as solids cannot be directly analyzed. The system converts a sample into an aerosol, and the converted sample links into the plasma central channel. The operational temperature of the inductively coupled plasma in an ideal situation is approximately 10.000 K. This condition

makes the converted sample vaporize quickly. The quick vaporization allows the element of the analyte to be free atoms in the gaseous state. The peristaltic pump transports the liquid sample into nebulizer at ml/min. By the aid of argon gas with a volumetric flow rate of 1 L/min, the sample is converted into a fine aerosol. From the large sample droplet, the fine aerosol droplet (around 2 micrometers in diameter) is separated in the spray chamber. Subsequently, through the injector, the fine droplet is directed from the spray chamber to the plasma torch [36]. The plasma torch generates positively charged ions. Via the interface region, that has a vacuum pressure of 1-2 torr, these ions are transported to the mass spectrometer. From the region of the interface, the ions are extracted, and subsequently exit the ion optics (electrostatic lenses) into the main vacuum chamber. In the mass separation device, the ion optics transport the ion beam and stops neutral species, photon, and particulates to reach the detector. Finally, Ion detector converts the ions into an electrical signal and the data handling systems process the signal conventionally. Lastly, the calibration set for ICPMS converts the signal into the analyte concentration.

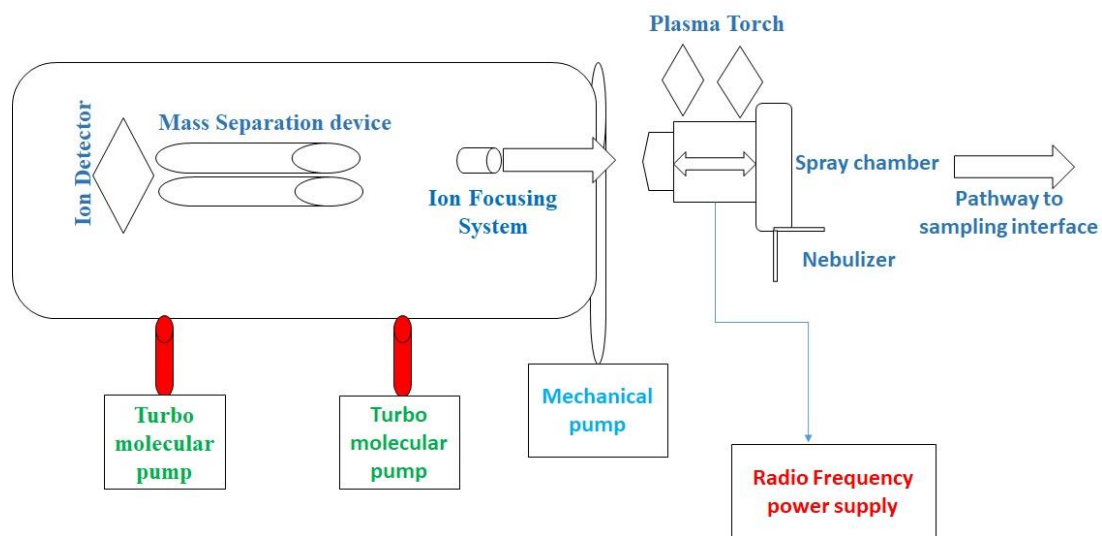


Figure 3.6 The ICPMS Set-Up

3.10 Fish Sample Preparation

Five different fish samples were bought from a hypermart in Dhahran mall, Saudi Arabia. The fish meat was dried in an oven at 60 - 80°C for around 2-3 hours. The dried fish samples were then grinded with a grinding machine a fine powder was attained. Subsequently, By applying a hydraulic pressure of around 6 bars (for dry samples), 2 bars (for wet samples) and 4 bars (for medium condition) around 10 minutes, while placed in a cylindrical dye (2 cm in diameter and of 2 mm thickness), The fish powders were pressed into highly-compacted rigid pellets to withstand the laser pulse. In addition, the pelleting process produces a smooth surface necessary for getting the best signals with minimum noise. Figure 3.7 shows the pictorial view of the pelleting process of the fish muscle powders. In this process, we did not use any type of chemical binder since the powder has its own intrinsic binding strength. The fish pellets were then kept in a clean petri dish to avoid contaminations.

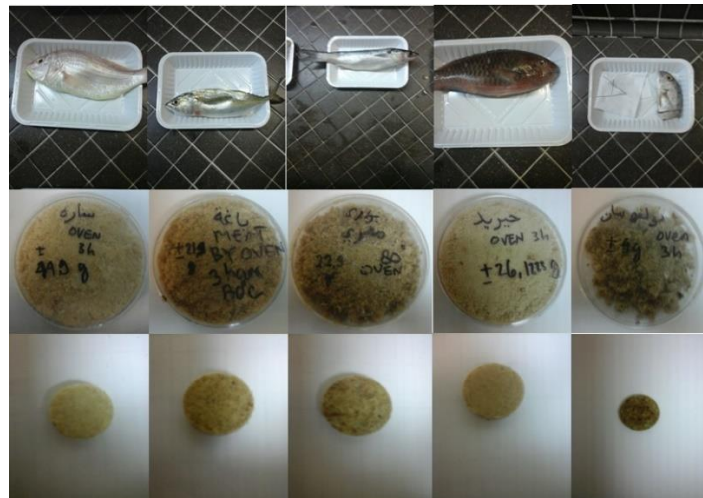


Figure 3.7 Pelletized fish samples, from the right to the left, the sample names are Sarah, Bagoh, Bory, Hered, Bulfusyan

3.11 Preparation of fish samples for ICP (Inductively coupled plasma) analysis

For ICP analysis, the fish samples must be in liquid form by the following standard dilution process,

1. Weigh 0.5 gram of each of the fish samples and put every weighed mass into five free tubes.
2. Add 2 ml distilled water to every tube.
3. Add 10 mL concentrated nitric acid to every tube
4. Add 2 mL Perchloric acid 70 % to every tube
5. Leave the samples overnight.
6. Heat the samples, partially covered, using a hot block at 95 °C for 10 hours, until the volume decreases to 3 mL.
7. Add 2 mL nitric acid to every tube until the total volume reach 5 mL each.
8. Open the partial cover and apply the heating process for 3 hours inside the hot black until the volume reduces into 2 mL.
9. After cooling, top up with distilled water until every tube has 25 mL.
10. The last volume needs to be filtered using filter papers prior to the ICP analysis.

3.10 Preparation Of Standard Samples For Calibration

The goal of this section is to determine the Magnesium, Calcium, Iron, Manganese, and Barium concentration levels in the fish sample 1-5. Calibration standards of different elemental concentrations of Calcium are (a) 50.91 ppm (b) 101.83 ppm (c) 220.63 ppm (d) 412.83 ppm (e) 869.79 ppm. Standards for Manganese are (a) 53.62 ppm (b) 71.63 ppm (c) 312.74 ppm (d) 648.915 ppm (e) 1228.036 ppm and Those for Barium are (a) 13.62 ppm (b) 33.15 ppm (c) 55.2 ppm (d) 82.8 ppm (e) 105.92 ppm. The standard samples were prepared by mixing the sample matrix with 33.33 percent solution of $\text{Ca}(\text{NO}_3)_2 \cdot 4\text{H}_2\text{O}$, $\text{Mn}(\text{NO}_3)_2$, and $\text{C}_4\text{H}_6\text{BaO}_4$ for Calcium, Manganese and Barium respectively. The calibration standards of different elemental concentrations of Magnesium are (a) 60.033 ppm (b) 148.503 ppm (c) 263.831 ppm (d) 420.234 ppm (e) 666.687 ppm and those for Iron are (a) 4.212 ppm (b) 12.55 ppm (c) 18.518 ppm (d) 25.62 ppm and (e) 31.997 ppm. The standard samples were prepared by mixing the sample matrix with 16.67 or 1/6 wt % solution of $\text{Mg}(\text{NO}_3)_2 \cdot 6\text{H}_2\text{O}$ and 0.2849 or 1/351 wt % solution of FeCl_2 for Magnesium and Iron respectively.

The marker wavelengths that we used for constructing the calibration curve are Mg 280.27, Ca II 315.8, Fe I 358.12, Mn I 407.94, and Ba I 778.04 nm. The new sample matrixes were then put into a cylindrical dye of 2 cm diameter and 2 mm thickness to be pelleted using hydraulically pressing machine. The surface of the new standardized samples needs to be smooth to obtain smoothly-superimposed peaks of the element of interest on the background line.



Figure 3.8 The grinder of the LIBS Samples

3.12 Precautions taken during experiment

1. To avoid sample contamination, pestle and mortar should be clean, and to reduce water absorption, these should be dry and isothermal.
2. To ensure that the calibration samples have excellent homogeneity, the powder should be first ground using grinding machine, and ground thoroughly using the pestle and mortar.
3. To avoid contamination, all pellets were stored in an aluminum foil inside a dash.

3.13 LIBS Data Accumulation and Analysis

The built in Andor I-star software in the LIBS computer records and displays the LIBS spectra. All LIBS data spectra are further analyzed using Microsoft Excel and NIST database for qualitative analysis of spectral assignments and quantitative analysis using calibration curves, and using Origin 9.0 for the evaluation of the plasma parameters, which are the stark broadening parameter for electron number density estimation and The Boltzman plot for calculation of the electron temperature.

CHAPTER 4

LIBS Analysis of Arabian Fish Samples

4.1 Introduction

Fish meat contains many trace elements, including toxins and nutrients. At low concentrations, most of the trace elements in fish are beneficial. But in high concentrations, these trace elements are dangerous for human consumption [79].

It has been reported that the beneficial elements present in fish are Zn, Mn, and Fe, and the toxic elements are Pb and Cd [6]. For people living in the Arabian Gulf, fish is a favorite food item. In fact, for all humanity, fish has become a primary source of nutrition and has consequently become a major source of toxic exposure since the fish may contain some toxins and heavy metals. The food regulatory organizations should set proper legislation and act urgently to perform online screening before the fish is commercially sold in the market so that the incidence of heavy metals poisoning can be prevented amongst humans. Some international organizations such as European Commission, FAO, and WHO require the monitoring of toxins and heavy metals such as (Fe, Zn, Pb, Cu, and Cd) and suggest monitoring of other elements (F, Al, J, Cr, Ni, Sb) in water and food [105]. The maximum permissible limit of heavy toxins in fish species is 20; 50; 1; 1; 0.5, and 2 ppm for Cu, Zn, As, Hg, Cd, Pb [31], and maximum permissible limit of heavy metals is 100 [23], 0.5, and 0.3 ppm [3] for Fe, Mn and Ba respectively.

The main source of toxins in the fish of the Arabian Gulf marine environment is environmental pollution, coming from the petrochemical refineries, industries and wastes. The marine environment has been contaminated with oil spill previously. During 1991, the oil spill contributed to heavy metal contamination in Kuwait, wherein it was reported that the levels of Cu and Zn increased very significantly [17].

Atomic absorption spectroscopy (AES) [79] and Inductively Coupled Plasma Mass Spectrophotometry[62] are frequently used to qualitatively and quantitatively determine the elements present in the fish samples. In this study, we utilized the UV Pulsed LIBS technique to detect nutritious elements like Calcium and Magnesium and heavy metals, especially Iron, Manganese and Barium.

4.2 LIBS Signal Intensity Optimization

Figure 4.1 shows the dependence of the LIBS signal intensity on the time delay between the laser pulse and the intensified charged coupled device (ICCD) Camera that records the LIBS signal. From the figure, we can observe that at time delay of 25 ns, the plasma starts to heat up with the result that the signal intensity becomes more and more increasing from initial intensity (20600) to the optimum intensity (290000) at the time delay of 125 ns. After this peak, the intensity becomes more and more decreasing to lower intensity until 12779 a.u. at the time delay 150 ns because of the cooling down of the plasma. Therefore, we found that the most optimal signal intensity is at 125 ns for the detection of Calcium Ca II 315.8 with the maximum intensity of 290000 a.u. This optimum time delay is applicable to scan all spectra ranging from 200 - 800 nm, depicted in Figure 4.7 until Figure 4.35

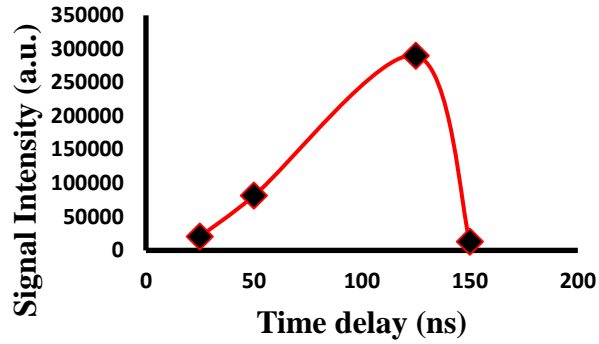


Figure 4.1 Dependence of the LIBS intensity on time delay

The study of energy dependence was observed to find the best signal at the center wavelength of 315 nm, which can show Iron (Fe I 298.357 nm), Carbon (C II 299.2618 nm), and Calcium (315.8 nm). The pulse energy range is from 30 to 47.7 mJ. Figure 4.2 shows that the LIBS Signal intensity is also proportional to the laser energy. The higher the incident laser energy is, the higher the LIBS intensity will be. The LIBS experiment was done using the Optimum energy, around 47.7-50 mJ.

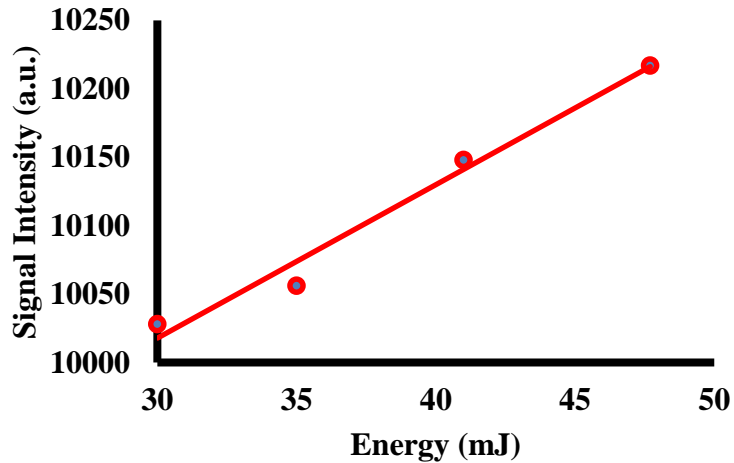


Figure 4.2 Dependence of the LIBS intensity on incident laser energy

4.3 The Plasma Parameter Analysis

To accurately quantify the elements, the plasma must be optically thin and in Local thermodynamic equilibrium (LTE). The analyzed sample has the same elemental composition with the thin plasma. In a laser ablation plasma, the LTE condition applies if the collision processes of the electron-atoms and electron-ion are rapid and prevail the radiative process. By the following physical laws, the laser ablation plasma can be explained. The distribution of Maxwellian velocity explains the plasma particle, the statistics of Boltzmann explain the energy level population, the Saha's equation explains the ionization process, and the plank's law explains the intensity of radiation. The LTE is not a good assumption along the fast-moving plasma boundary, which has a low electron density [26][43][57]. LTE requirements stipulate that equilibrium occurs over a small region in space, even though the equilibrium is different from one region to another [26]. The LTE Condition is valid if the region is slightly deeper into the volume of the plasma with the reason that the collisions occur more rapidly and the conditions could change more slowly. To make sure that LTE condition applies, the collision processes in the population level must be dominant. This is the reason why there must be a sufficiently high enough density of electron. The formulation of this condition was given by equation (7), the McWhirter Criterion, explained in section 1.2.8 Plasma Study as an Ionization process. To make sure that the plasma reaches the LTE conditions, the stark broadening in equation (16) and the Boltzmann's plot method applying equation (14) were used to calculate the electron number density and the plasma temperature respectively.

Some essential criteria to obtain a good Boltzmann Plot are well spaced upper level, accurate transition probabilities and line intensities [91][20]. To get the Boltzmann plot in Figure 4.4, giving electron temperature of $T = 14137.55 \pm 3448.289$ K, different Calcium wavelengths were chosen based on Figure 4.3 and listed in table 4.1.

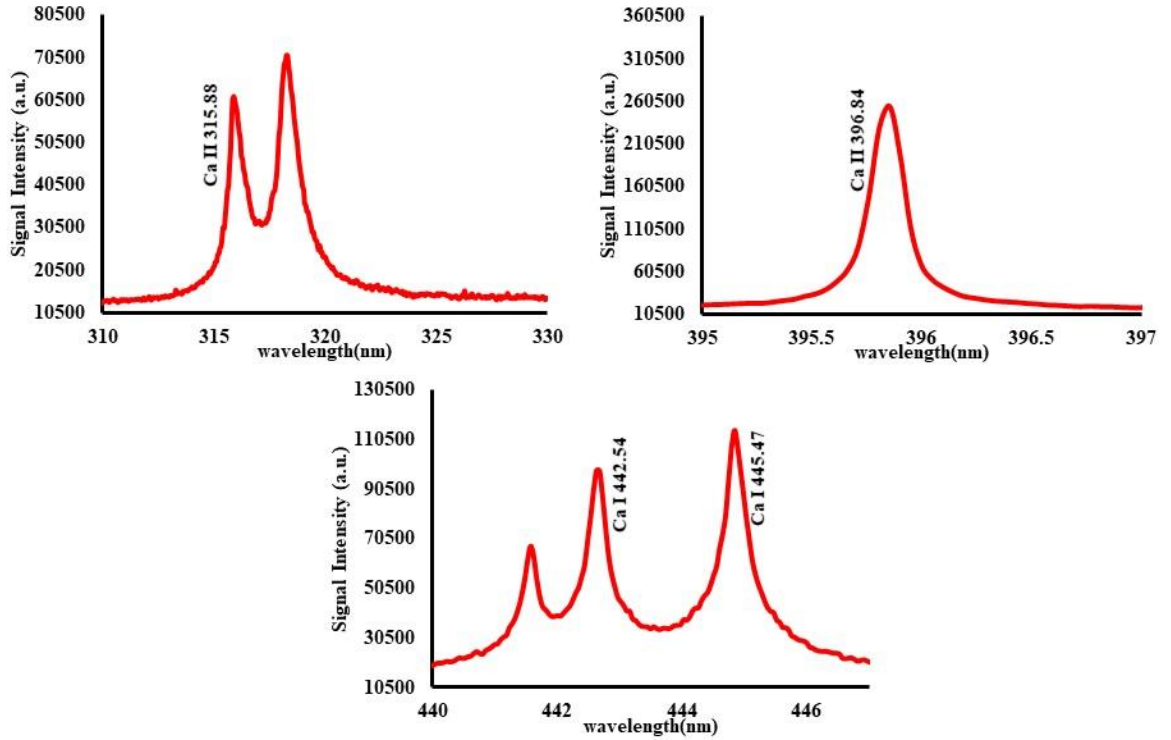


Figure 4.3 LIBS spectra of Calcium lines selected for Boltzman plot for calculation of plasma temperature

Table 4.1 Selected wavelengths for characteristic atomic transition lines of calcium and other parameter for Boltzman plot

Element	Fingerprint		$A_{ik} \times 10^8 (s^{-1})$	$E_k (eV)$	Optical Transition Assignment	LIBS signal Intensity(arb.units)
	Wavelength (nm)	g_k			Lower State \rightarrow Higher State	
Ca II	315.88	4	3.1	7.04	$3p^6 4p \ ^2P_{1/2}^o \rightarrow 3p^6 4d \ ^2D_{3/2}$	61390
Ca II	396.84	2	1.4	3.12	$3p^6 4s \ ^2S_{1/2} \rightarrow 3p^6 4p \ ^2P_{1/2}^o$	254648
Ca I	442.54	3	0.498	4.68	$3p^6 4s 4p \ ^3P_0^o \rightarrow 3p^6 4s 4d \ ^3D_1$	97918
Ca I	445.47	7	0.87	4.68	$3p^6 4s 4p \ ^3P_2^o \rightarrow 3p^6 4s 4d \ ^3D_3$	114010

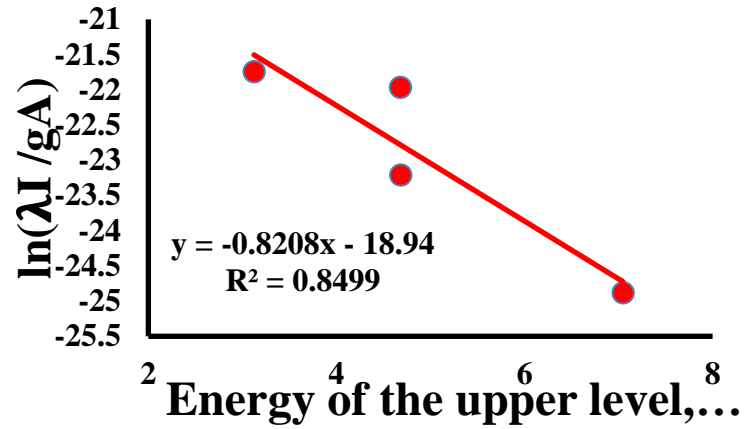


Figure 4.4 Boltzman plot to calculate the plasma temperature

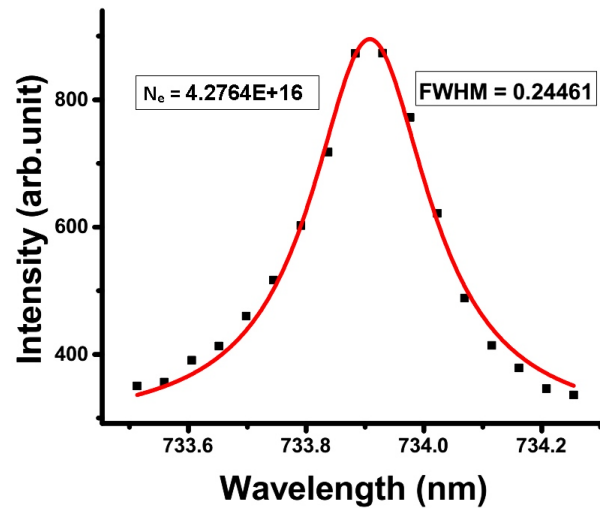


Figure 4.5 Stark broadening profile of Ca I 732.61 for estimation of electron density

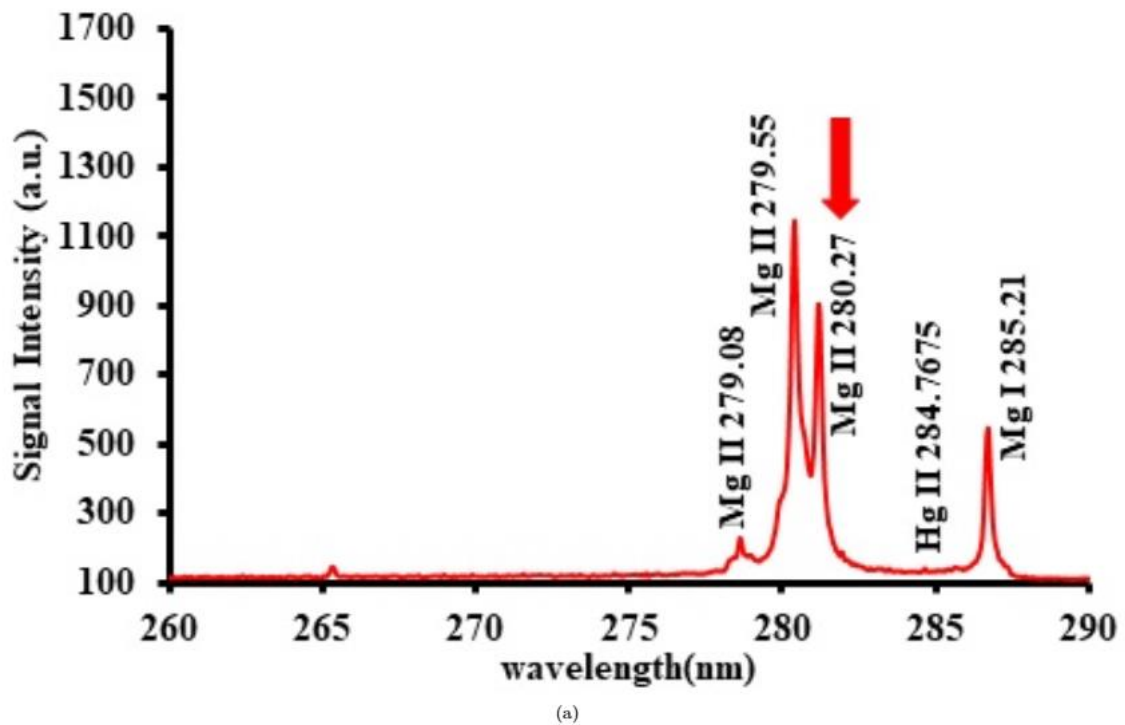
The electron impact parameter, w is from the reference [68]. Using the reduced stark broadening equation, the experimental electron number density N_e was found to be 4.2764×10^{16} which is much higher than the critical n_e , 1.1493×10^{16} . This result explains that the Mc whirter criterion holds. Since the experimental $N_e > 10^{16}$ and $kT = 1.218 \text{ eV} < 5 \text{ eV}$ then the Electron energy distribution function (EEDF) criterion also holds. The two criteria prove that plasma is optically thin and in Local thermodynamic equilibrium.

4.4 Elemental Detection and calibration curves

We purchased 5 different varieties of fish samples (Figure 3.7, Sarah, Bagoh, Bory, Hered, and Bulfusyan). The scan for elemental detection was in the range of **260 - 830 nm**. In the whole range, the developed LIBS system mainly detected and quantified nutrients like (Calcium and Magnesium) and heavy metals like (Iron, manganese, and Barium). Along with the mainly detected elements, we also found Phosphorus, Silicon, Sodium, Chlorine, Copper, Bromine, and Mercury.

In the range of **260-290 nm**, depicted in Figure 4.6 until Figure 4.8, we found the laser line (266 nm), 1 neutral line and 3 singly ionized lines of Magnesium. The existence of four Magnesium lines is, as a result, of high enough laser energy, having the 266 nm laser wavelength. This energy is high enough to create the multiphoton ionization process in such a way that the LIBS system were able to record the emission of 3 ionic transition for singly ionized wavelengths of Mg II 279.08 nm $\{2p^63p^2P^{\circ}_{1/2} \rightarrow 2p^63d^2D_{3/2}\}$, Mg II 279.55 nm $\{2p^63s^2S_{1/2} \rightarrow 2p^63p^2P^{\circ}_{3/2}\}$ and Mg II 280.27 nm $\{2p^63s^2S_{1/2} \rightarrow 2p^63p^2P^{\circ}_{1/2}\}$, and 1 atomic transition for 1 neutral wavelength of Mg I 285.21 nm $\{2p^63s^1S_0 \rightarrow 3s3p^1P^{\circ}_1\}$, having well known probability of transition. The Magnesium detection in all samples relies on the persistent line of Mg II (280.27 nm) as a fingerprint wavelength. The proof of magnesium detection, relying on this wavelength is that after adding different linearly known concentration of $Mg(NO_3)_2 \cdot 6H_2O$ into a set of standard samples, the chosen fingerprint wavelength, depicted in Figure 4.9 grows linearly. At the wavelength of Mg II (280.27 nm), All samples in Figure 4.6 until Figure 4.8 also have different intensities, indicating different magnesium concentration. Between the two magnesium lines (Mg II 280.27 and Mg I 285.21), we also detected mercury line that has fingerprint wavelength of

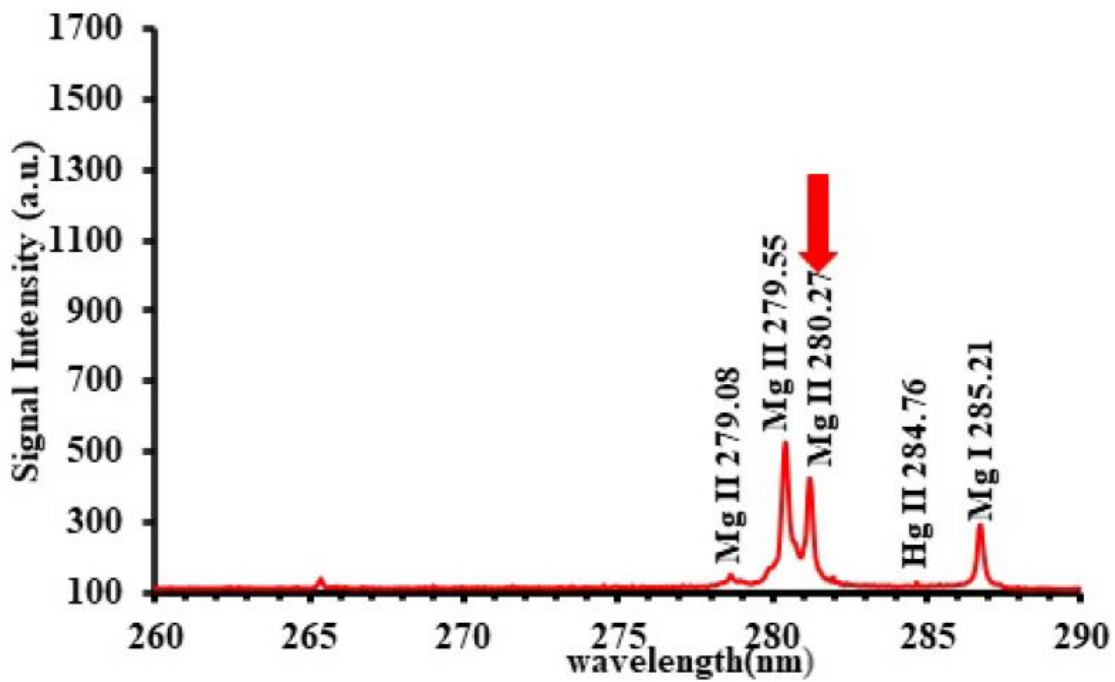
284.76 nm. Refer to the figures, the mercury intensity follows the following order: Sarah < Hered < Bagoh < Bulfusyan < Bory misr. This means that based on the contents of Mercury, Bory Misr is the most harmful fish of the 5 samples that we analyze in our laboratory.



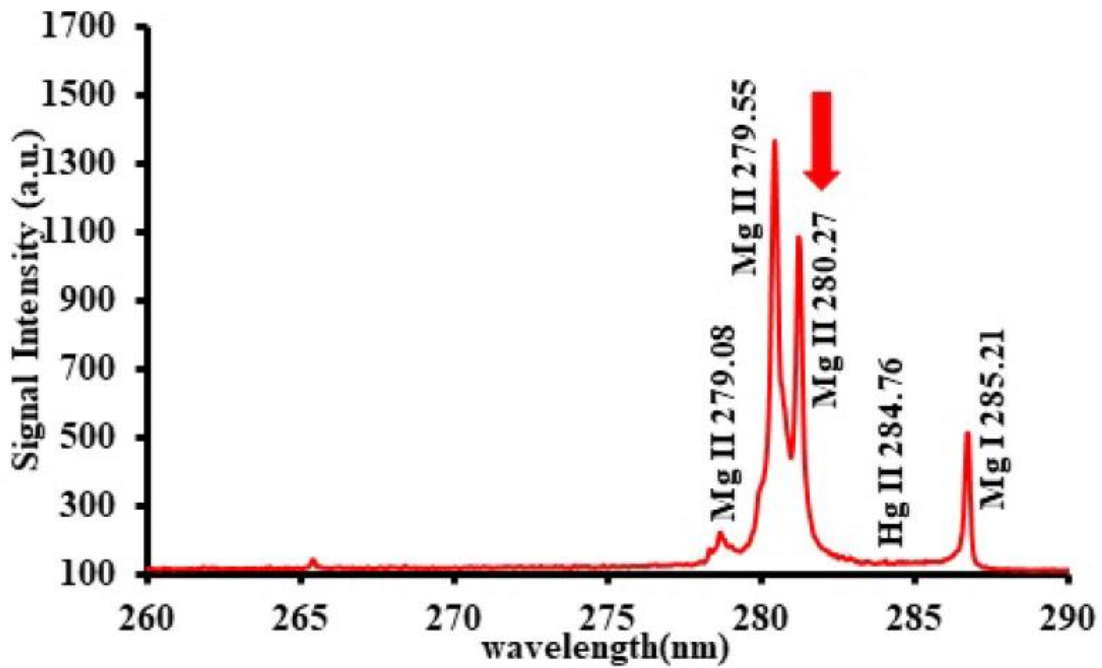
© Lutfi Mulyadi Surachman 2018

Figure 4.6 Typical LIBS Spectrum indicating persistent Mg lines in 260-290 nm region for (a) Bulfusyan fish at 280.27 nm

MAGNESIUM AND MERCURY DETECTION



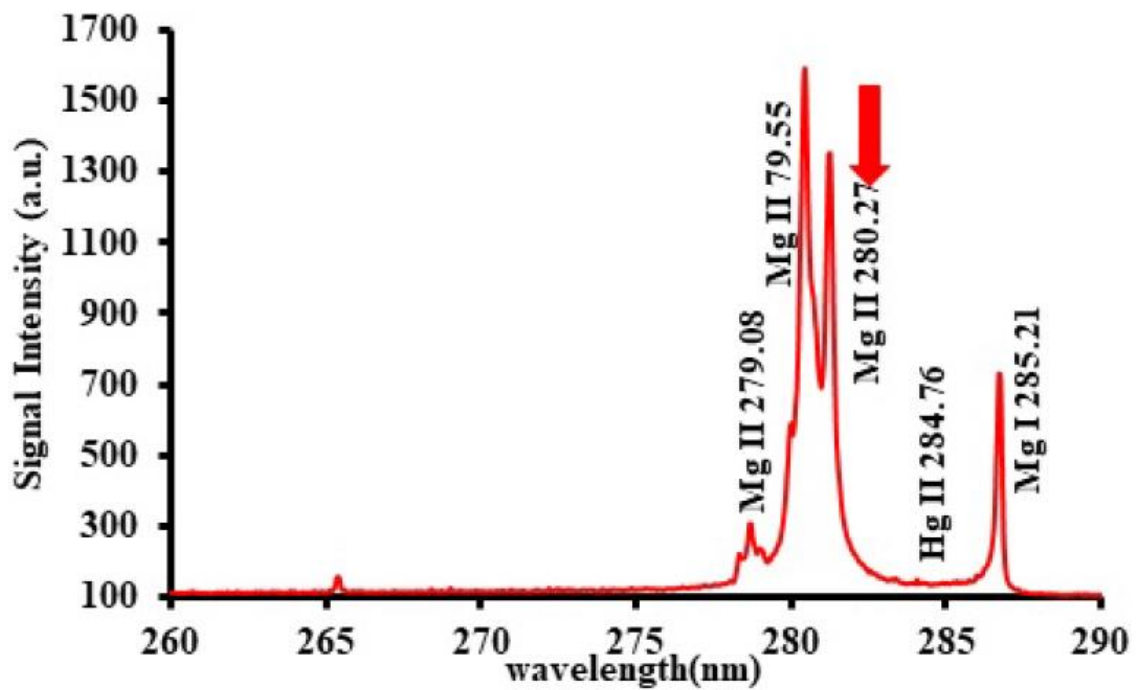
(a)



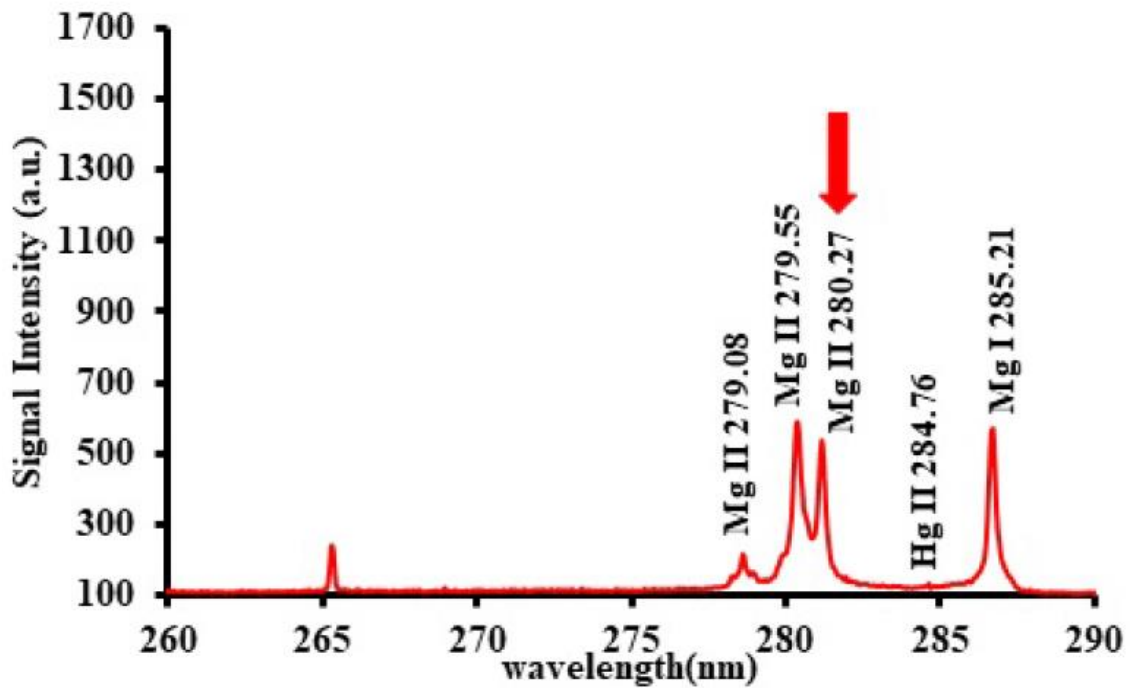
(b)

© Lutfi Mulyadi Surachman 2018

Figure 4.7 Typical LIBS Spectrum indicating persistent Mg lines in 260-290 nm region for (a) Sarah fish and (b) Bagoh fish at 280.27 nm



(a)

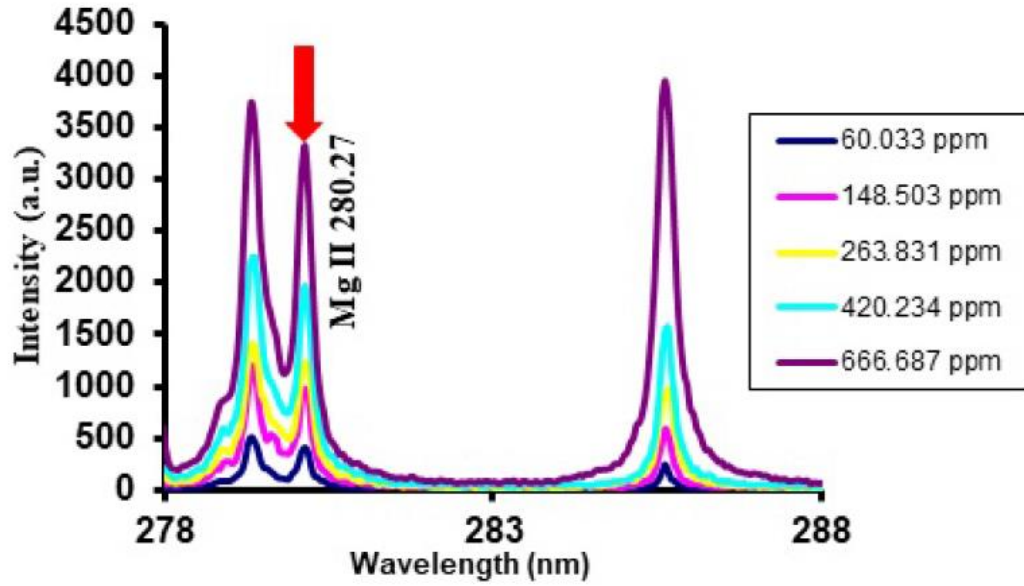


(b)

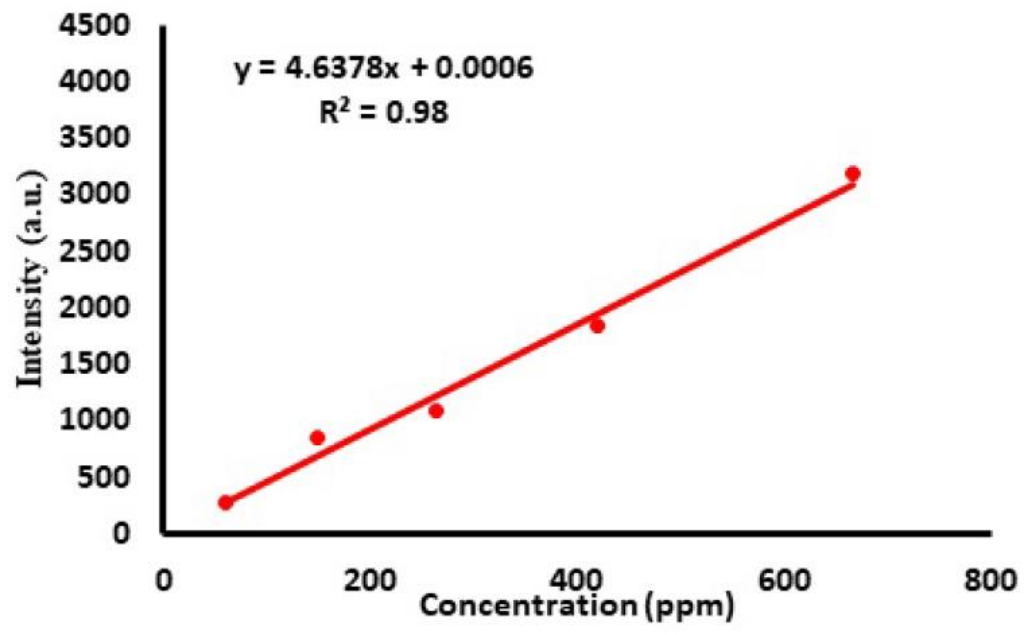
© Lutfi Mulyadi Surachman 2018

Figure 4.8 Typical LIBS Spectrum indicating persistent Mg lines in 260-290 nm region for (a) Bory fish and (b) Hered fish at 280.27 nm

MAGNESIUM CALIBRATION CURVES



(a)

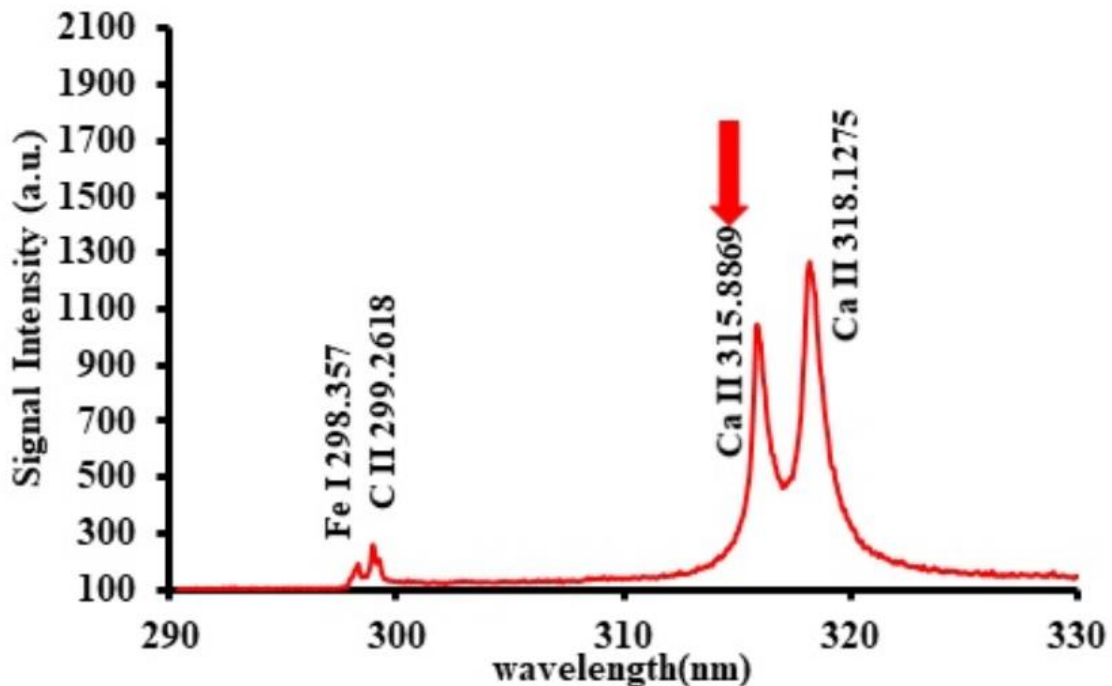


(b)

© Lutfi Mulyadi Surachman 2018

Figure 4.9 Calibration curve for detection of Magnesium

The same analysis can be applied to explain the contents of Ca, and the main heavy metals (Fe, Mn, Ba). Figure 4.10 until Figure 4.12 depict LIBS spectra of the fish samples in the range of **290-330 nm**. In this range, Calcium identification in all samples relies on the persistent line of **Ca II 315.88 nm** { $3p^64p^2P^o_{1/2} \rightarrow 3p^64d^2D_{3/2}$ } as a fingerprint wavelength. The proof of calcium detection, relying on this wavelength is that after adding different linearly known concentration of $\text{Ca}(\text{NO}_3)_2 \cdot 4\text{H}_2\text{O}$ into a set of standard samples, the chosen fingerprint wavelength, depicted in Figure 4.13 grows linearly. The fish samples in Figure 4.10 until Figure 4.12 also have different fingerprint wavelength intensities, indicating different calcium concentration. In the same range, we also found atomic emission of Iron, Fe I 298.35 nm and ionic emission of Carbon, C II 299.26 nm and Calcium, Ca II 318.12 nm.

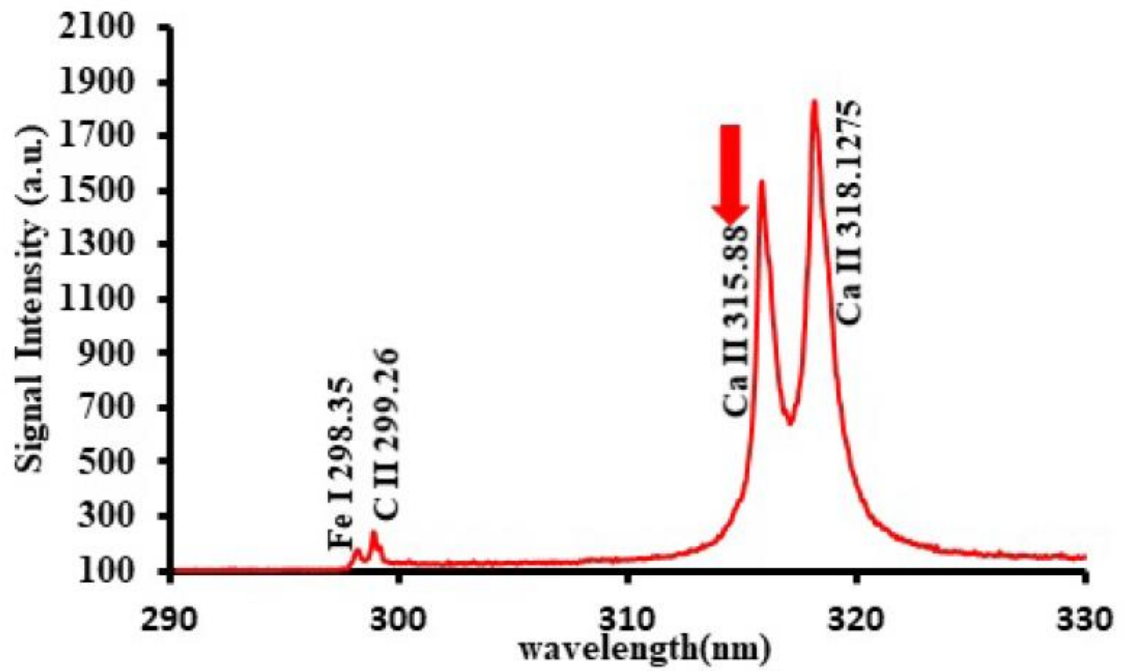


(a)

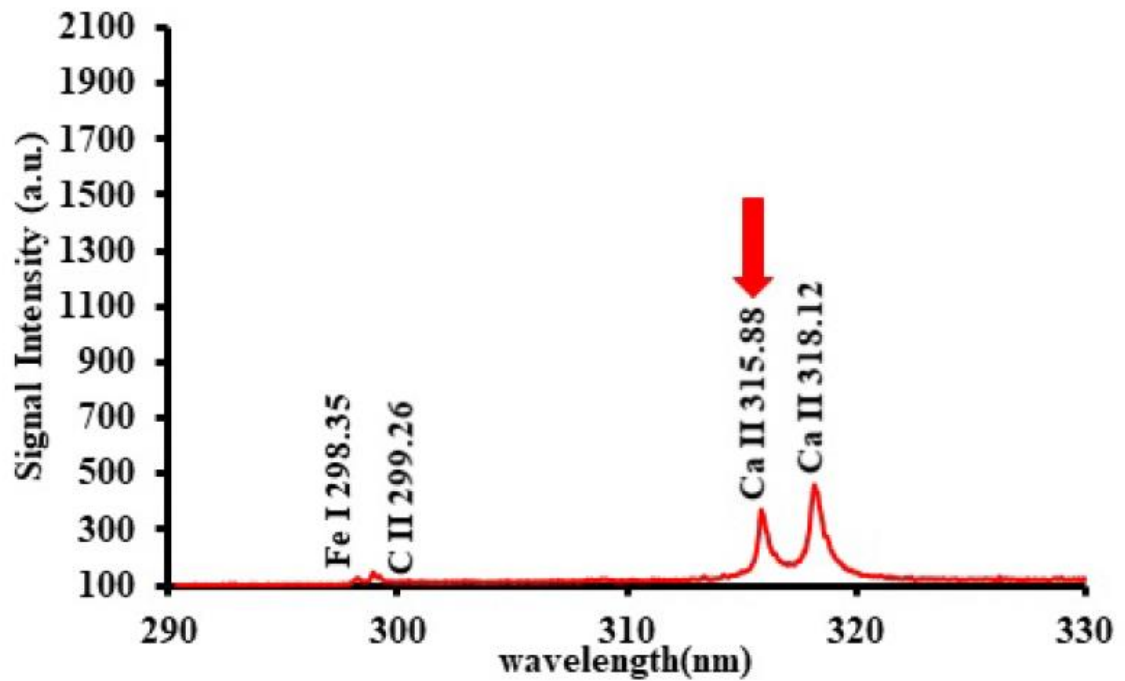
© Lutfi Mulyadi Surachman 2018

Figure 4.10 Typical LIBS Spectrum indicating persistent Ca lines in 290-330 nm region for (a) Bulfusyan fish at 315.8 nm

CALCIUM DETECTION



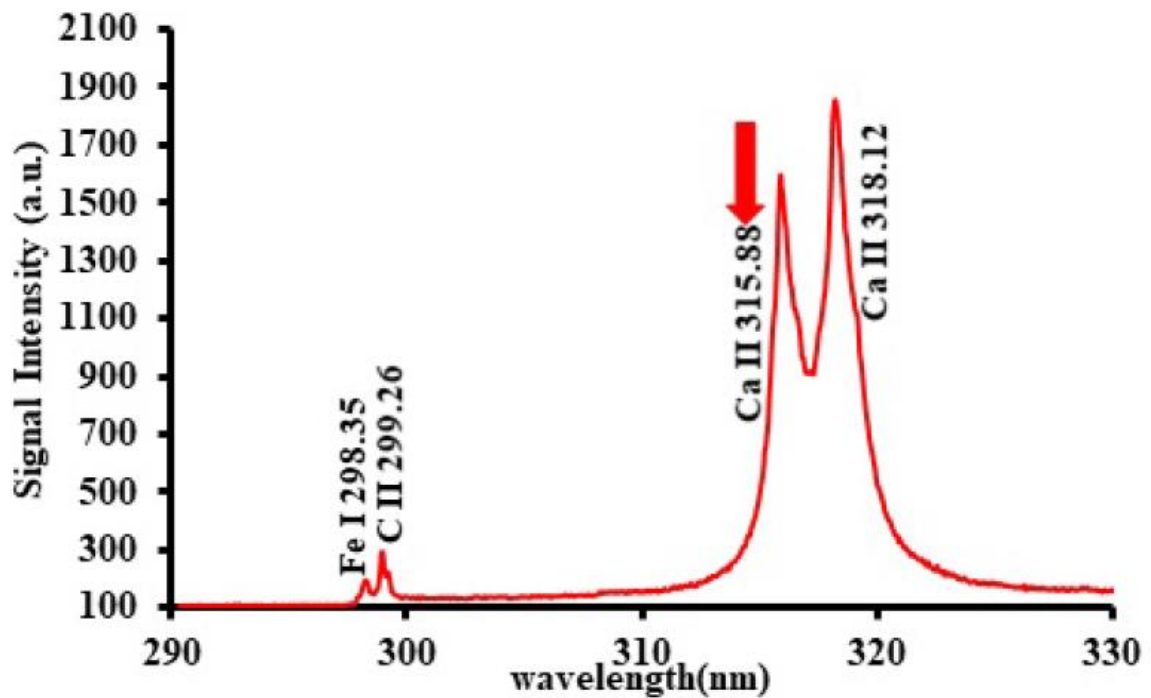
(a)



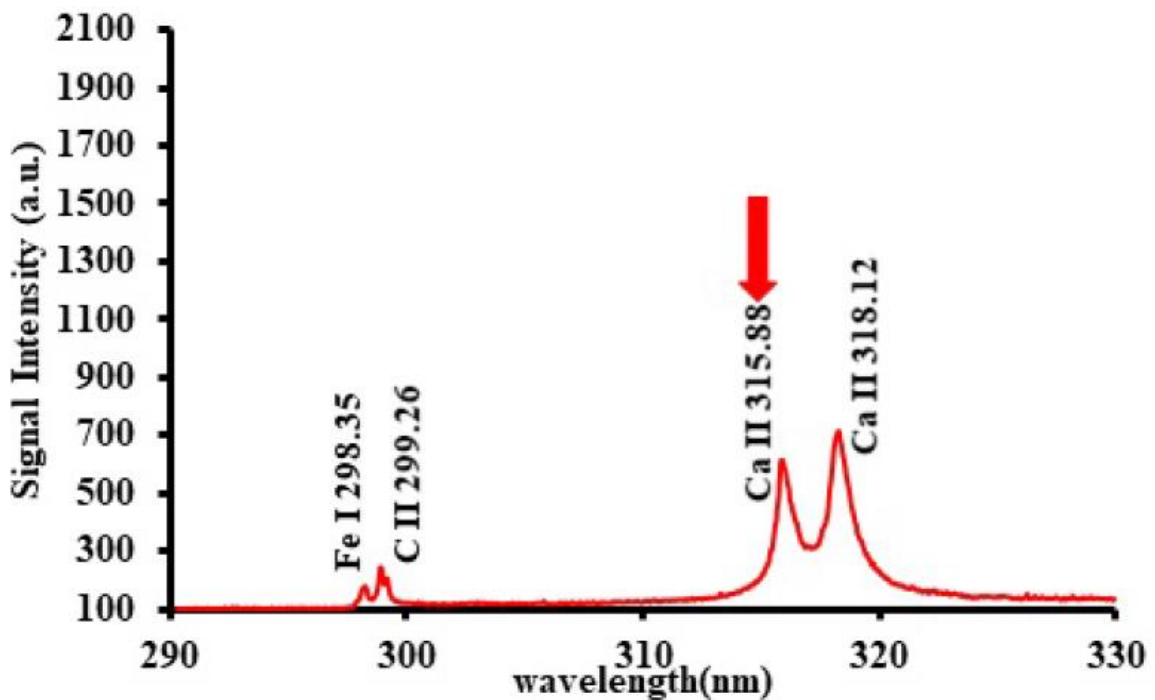
(b)

© Lutfi Mulyadi Surachman 2018

Figure 4.11 Typical LIBS Spectrum indicating persistent Ca lines in 290-330 nm region for (a) Sarah fish and (b) Bagoh fish at 315.8 nm



(a)

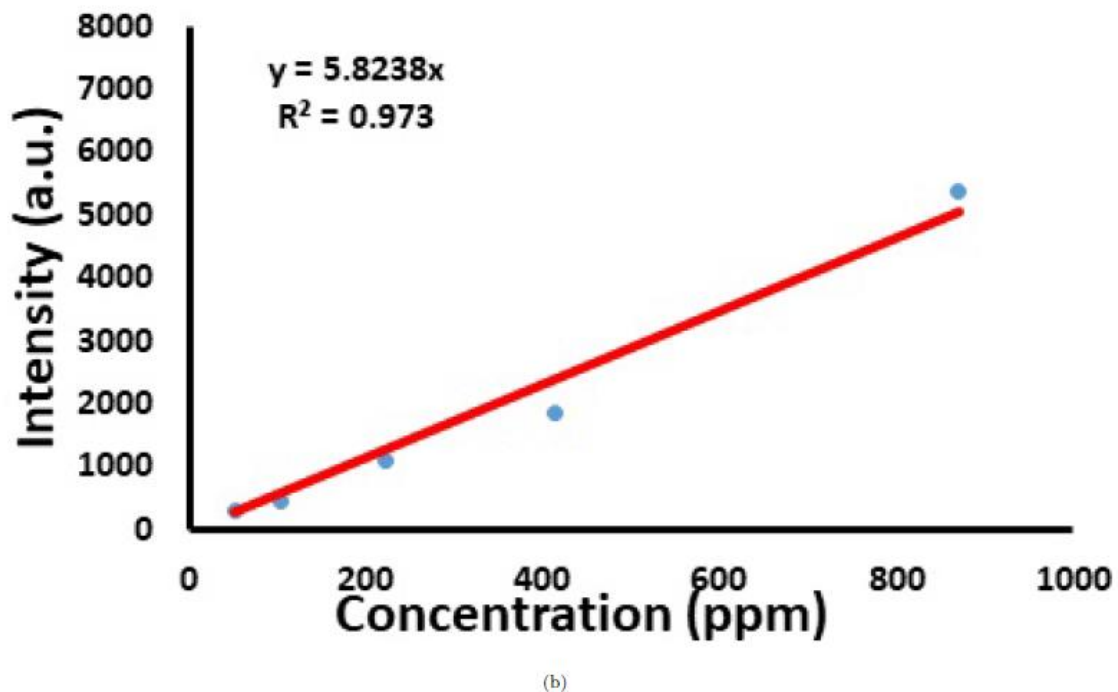
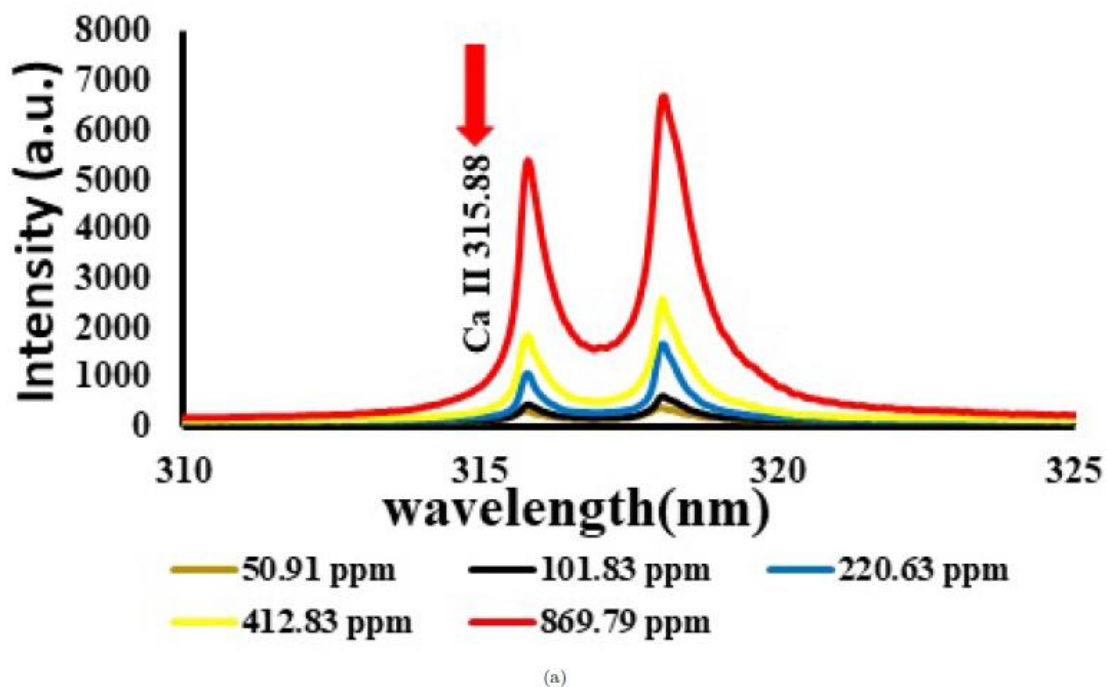


(b)

© Lutfi Mulyadi Surachman 2018

Figure 4.12 Typical LIBS Spectrum indicating persistent Ca lines in 290-330 nm region for (a) Bory fish and (b) Hered fish at 315.8 nm

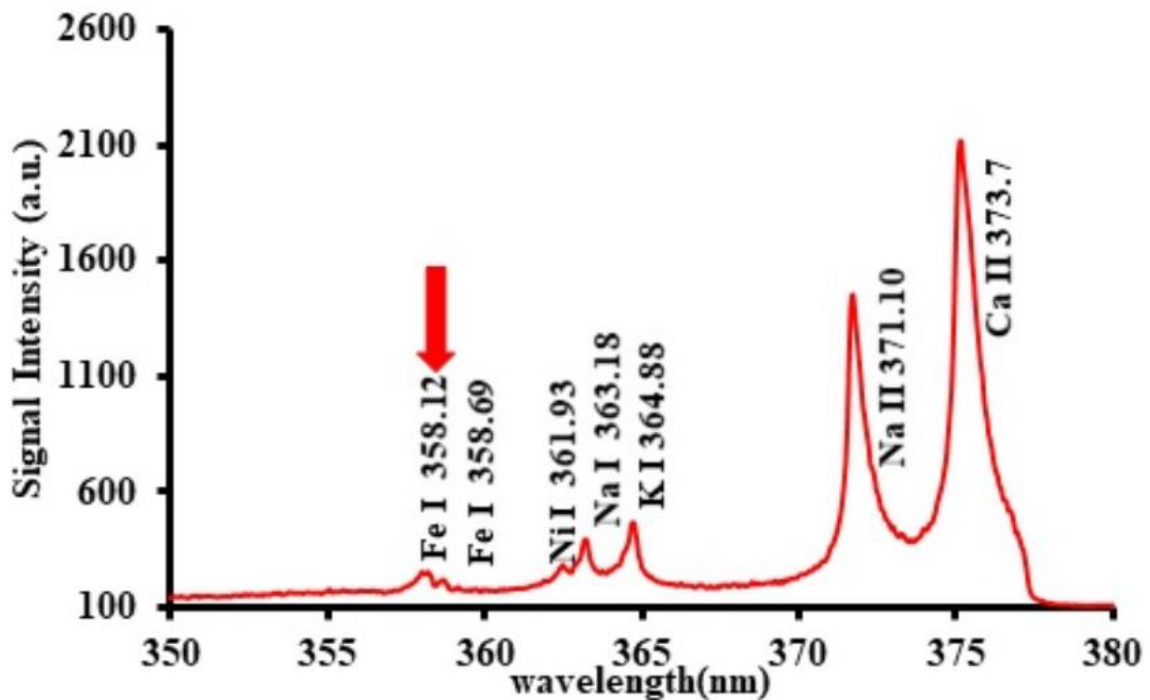
CALCIUM CALIBRATION CURVES



© Lutfi Mulyadi Surachman 2018

Figure 4.13 Calibration curve for detection of Calcium

Figure 4.14 until Figure 4.16 show the spectra of the five fish samples in the range of 350-380 nm. In this range, Iron identification in all samples relies on the persistent line of Fe II 358.12 nm $\{3d^7(^4F)4s\ a^5F_5 \rightarrow 3d^7(^4F)4p\ z^5G^o_6\}$ as a fingerprint wavelength. The proof of iron detection, relying on this wavelength is that after adding different linearly known concentration of FeCl₂ into a set of standard samples, the chosen fingerprint wavelength, depicted in Figure 4.17 grows linearly. The fish samples in Figure 4.14 until Figure 4.16 also have different fingerprint wavelength intensities, indicating different iron concentration. In the same range, we also found atomic emission of Nickel (Ni I 381.93 nm), Sodium (Na I 363.18 nm), Potassium (K I 364.88 nm) and ionic emission of Sodium (Na II 371.10 nm) and (Calcium, Ca II 373.7 nm).

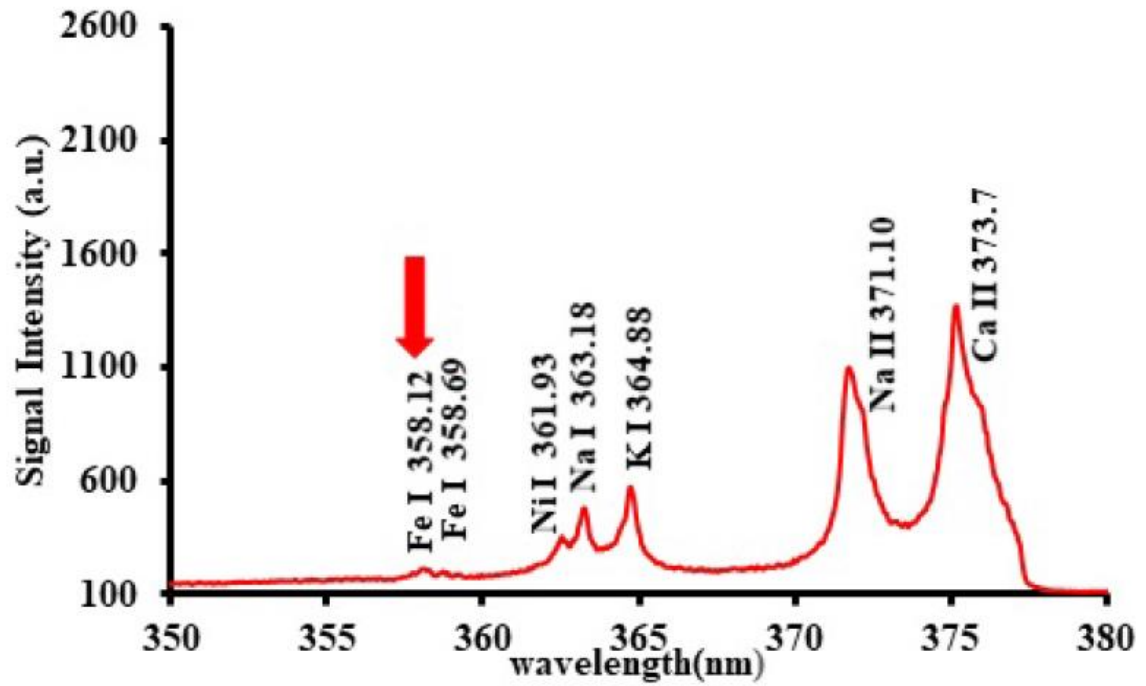


(a)

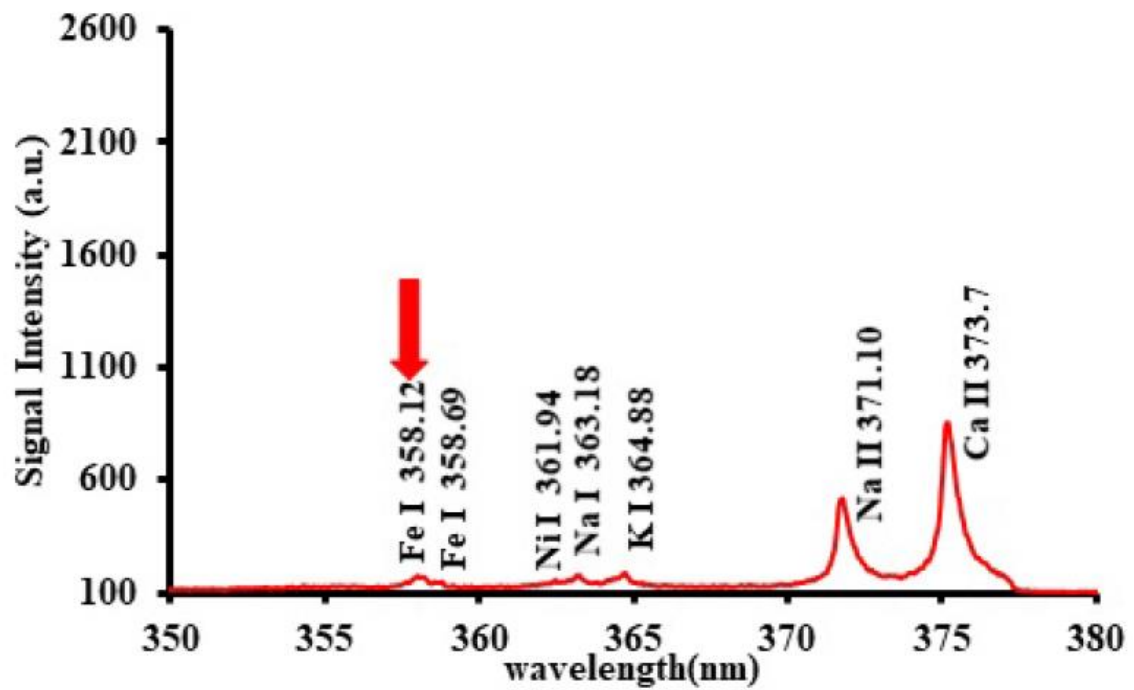
© Lutfi Mulyadi Surachman 2018

Figure 4.14 Typical LIBS Spectrum indicating persistent Fe line in 350-380 nm region for (a) Bulfusyan fish at 358.12 nm

IRON DETECTION



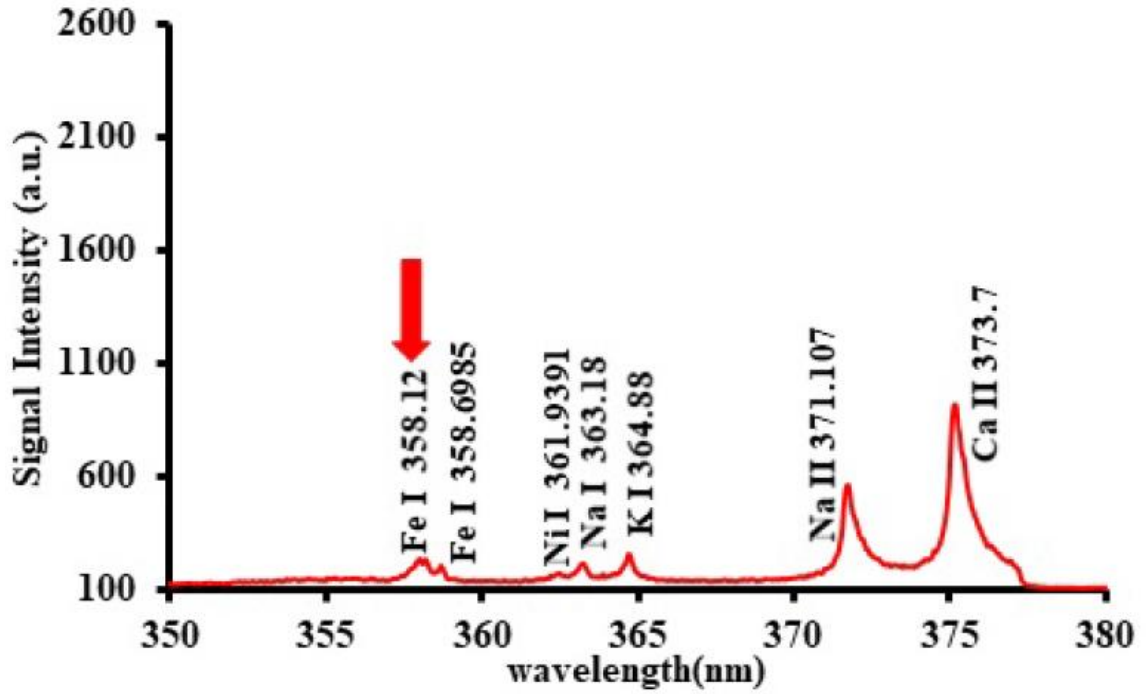
(a)



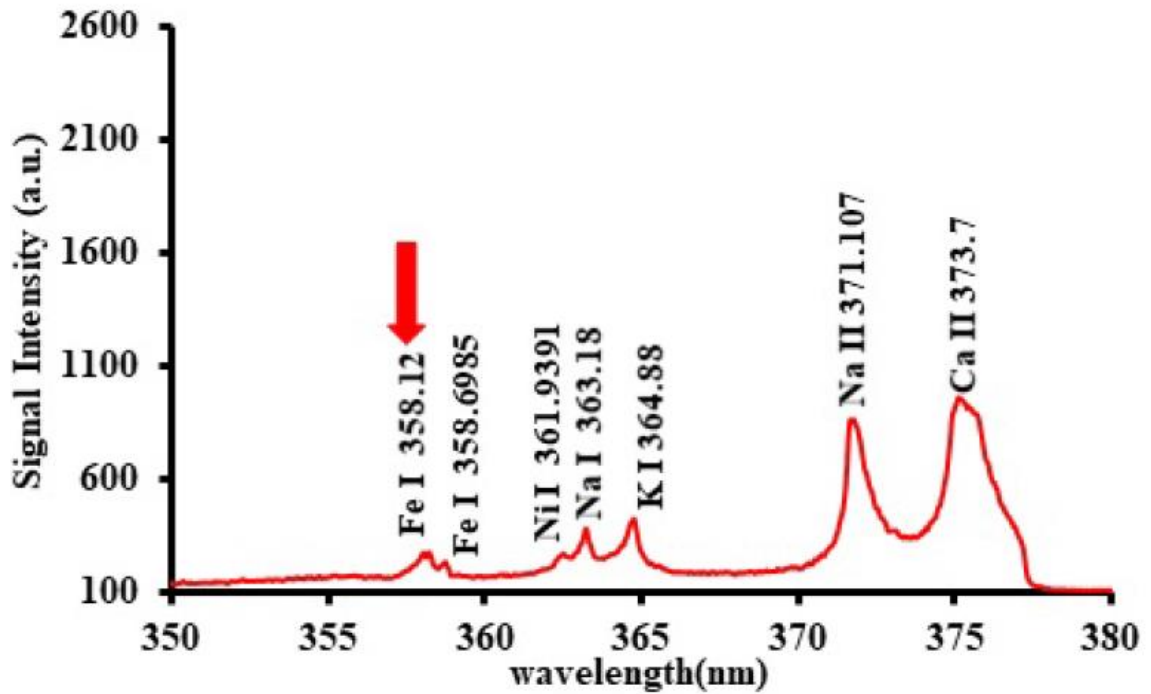
(b)

© Lutfi Mulyadi Surachman 2018

Figure 4.15 Typical LIBS Spectrum indicating persistent Fe line in 350-380 nm region for (a) Sarah fish and (b) Bagoh Fish at 358.12 nm



(a)

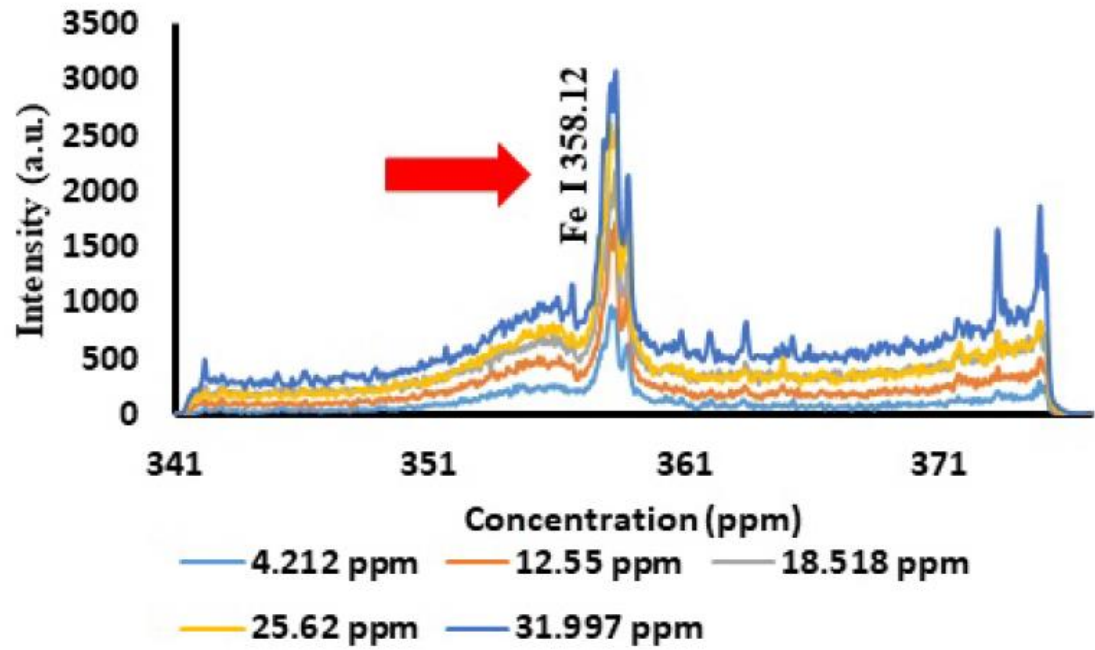


(b)

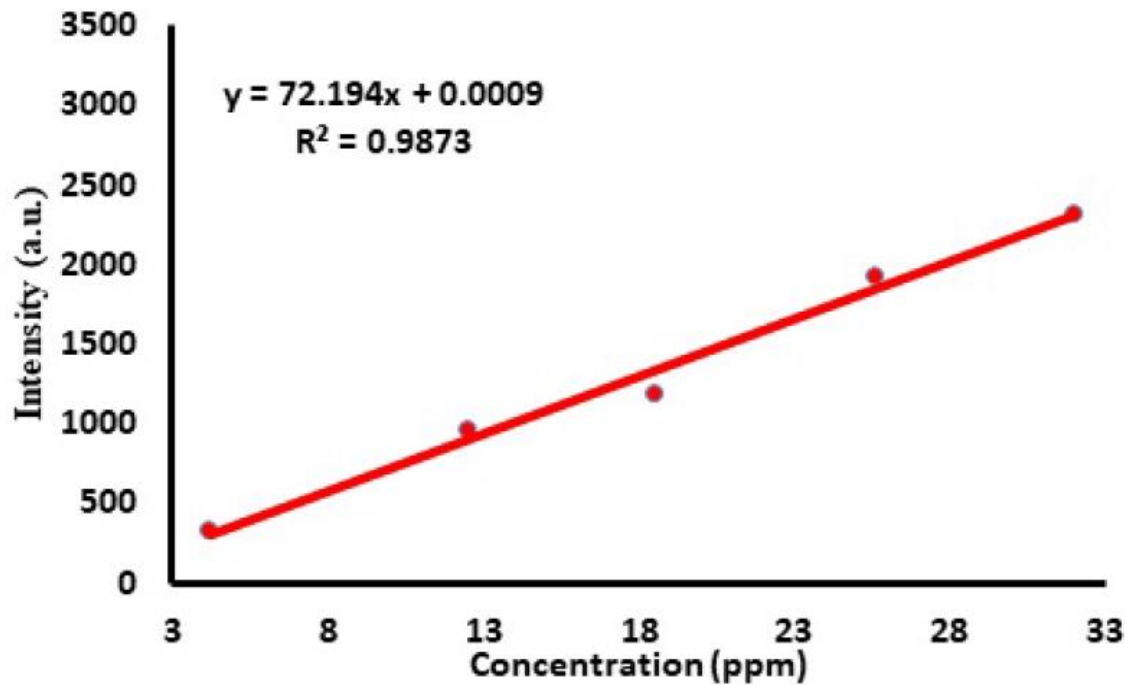
© Lutfi Mulyadi Surachman 2018

Figure 4.16 Typical LIBS Spectrum indicating persistent Fe line in 350-380 nm region for (a) Bory fish and (b) Hered Fish at 358.12 nm

IRON CALIBRATION CURVES



(a)

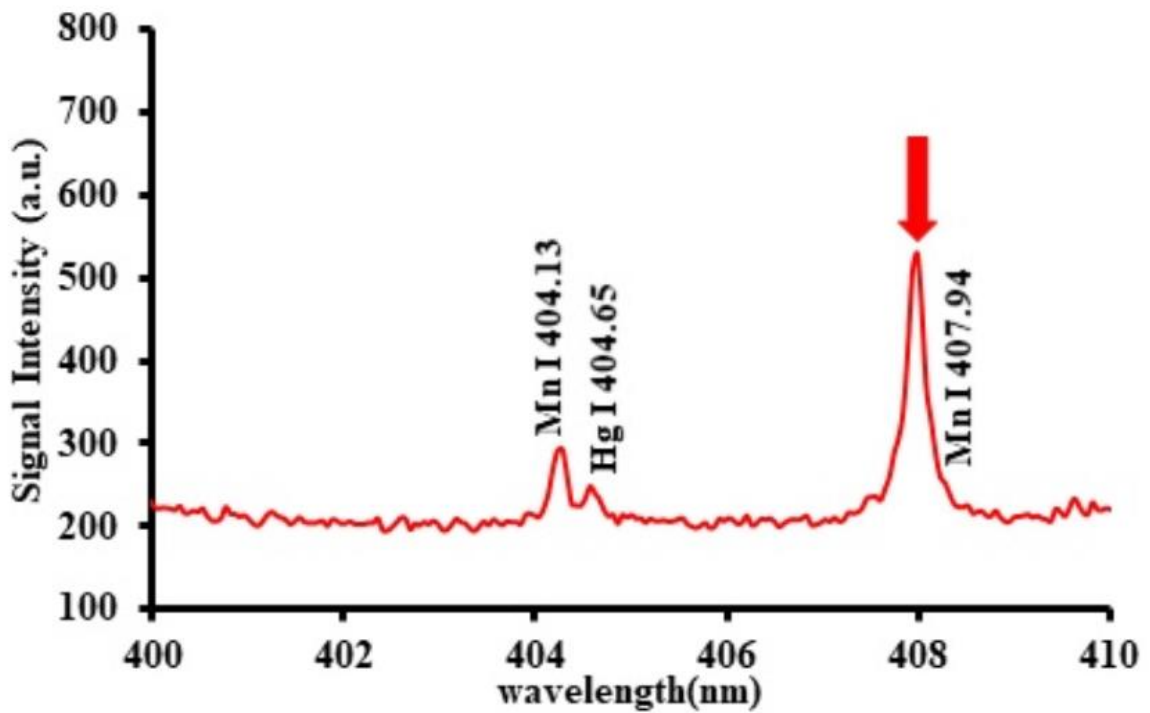


(b)

© Lutfi Mulyadi Surachman 2018

Figure 4.17 Calibration curve for detection of Iron

Figure 4.18 until Figure 4.20 show the spectra of the five fish samples in the range of 400 - 410 nm. In this range, Manganese identification in all samples relies on the strong line of atomic emission of Mn I 407.94 nm $\{3d^6(^5D)4s\ a^6D_{1/2} \rightarrow 3d^6(^5D)4p\ z^6D^{\circ}_{3/2}\}$ as a fingerprint wavelength. The proof of manganese detection, relying on this wavelength is that after adding different linearly known concentration of $Mn(NO_3)_2$ into a set of standard samples, the chosen fingerprint wavelength, depicted in Figure 4.21 grows linearly. The fish samples in the Figure 4.18 until Figure 4.20 also have different fingerprint wavelength intensities, indicating different manganese concentration. In the same range, we also found atomic emission of another Manganese (Mn I 404.13 nm) and Mercury (Hg I 404.65 nm).

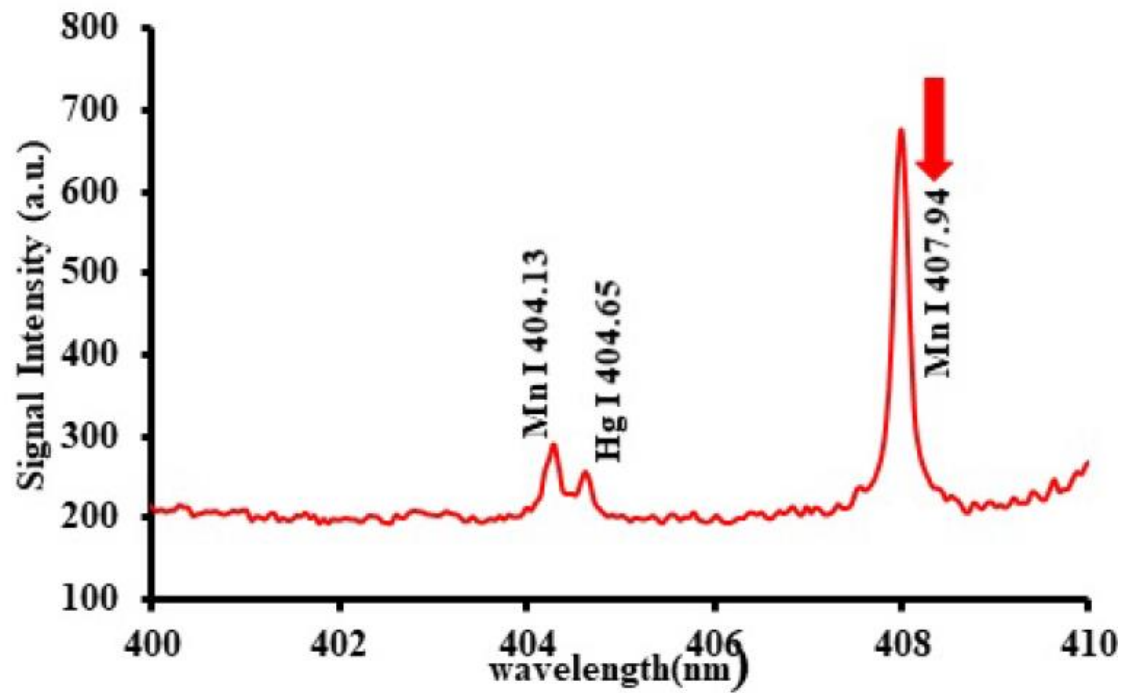


(a)

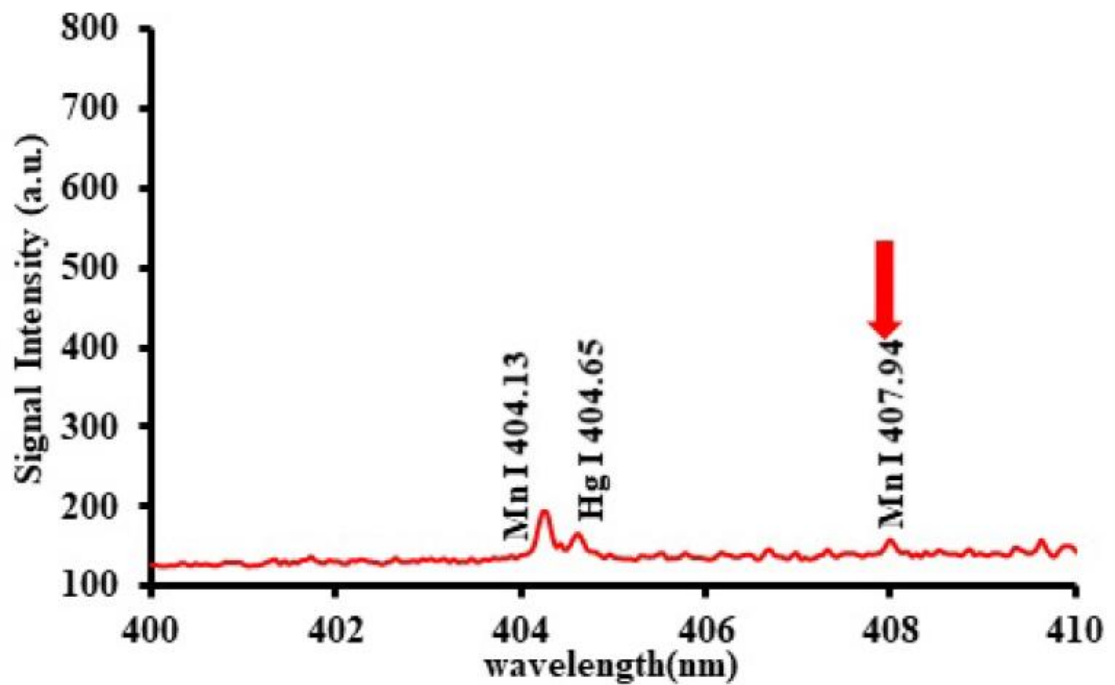
© Lutfi Mulyadi Surachman 2018

Figure 4.18 Typical LIBS Spectrum indicating strong Mn line in 400-410 nm region for (a) Bulfusyan fish at 407.94 nm

MANGANESE DETECTION



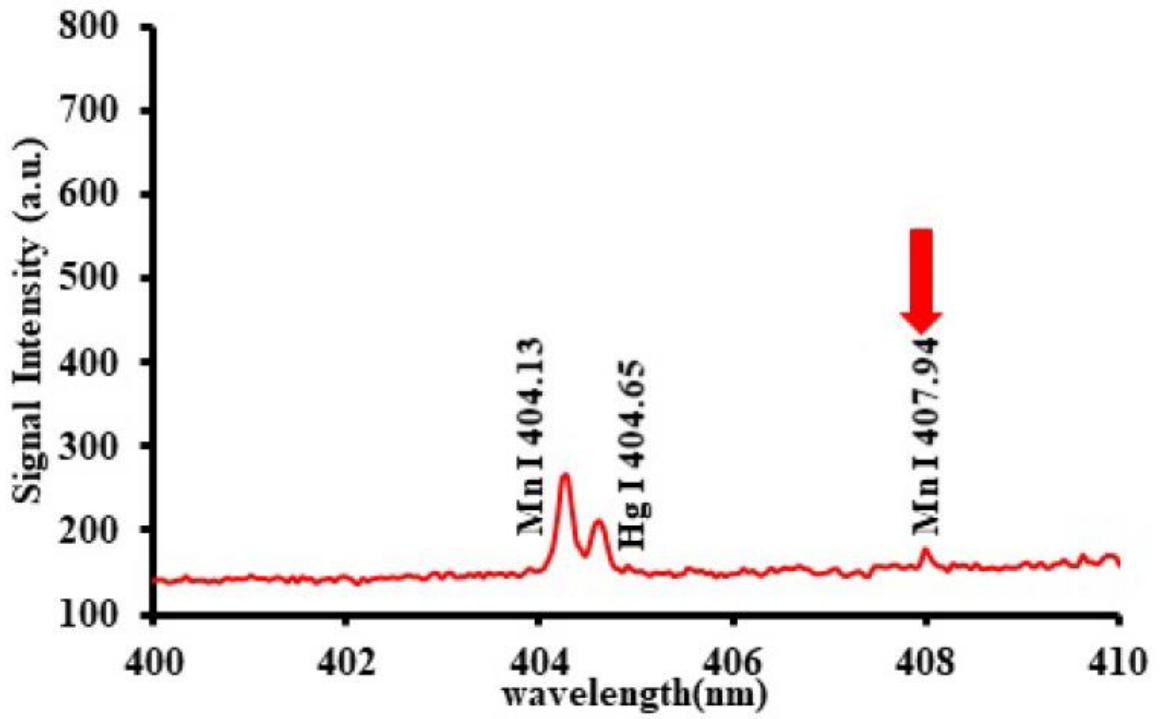
(a)



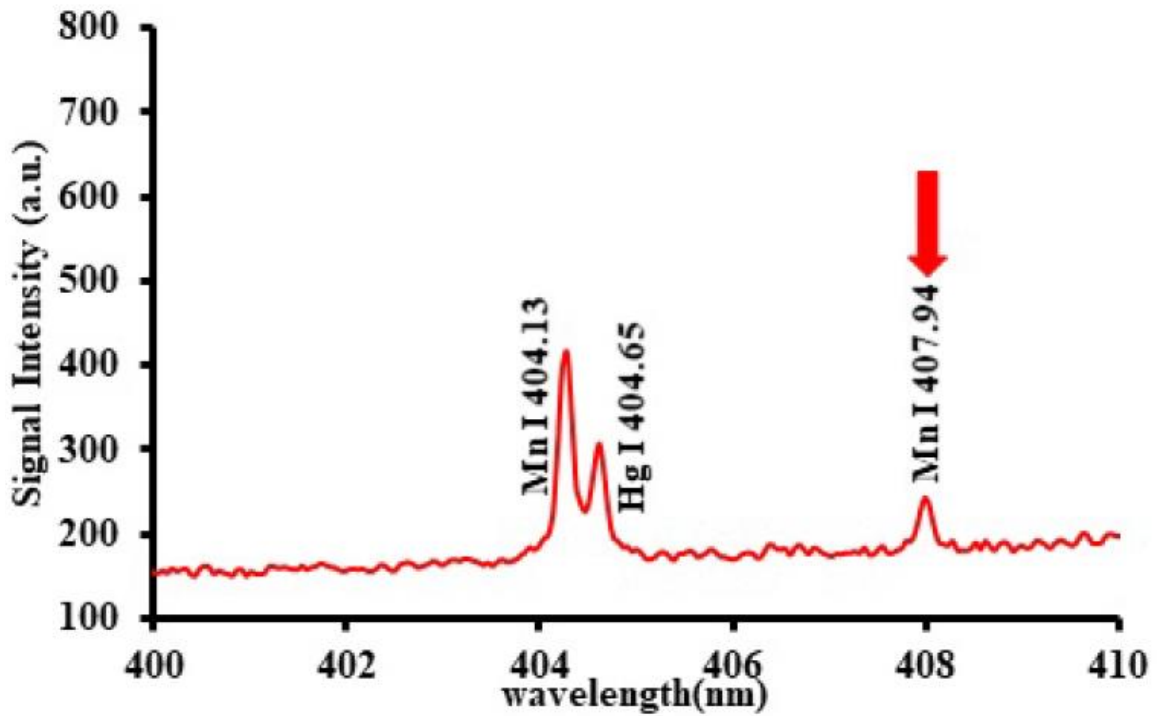
(b)

© Lutfi Mulyadi Surachman 2018

Figure 4.19 Typical LIBS Spectrum indicating strong Mn line in 400-410 nm region for (a) Sarah fish and (b) Bagoh fish at 407.94 nm



(a)

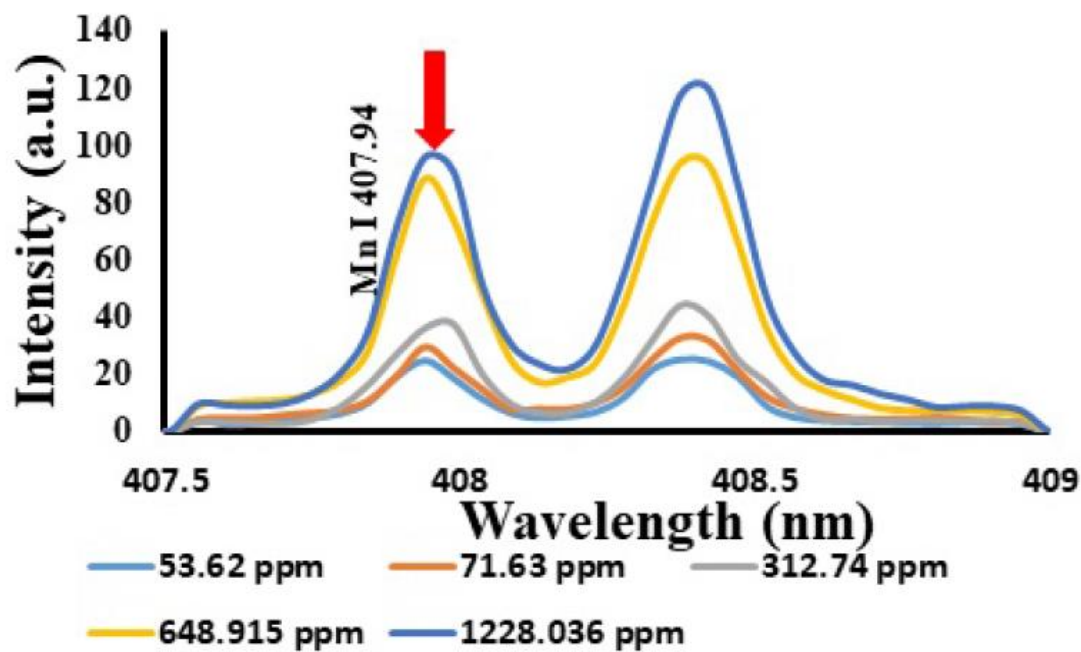


(b)

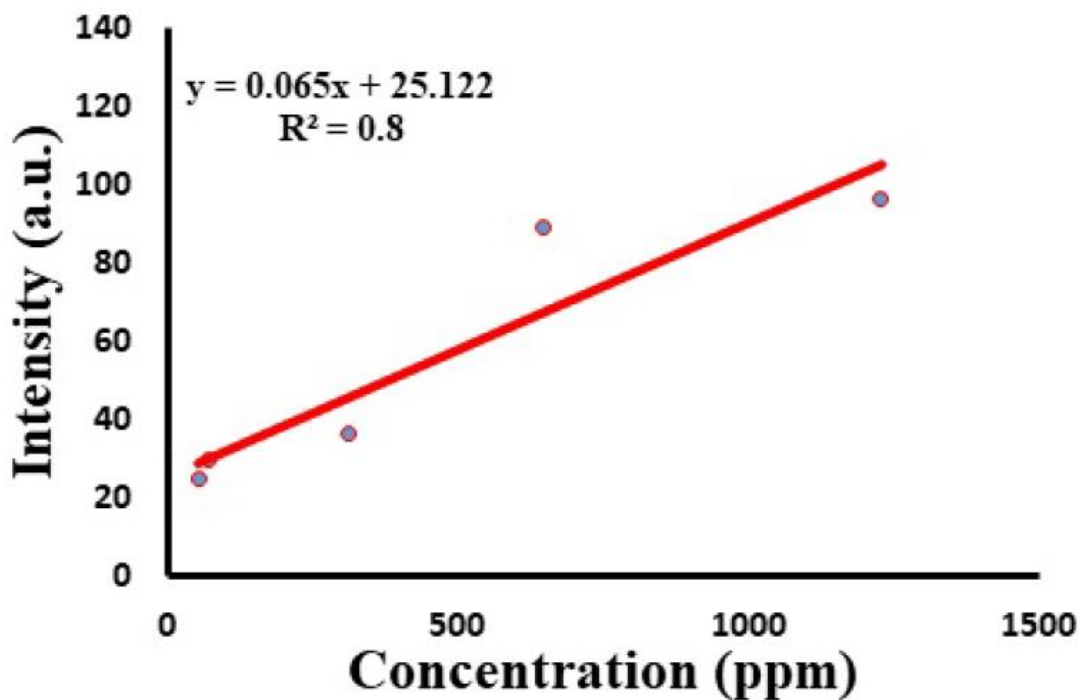
© Lutfi Mulyadi Surachman 2018

Figure 4.20 Typical LIBS Spectrum indicating strong Mn line in 400-410 nm region for (a) Bory fish and (b) Hered fish at 407.94 nm

MANGANESE CALIBRATION CURVES



(a)

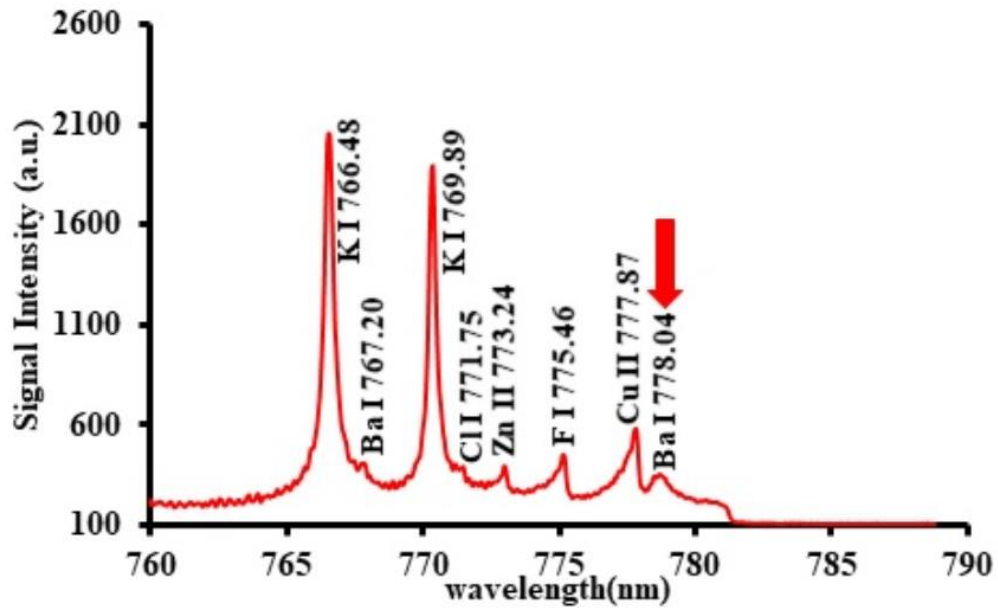


(b)

© Lutfi Mulyadi Surachman 2018

Figure 4.21 Calibration curve for detection of Manganese

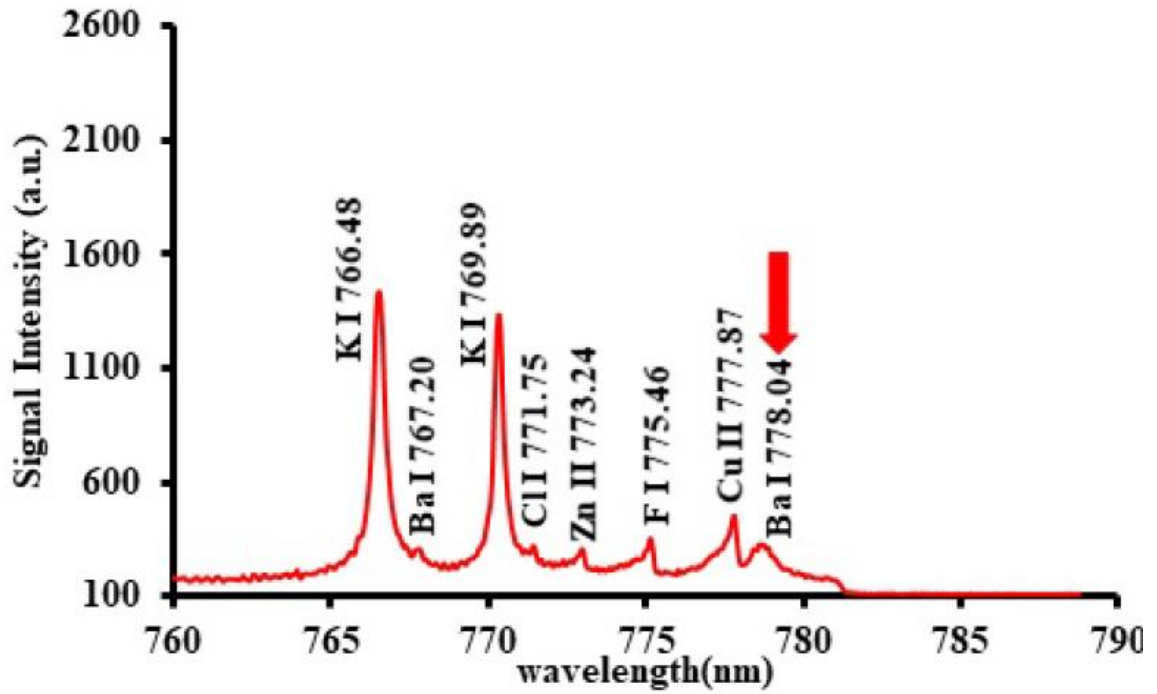
Figure 4.22 until Figure 4.24 depict the spectra of the five fish samples in the range of 760 - 790 nm. In this range, Barium identification in all samples relies on the strong line of atomic emission of **Ba I 778.04 nm** { $6s5d\ ^3D_2 \rightarrow 5d6p\ ^3F^o_2$ } as a fingerprint wavelength. The proof of barium detection, relying on this wavelength is that after adding different linearly known concentration of $C_4H_6BaO_4$ into a set of standard samples, the chosen fingerprint wavelength, depicted in Figure 4.25 grows linearly. The fish samples in the Figure 4.22 until Figure 4.24 also have different fingerprint wavelength intensities, indicating different barium concentration in all samples. In the same range, we also found atomic emission of two potassium lines (K I 766.48 nm and K I 769.89 nm), another atomic emission of Barium (Ba I 767.20 nm), atomic emission of Chlorine (Cl I 771.75 nm), Fluoride (F I 775.46 nm), ionic emission of Zinc (Zn II 773.24 nm) and ionic emission of Copper (Cu II 777.87 nm). For all elements in different ranges, all emissions have different intensities, indicating different concentrations of the elements in all fish samples.



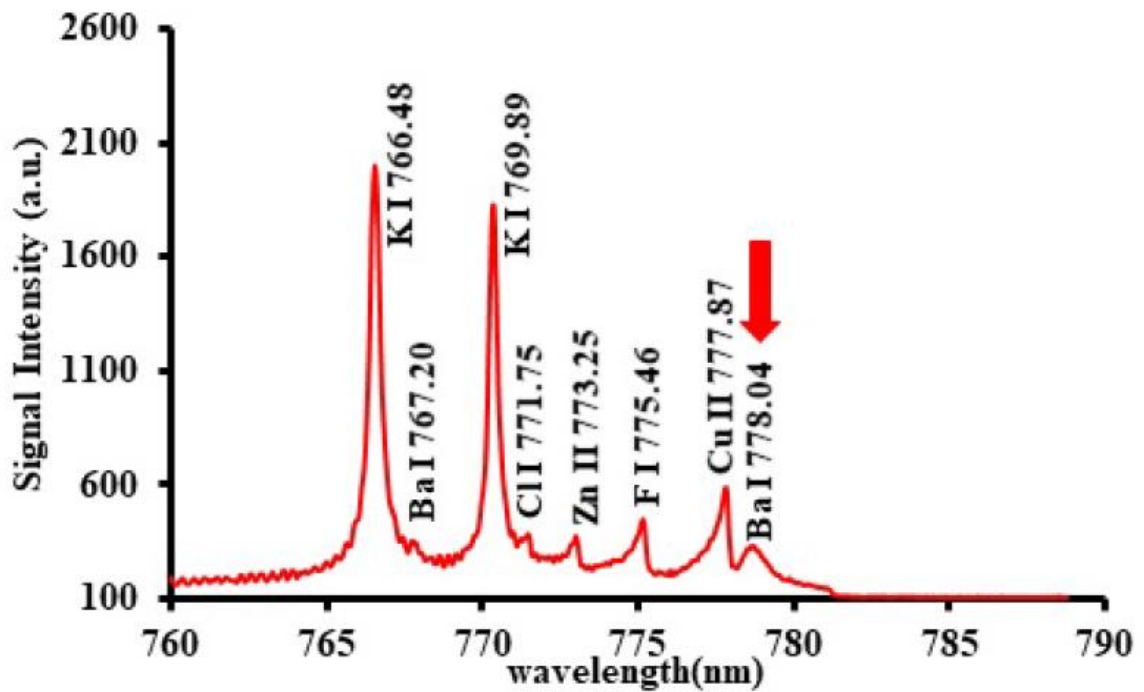
(a)
© Lutfi Mulyadi Surachman 2018

Figure 4.22 Typical LIBS Spectrum indicating strong Ba line in 760-790 nm region for (a) Bulfusyan fish at 778.04 nm

BARIUM DETECTION



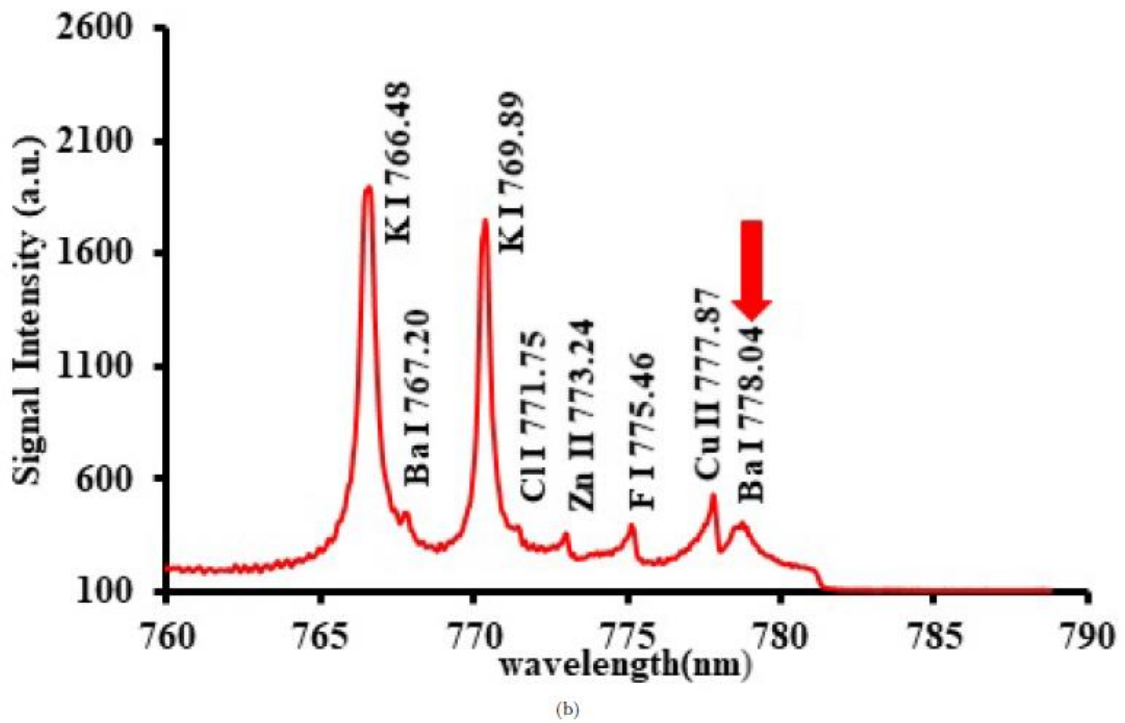
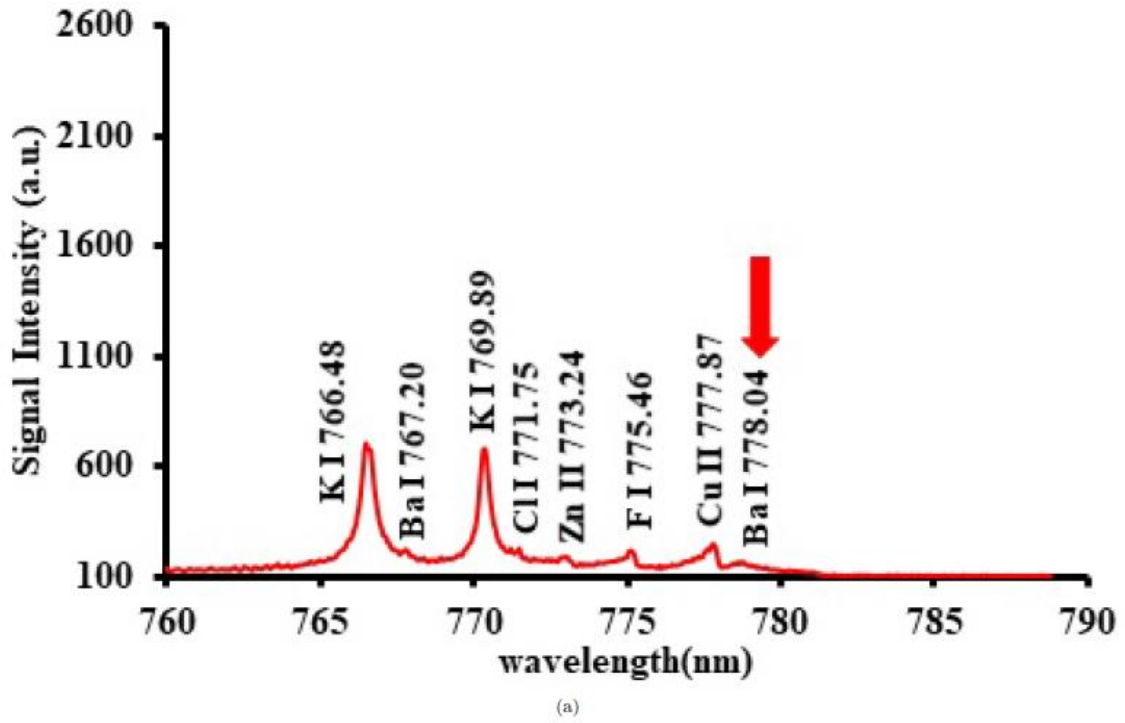
(a)



(b)

© Lutfi Mulyadi Surachman 2018

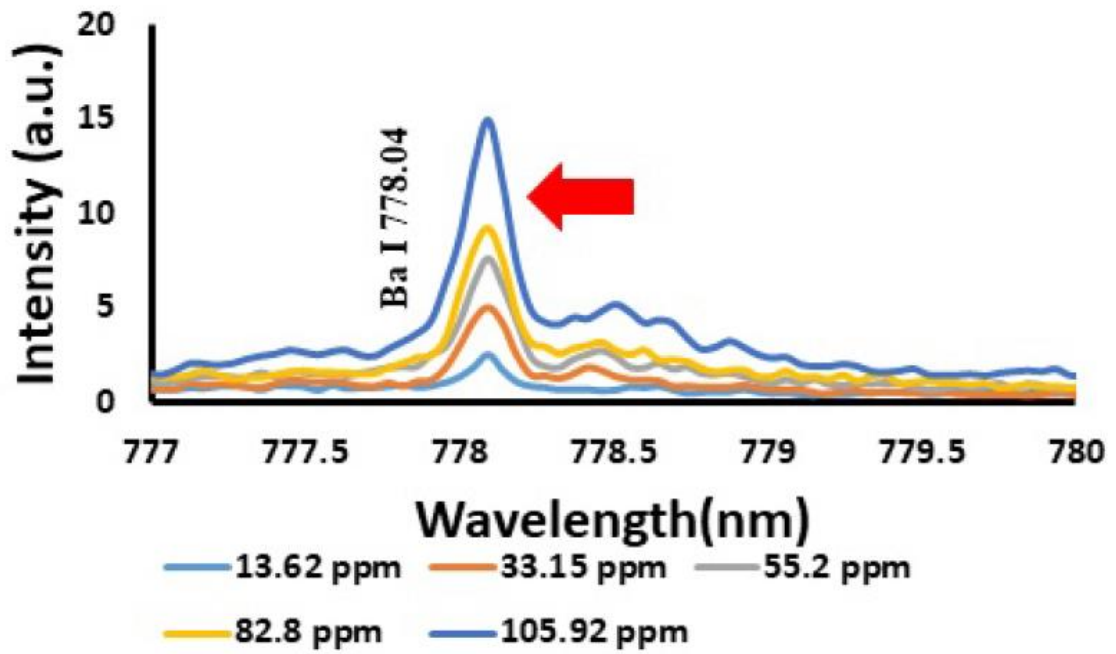
Figure 4.23 Typical LIBS Spectrum indicating strong Ba line in 760-790 nm region for (a) Sarah fish and (b) Bagoh fish at 778.04 nm



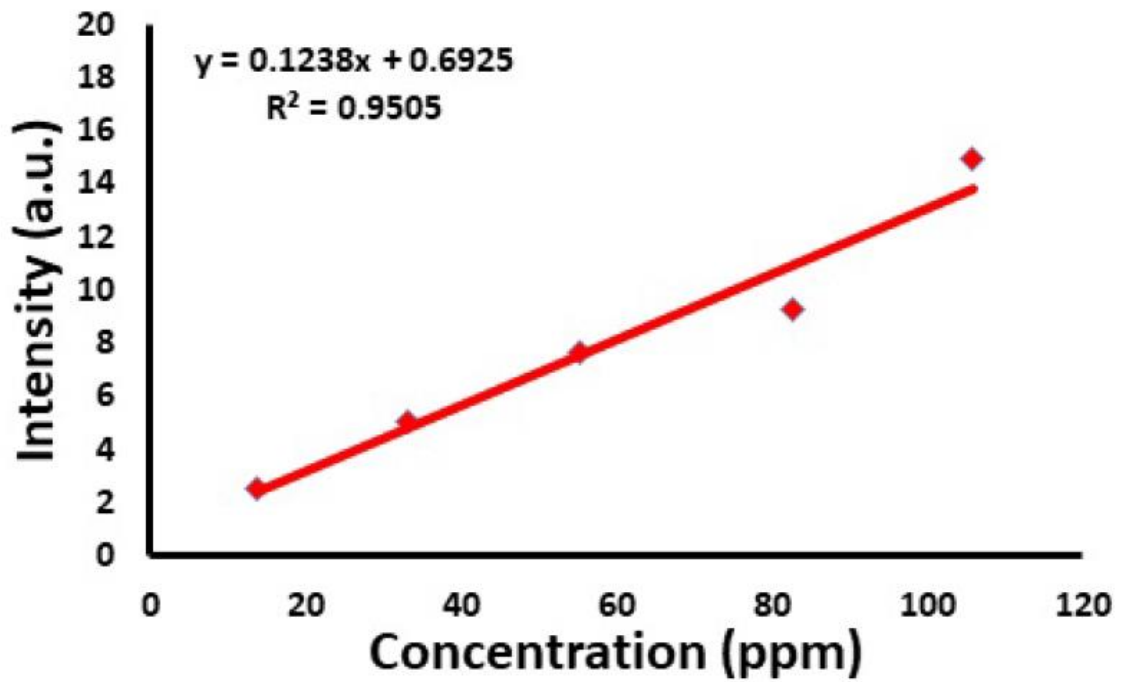
© Lutfi Mulyadi Surachman 2018

Figure 4.24 Typical LIBS Spectrum indicating strong Ba line in 760-790 nm region for (a) Bory fish and (b) Hered fish at 778.04 nm

BARIUM CALIBRATION CURVES



(a)

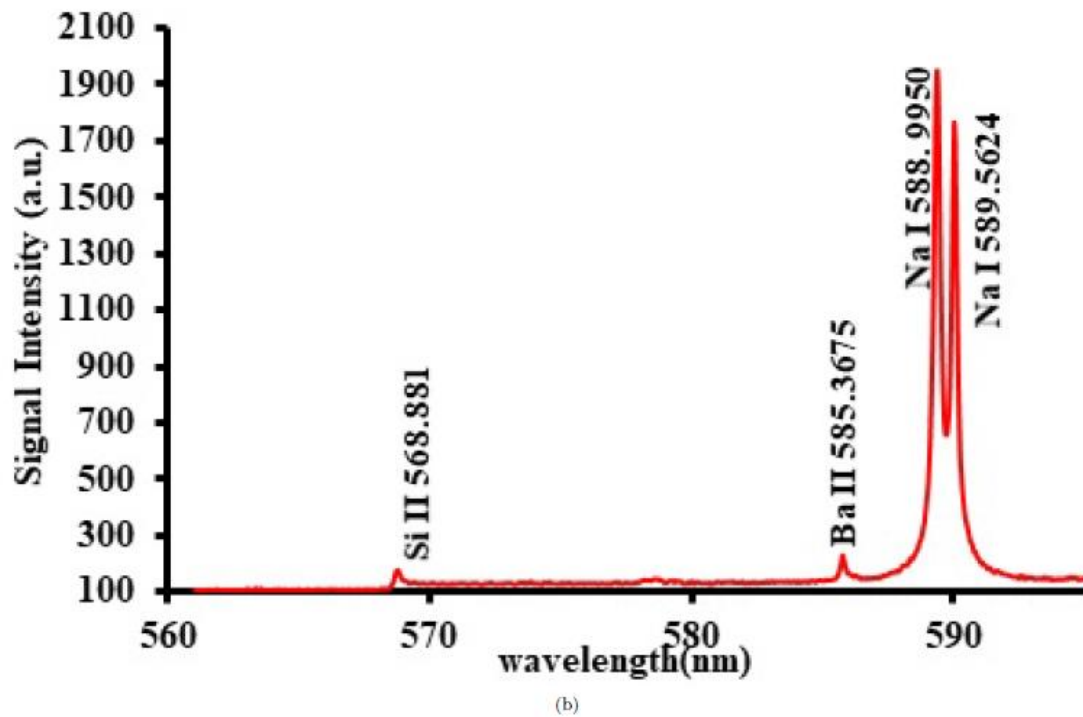
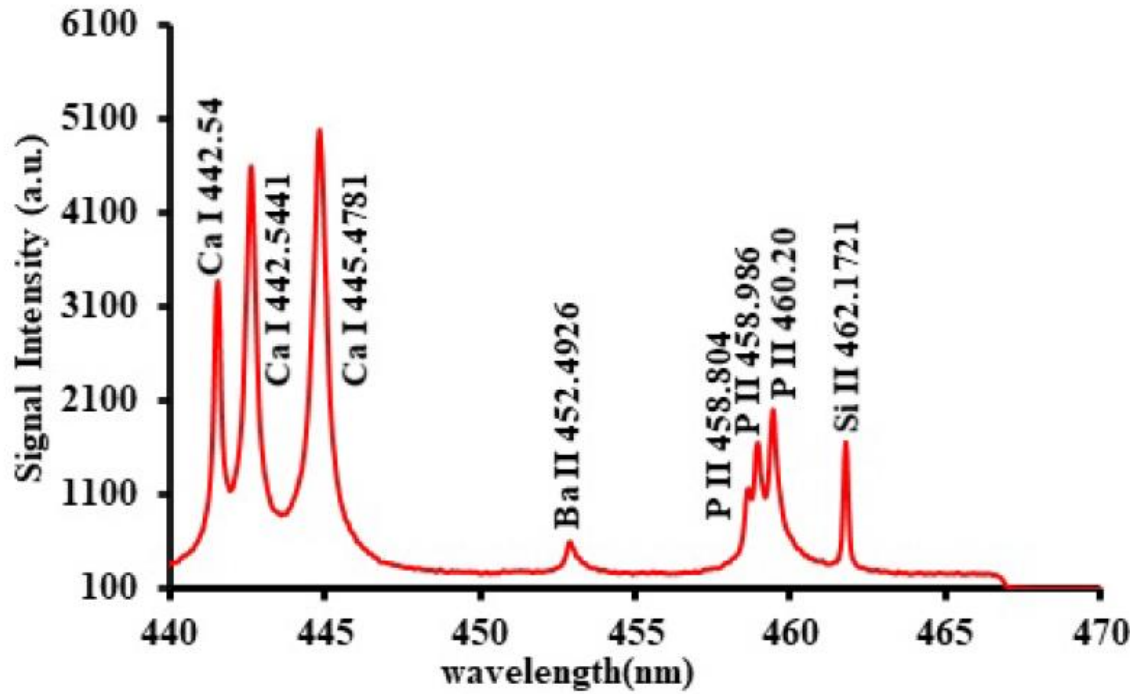


(b)

© Lutfi Mulyadi Surachman 2018

Figure 4.25 Calibration curve for detection of Barium

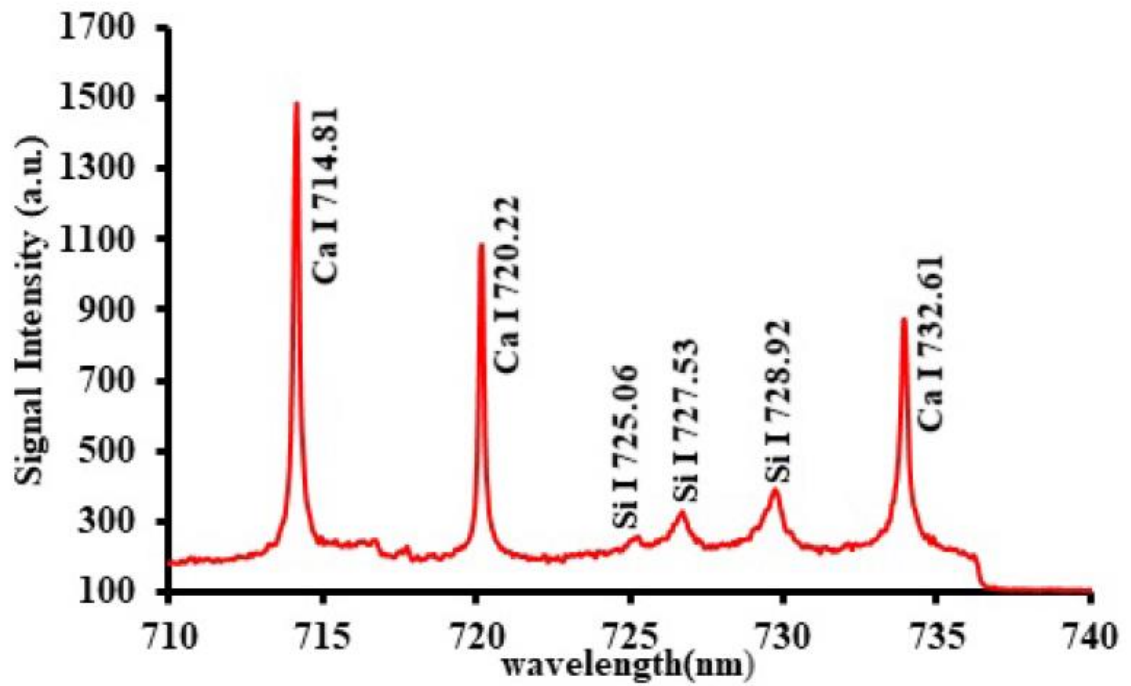
SAMPLE 1 (SARAH)



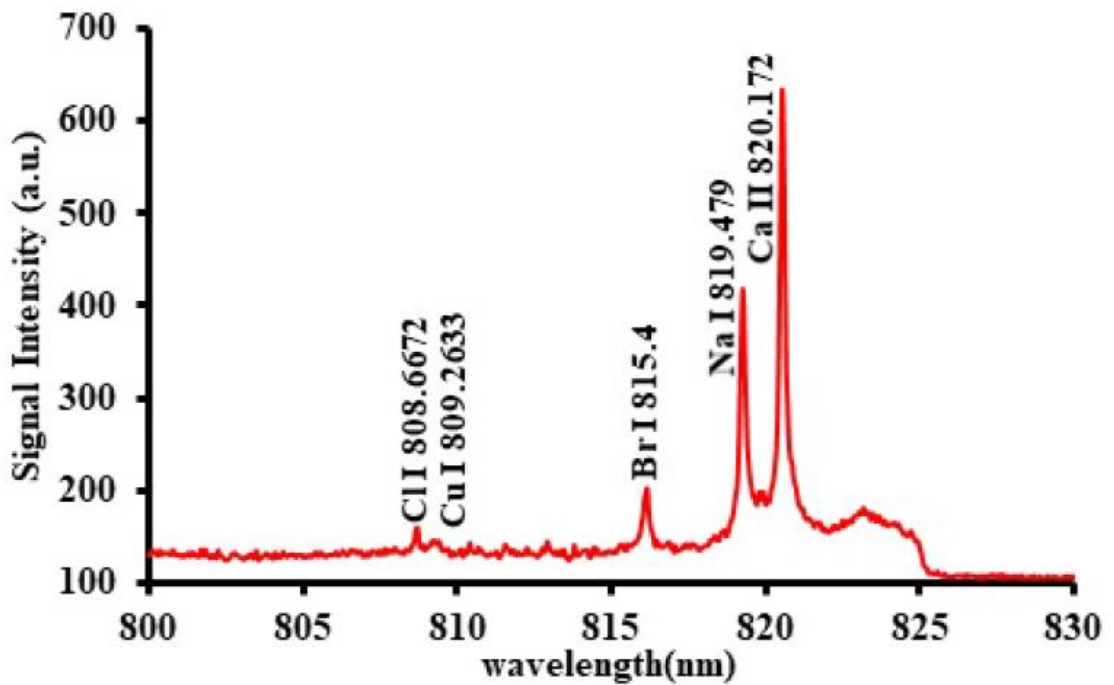
© Lutfi Mulyadi Surachman 2018

Figure 4.26 LIBS spectra of sample 1 Sarah fish at (a) 450nm and (b) 585 nm central wavelength

SAMPLE 1 (SARAH)



(a)

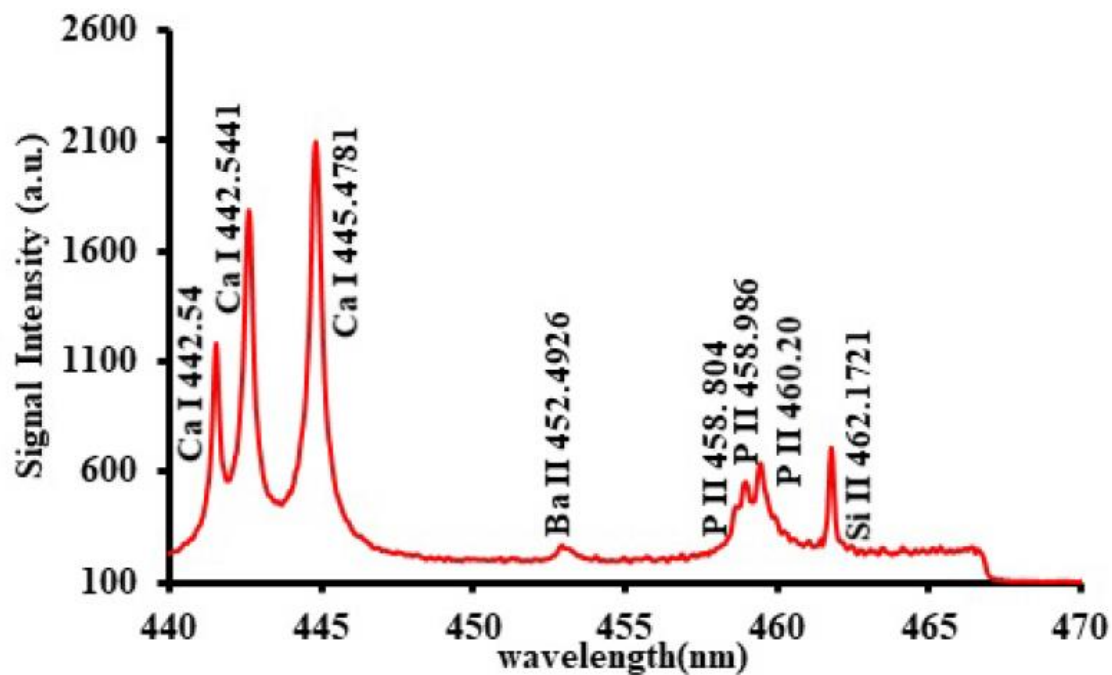


(b)

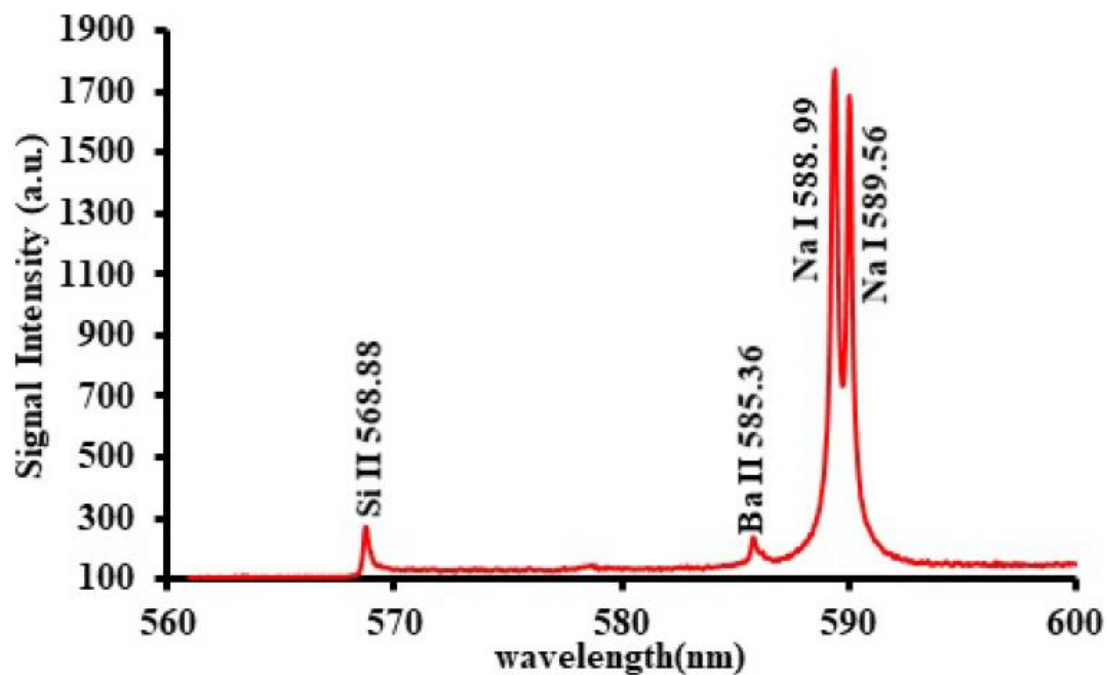
© Lutfi Mulyadi Surachman 2018

Figure 4.27 LIBS spectra of sample 1 Sarah fish at (a) 720 nm and (b) 810 nm central wavelength

SAMPLE 2 (BAGOH)



(a)

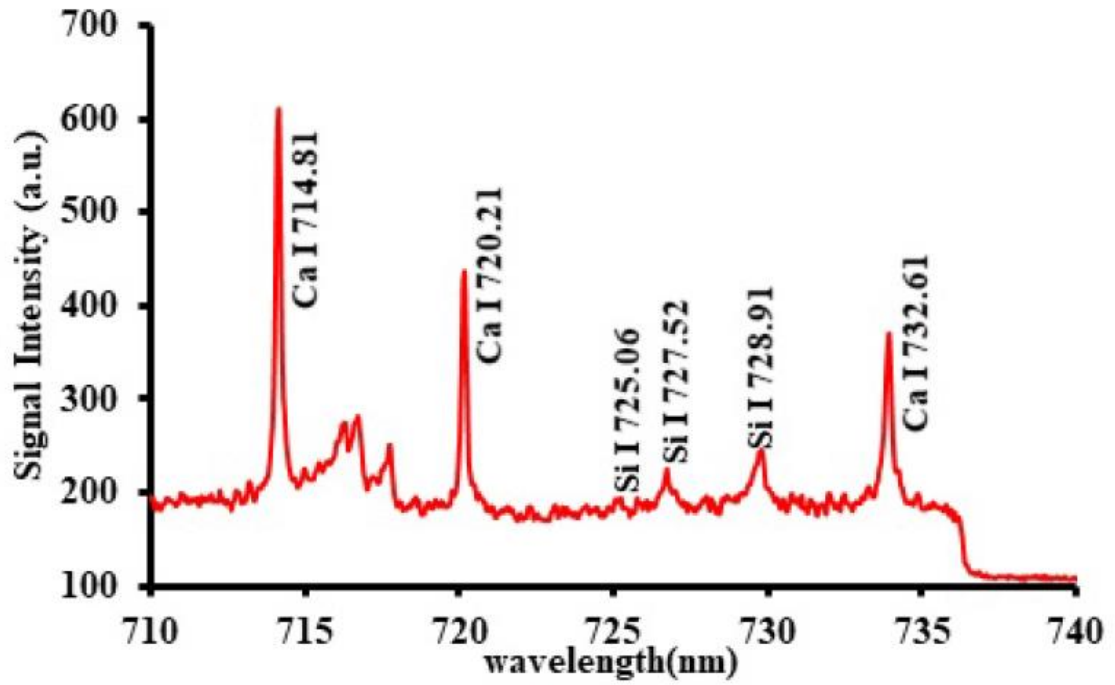


(b)

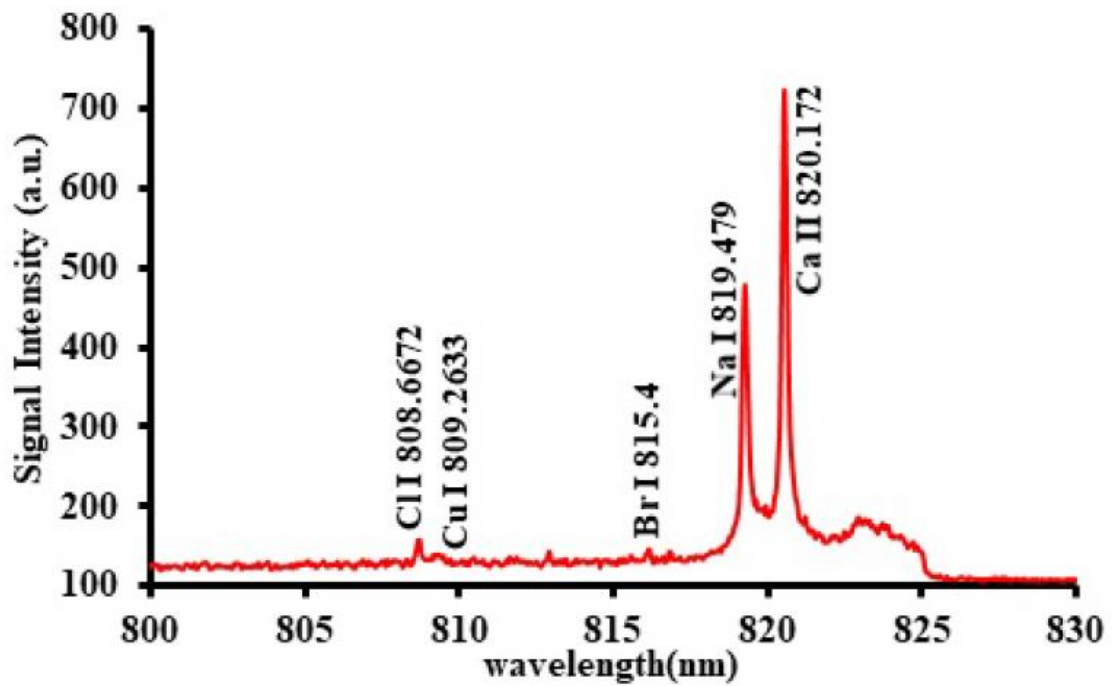
© Lutfi Mulyadi Surachman 2018

Figure 4.28 LIBS spectra of sample 2 Bagoh fish at (a) 450nm and (b) 585 nm central wavelength

SAMPLE 2 (BAGOH)



(a)

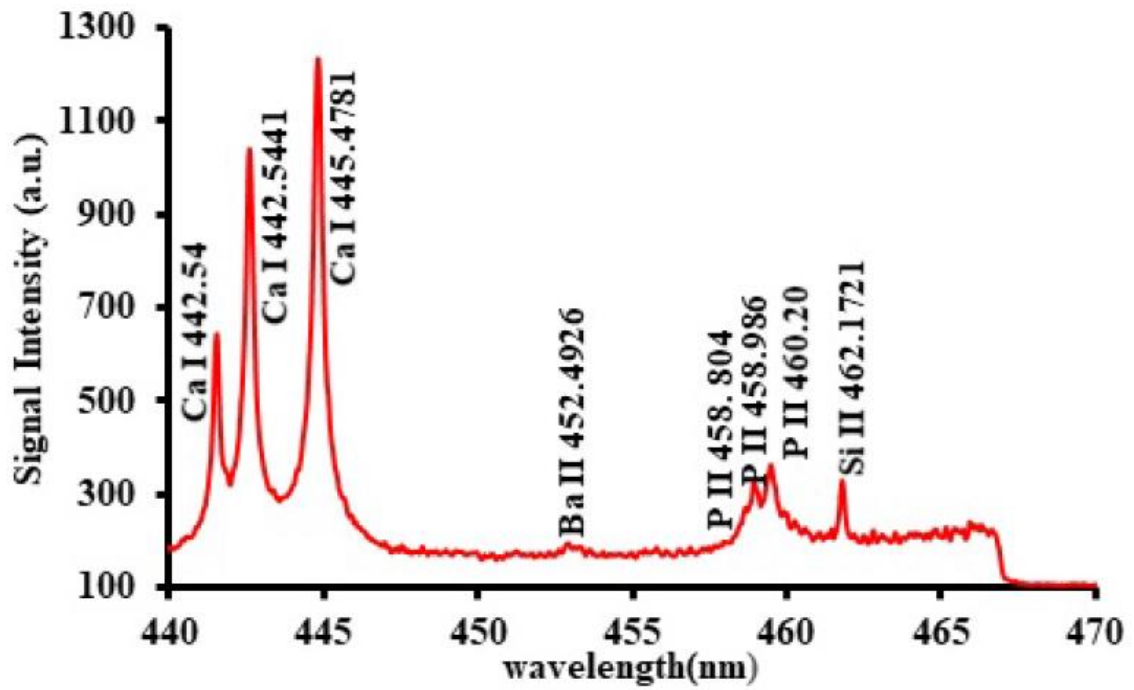


(b)

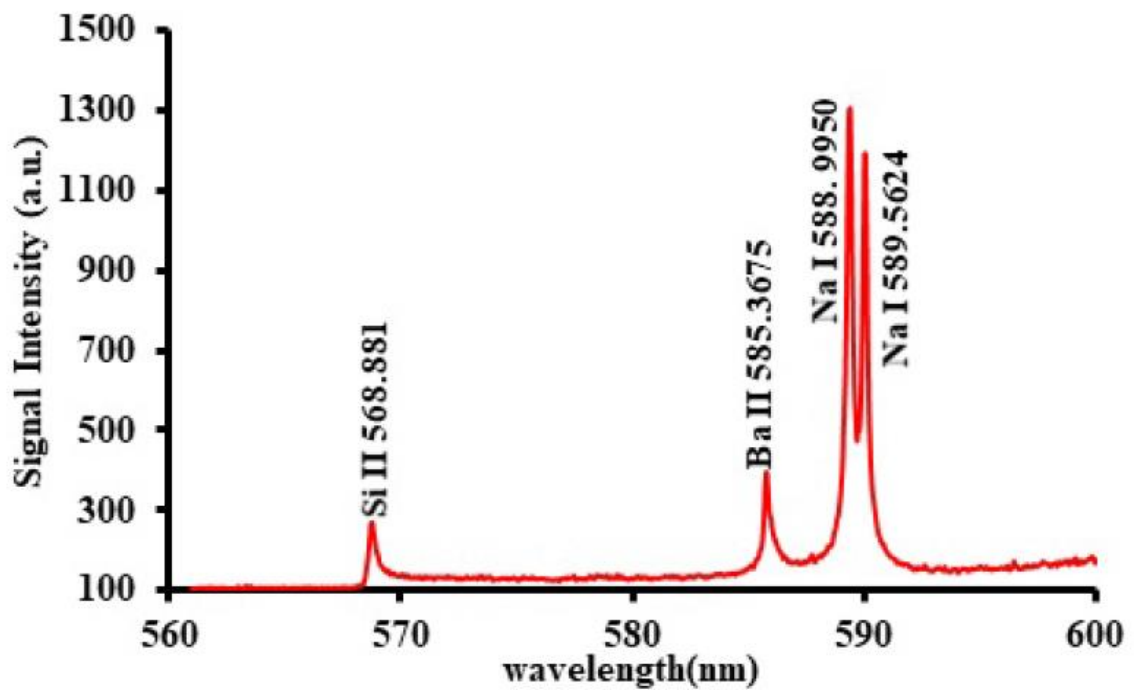
© Lutfi Mulyadi Surachman 2018

Figure 4.29 LIBS spectra of sample 2 Bagoh fish at (a) 720 nm and (b) 810 nm central wavelength

SAMPLE 3 (BORY MISR)



(a)

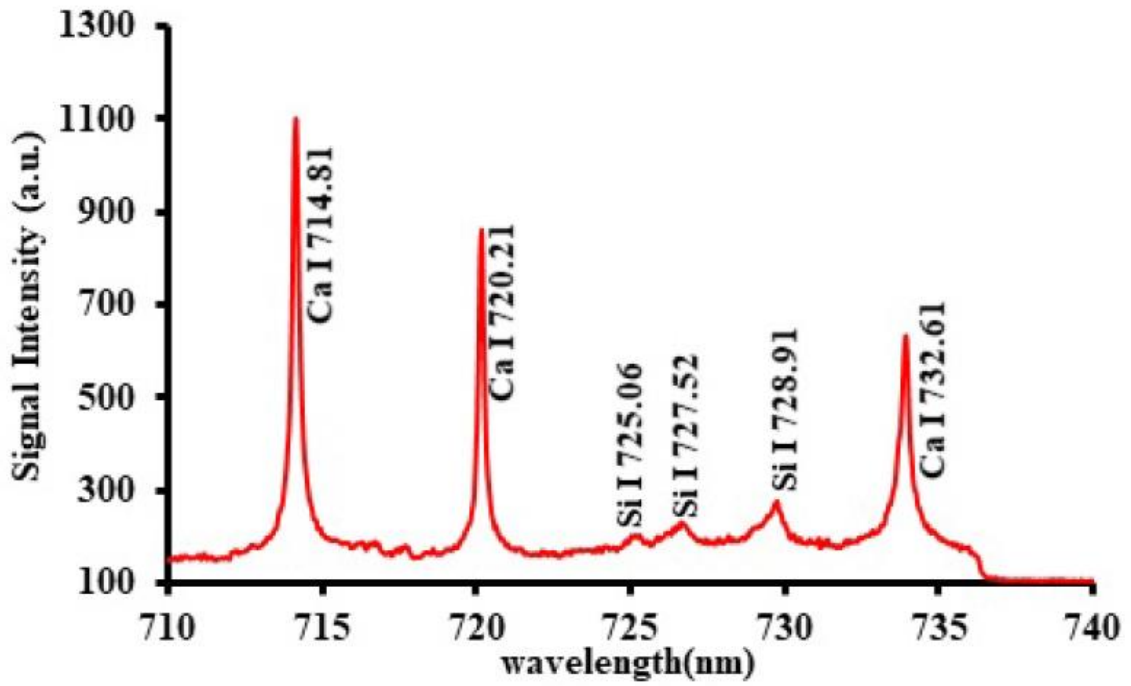


(b)

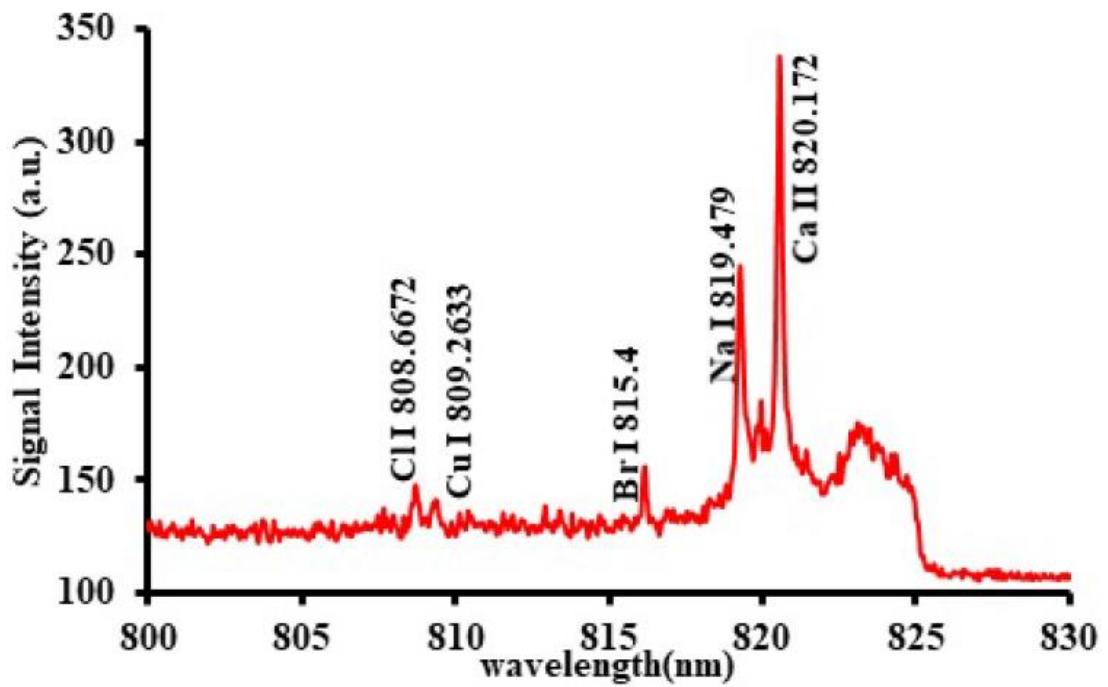
© Lutfi Mulyadi Surachman 2018

Figure 4.30 LIBS spectra of sample 3 Bory fish at (a) 450nm and (b) 585 nm central wavelength

SAMPLE 3 (BORY MISR)



(a)

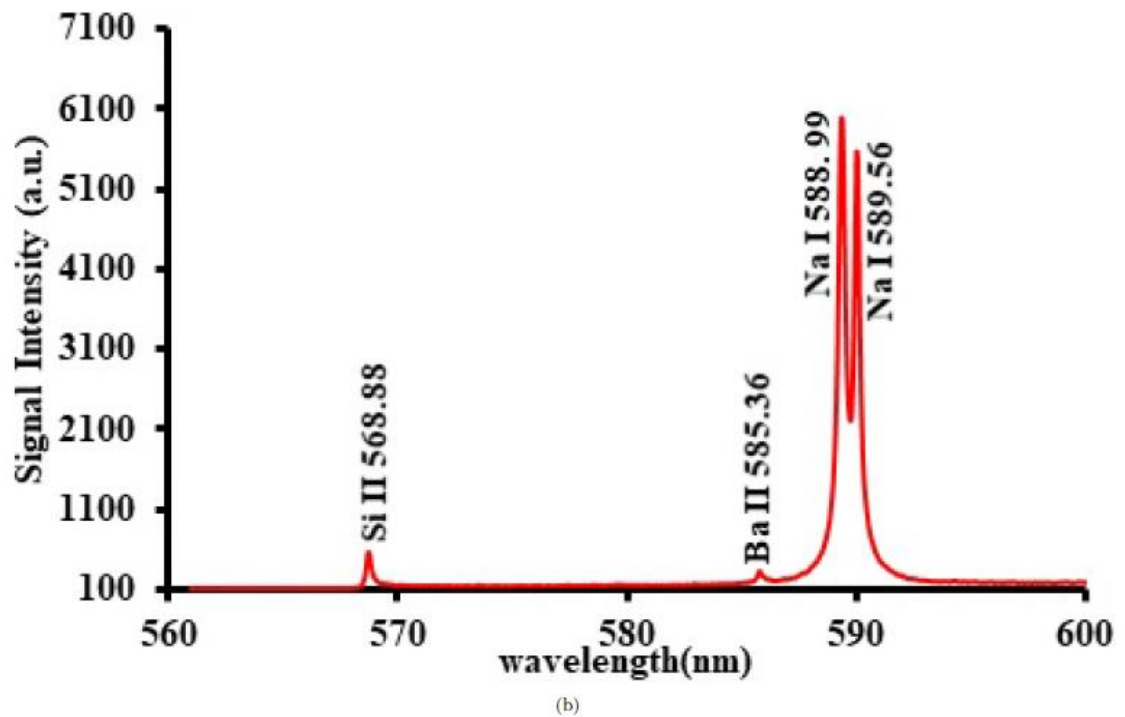
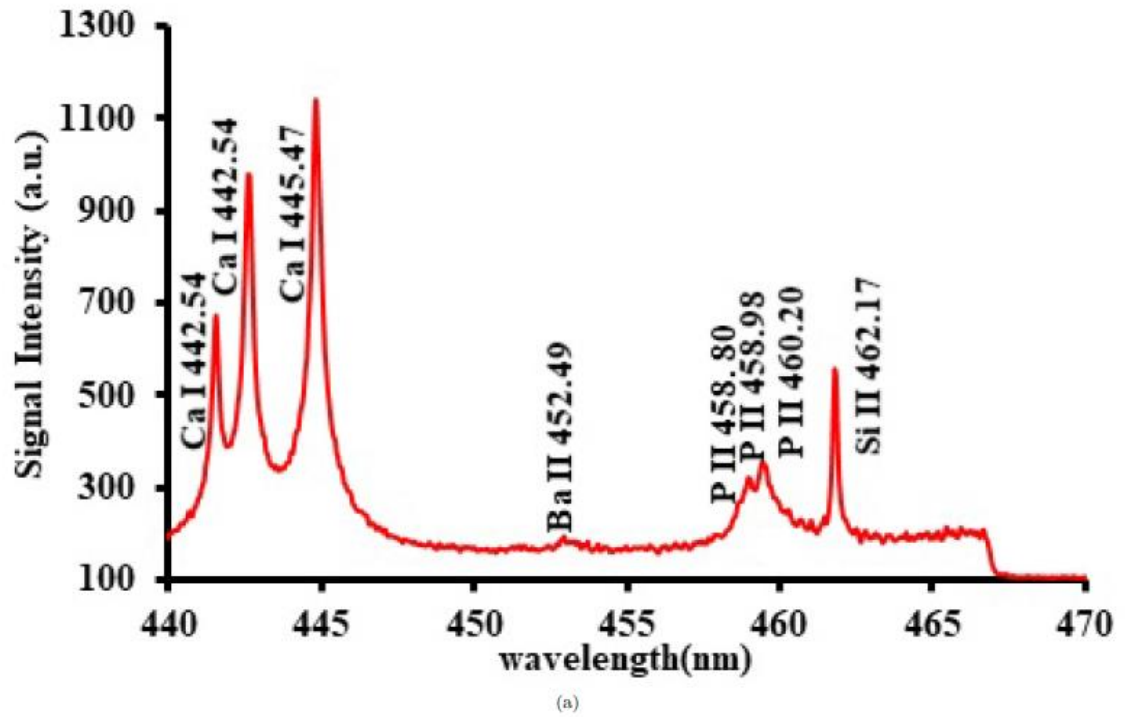


(b)

© Lutfi Mulyadi Surachman 2018

Figure 4.31 LIBS spectra of sample 3 Bory fish at (a) 720 nm and (b) 810 nm central wavelength

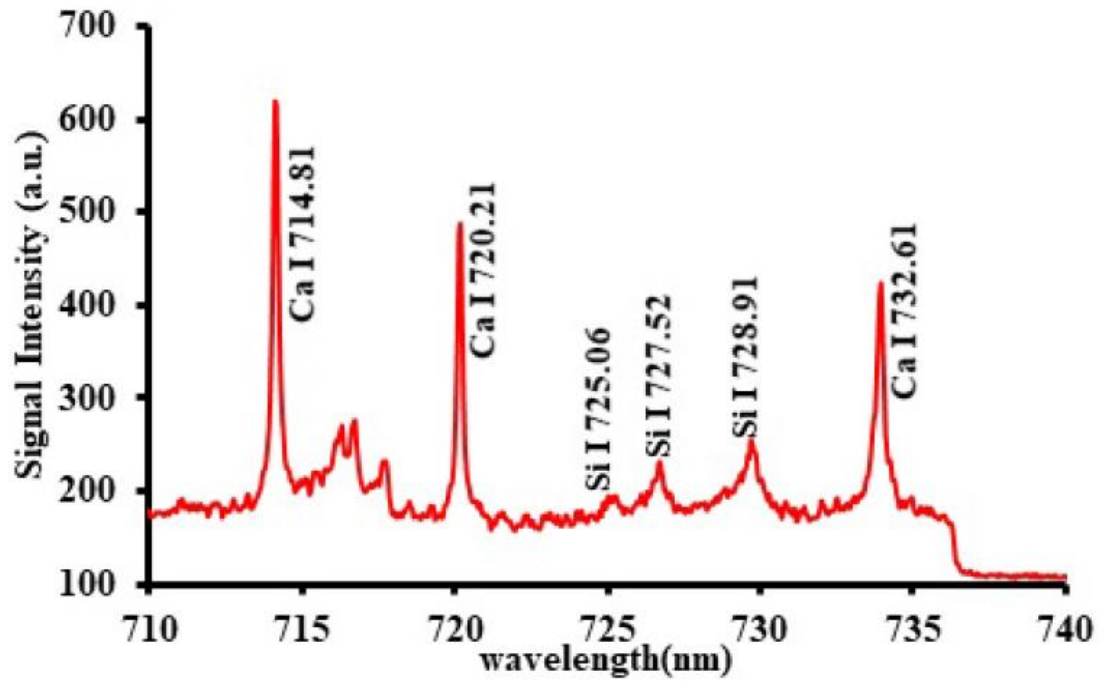
SAMPLE 4 (HERED)



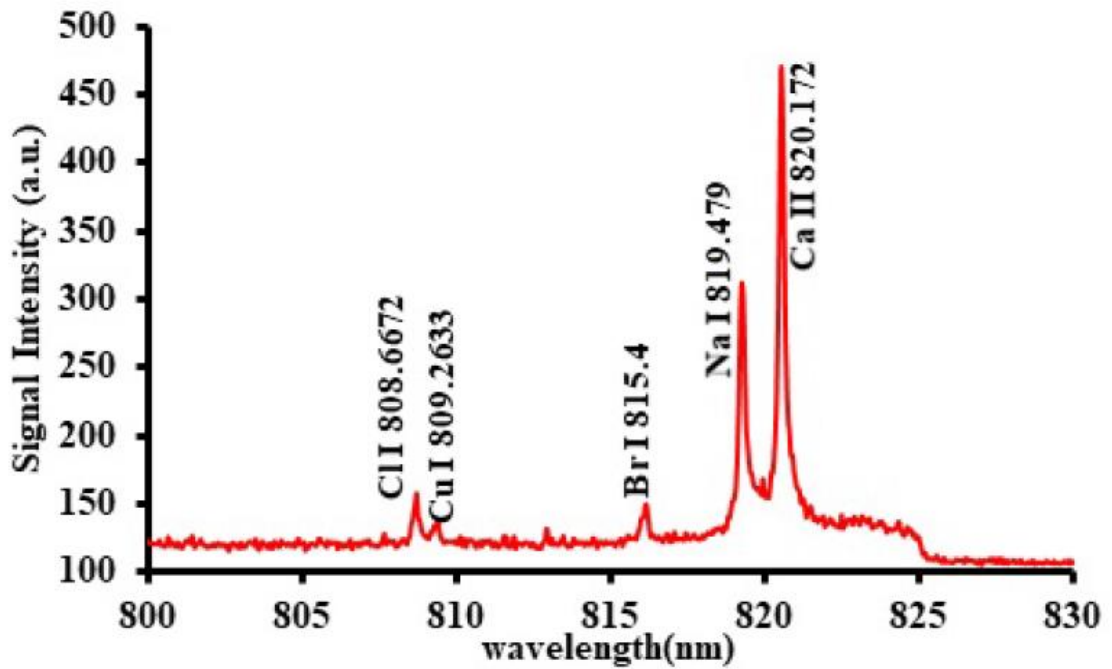
© Lutfi Mulyadi Surachman 2018

Figure 4.32 LIBS spectra of sample 4 Hered fish at (a) 450nm and (b) 585 nm central wavelength

SAMPLE 4 (HERED)



(a)

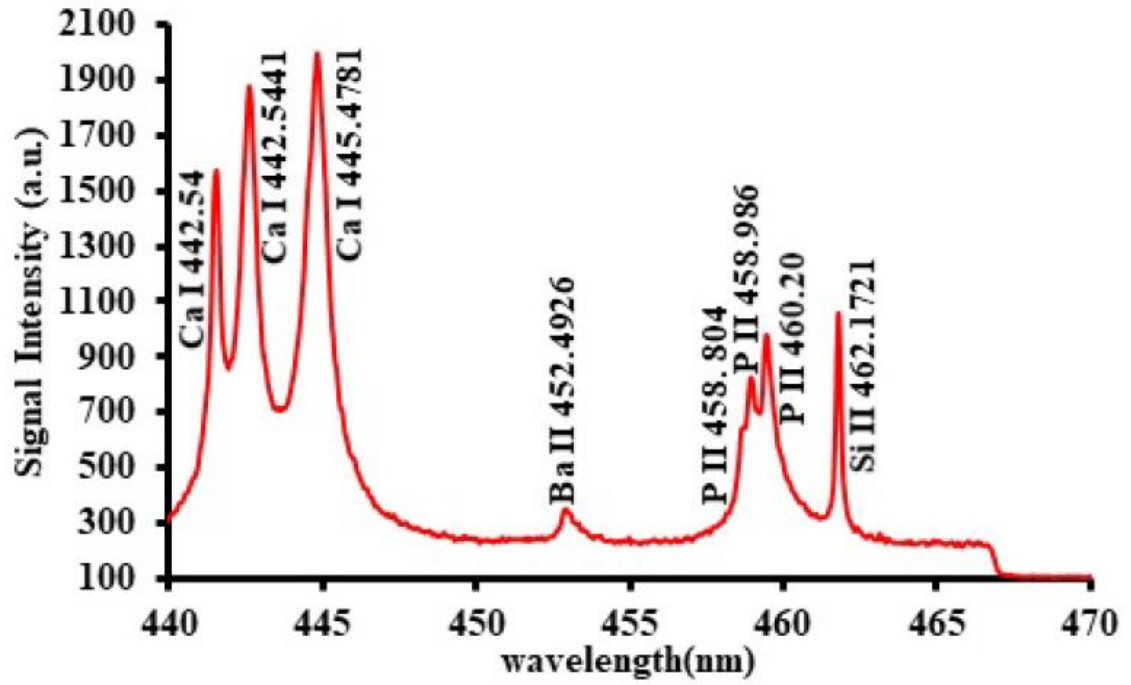


(b)

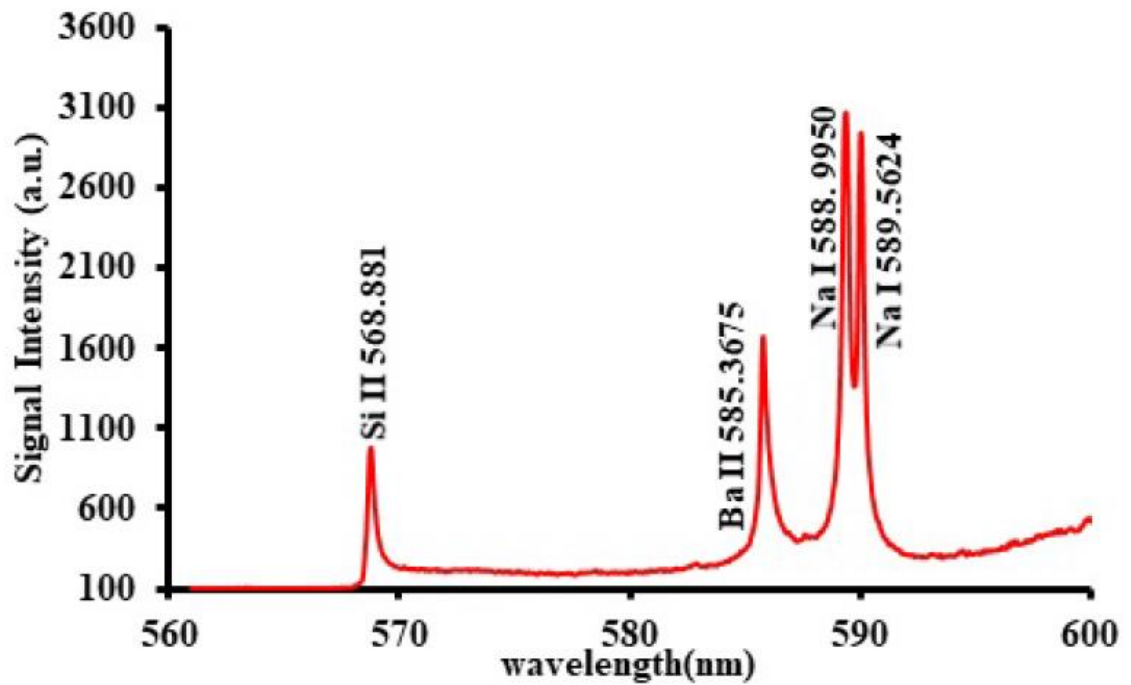
© Lutfi Mulyadi Surachman 2018

Figure 4.33 LIBS spectra of sample 4 Hered fish at (a) 720 nm and (b) 810 nm central wavelength

SAMPLE 5 (BULFUSYAN)



(a)

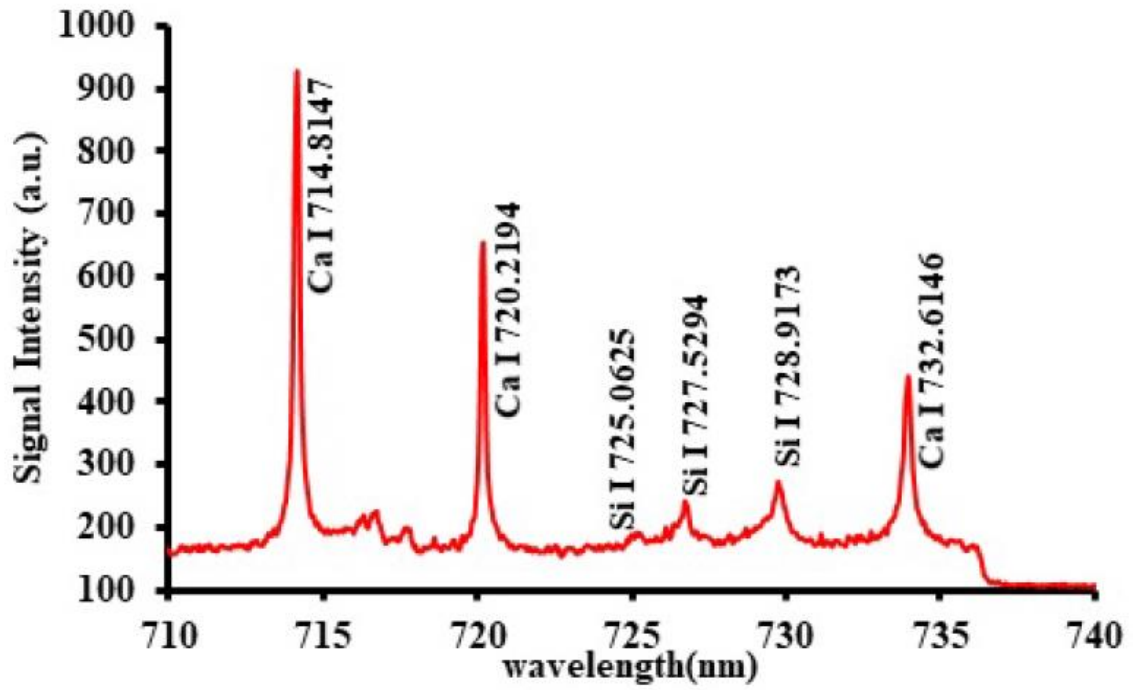


(b)

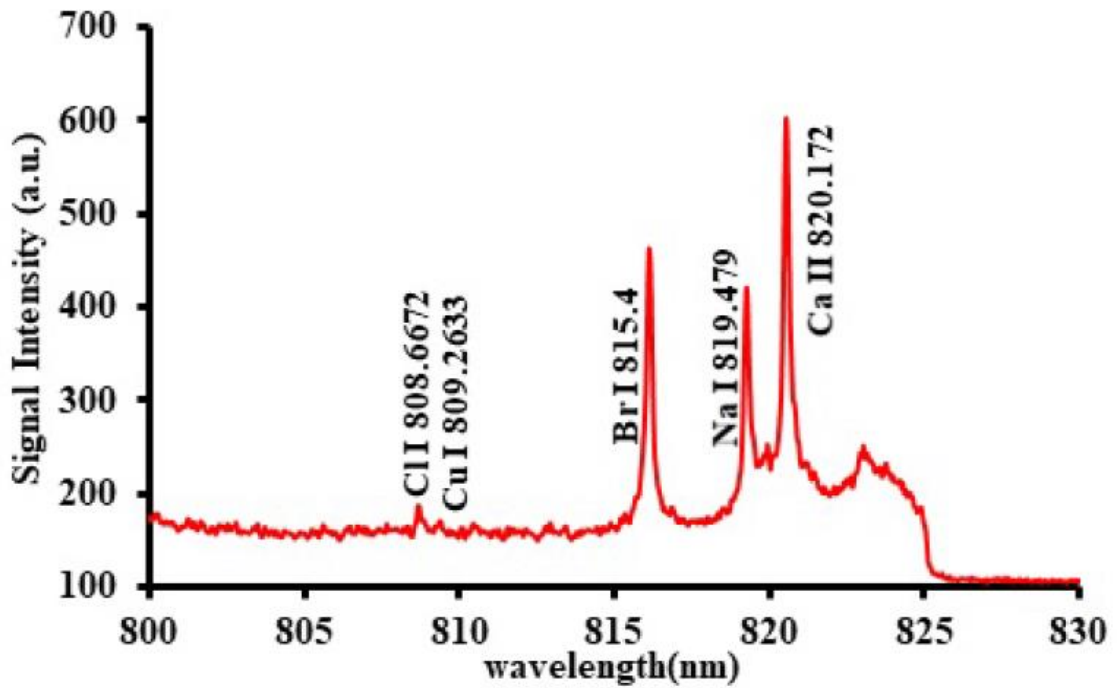
© Lutfi Mulyadi Surachman 2018

Figure 4.34 LIBS spectra of sample 5 Bulfusyan fish at (a) 450nm and (b) 585 nm central wavelength

SAMPLE 5 (BULFUSYAN)



(a)



(b)

© Lutfi Mulyadi Surachman 2018

Figure 4.35 LIBS spectra of sample 5 Bulfusyan fish at (a) 720 nm and (b) 810 nm central wavelength

Table 4.2 The common elements in the fish samples

	Ca		Mg		K	Na		Fe		C	S
Sample 1-5	Ca I 442.54	Ca II 315.8	Mg I 285.21	Mg II 270.08	K I 766.49	Na I 589.6	Na II 280.95	Fe I 278.81	Fe II 420.20	C II 299.26	S II 416.26
	Ca I 445.48	Ca II 318.1		Mg II 279.5	K I 769.89	Na I 819.48	Na II 371.10	Fe I 298.36		C II 392.07	
	Ca I 714.81	Ca II 396.8		Mg II 280.27				Fe I 358.7			
	Ca I 720.22	Ca II 820.1						Fe I 363.14			
	Ca I 732.61							Fe I 364.78			
								Fe I 421.61			
								Fe I 441.51			

	P	Si		Zn	Na	Cl	Mn	Cu	
Sample 1-5	P II 458.8	Si I 775.06	Si II 462.17	Zn II 773.25	Na II 280.95	Cl I 771.76	Mn I 357.78	Cu I 809.3	Cu II 270.09
	P II 458.9	Si I 727.5	Si II 568.89		Na II 371.10	Cl I 808.67	Mn I 404.13		Cu II 777.87
	P II 460.20	Si I 728.9					Mn I 407.9		

	Ba		Co		Ni	Se	F	Br	Hg	
Sample 1-5	Ba I 778.04	Ba II 452.5	Co I 344.92	Co II 270.66	Ni I 362.94	Se II 417.53	F I 775.5	Br I 815.4	Hg I 253.6	Hg II 284.8
		Ba II 585.4	Co I 347.4						Hg I 404.65	

4.5 Quantitative Analysis and Risk Assessment

Using the generated linear equation from the calibration curves for every element and the corresponding intensities in the previous section, we can calculate the concentration of 2 nutrients (Ca and Mg) and 3 heavy Metals (Fe, Mn, and Ba), listed in table 4.3. The three metallic elements will be further processed for health risk assessment in the next sub-section 4.5.1.1 until 4.5.1.3.

Based on table 4.3, the highest concentration of Magnesium, Calcium, Iron, Manganese and Barium is in the fish of Egyptian Bory, Bulfusyan, Hered, Bulfusyan, and Hered Respectively.

Table 4.3 the elemental concentration detected in the fish samples using the LIBS set-up

Element	Sample Name	LIBS (ppm)	Permissible limit (ppm)	LIBS LOD (ppm)
Mg II 280.27	Sarah	685.67 ± 44.16	-	93.06 ± 5.99
	Bagoh	2121.43 ± 136.63		
	Bory	2702.4 ± 174.04		
	Hered	929.27 ± 59.84		
	Bulfusyan	1729 ± 111.35		
Ca II 315.89	Sarah	246.08 ± 14.34	-	171.073 ± 9.96
	Bagoh	457.09 ± 26.63		
	Bory	257.48 ± 15.00		
	Hered	877.11 ± 51.11		
	Bulfusyan	1620.32 ± 94.41		
Fe I 358.12	Sarah	14.45 ± 0.94	100	4.28 ± 0.28
	Bagoh	10.26 ± 0.67		
	Bory	18.35 ± 1.2		
	Hered	23.96 ± 1.56		
	Bulfusyan	20.86 ± 1.36		
Mn I 407.9415	Sarah	74.63 ± 17.04	0.5	22.40 ± 5.116
	Bagoh	27.79 ± 6.34		
	Bory	36.54 ± 8.34		
	Hered	83.53 ± 19.07		
	Bulfusyan	522.26 ± 119.25		
Ba I 778.05	Sarah	66.514 ± 8.76	0.3	29.84 ± 3.93
	Bagoh	73.08 ± 9.63		
	Bory	65.60 ± 8.64		
	Hered	97.76 ± 12.88		
	Bulfusyan	64.27 ± 8.46		

4.5.1.1 Estimated daily intake (EDI) and Risk metal consumption

$$EDI = \frac{Mc \times IR}{Bw \times 10^{-3}} \quad (18)$$

Estimated daily intake is the estimation of elemental consumption of the people in certain country based on their consumption rates, average body weight and the consumed metal concentration in ppm. For Saudi Arabia, the consumption rate for fish is 21.917 Kg /day ([76];[104]). The average body weight is 79 Kg for male and 71.5 Kg for female [2].

The risk assessment of the metal consumption follows the following criteria,

1. $\frac{EDI}{RfD} \leq RfD$; Minimum Risk
2. $\frac{EDI}{RfD} > (1 - 5)RfD$; Low Risk
3. $\frac{EDI}{RfD} > (5 - 10)RfD$; Moderate Risk
4. $\frac{EDI}{RfD} > 10 RfD$; High Risk

Note that RfD is the reference dose that is unique for every element. For Iron, the Reference dose is 0.7 mg/kg/day.

Table 4.4 Estimated Daily Intake of Fe (mg/kg body-weight /day)

Sample Name	LIBS (Male)	LIBS (Female)
Sarah	4.01 ± 0.26	4.43 ± 0.28
Bagoh	2.85 ± 0.18	3.14 ± 0.20
Bory	5.09 ± 0.33	5.62 ± 0.36
Hered	6.65 ± 0.43	7.34 ± 0.47
Bulfusyan	5.78 ± 0.378	6.39 ± 0.41

Using the above criteria, by dividing all EDI values for iron in the table 4.4 with its Rfd value, the criteria for the iron risk consumption can be summarized in table 4.5 and thus, the iron risk consumption can be evaluated and listed in table 4.6. Due to the lower average body weight, the female in Saudi Arabia is prone to have higher estimated daily

intake of every metal (Fe, Mn, and Ba) with the result that the metal risk consumption will also be higher. This argument is in agreement with the results in table 4.6, table 4.9, and table 4.12. Based on table 4.6, we can also see that consumption of sarah and bagoh fish has moderate iron risk, while the consumption of Bory, Hered and Bulfusyan has high Iron risk for both males and females. It is also true that female has more moderate iron risk to consume sarah and bagoh fish, and has higher iron risk to consume Bory, Hered and Bulfusyan Fish. Of all fish samples, consumption of Hered fish induces the highest iron risk.

Table 4.5 Iron Risk Criteria

Iron Risk	EDI/Rfd
Minimum	<0.7
low	>0.7-3.5
Moderate	>3.5-7
High	>7

Table 4.6 Iron Risk Consumption

Fish Samples	LIBS (Male)	Risk	LIBS (Female)	Risk
Sarah	5.72 ± 0.37	Moderate	6.32 ± 0.41	Moderate
Bagoh	4.06 ± 0.26	Moderate	4.49 ± 0.29	Moderate
Bory	7.27 ± 0.47	High	8.03 ± 0.52	High
Hered	9.49 ± 0.62	High	10.49 ± 0.68	High
Bulfusyan	8.26 ± 0.54	High	9.13 ± 0.59	High

Table 4.7 Estimated Daily Intake of Mn (mg/kg body-weight /day)

Sample Name	LIBS (Male)	LIBS (Female)
Sarah	20.70 ± 4.72	22.87 ± 5.22
Bagoh	7.71 ± 1.76	8.52 ± 1.94
Bory	10.14 ± 2.31	11.20 ± 2.55
Hered	23.17 ± 5.29	25.60 ± 5.84
Bulfusyan	144.89 ± 33.08	160.09 ± 36.55

By dividing all EDI values of manganese in table 4.7 with its Rfd value, 0.14 mg/kg/day, risk criteria for Manganese consumption can be summarized in table 4.8 and therefore the Manganese risk can be evaluated and listed in table 4.9. Based on table 4.9, we can also see that consumption of all different fish samples has high Manganese risk for both males and females. It is also true that female has higher manganese risk to consume all fish samples. Especially, females have the highest manganese risk by consuming Bulfusyan fish.

Table 4.8 Manganese Risk Criteria

Mn Risk	EDI/Rfd
Minimum	<0.14
Low	>0.14-0.7
Moderate	>0.7-1.4
High	>1.4

Table 4.9 Manganese Risk Consumption

Fish Samples	LIBS (Male)	Risk	LIBS (Female)	Risk
Sarah	147.89 ± 33.77	High	163.41 ± 37.31	High
Bagoh	55.07 ± 12.56	High	60.85 ± 13.88	High
Bory	72.41 ± 16.52	High	80.00 ± 18.26	High
Hered	165.53 ± 37.79	High	182.89 ± 41.76	High
Bulfusyan	1034.97 ± 236.32	High	1143.53 ± 261.10	High

Table 4.10 Estimated Daily Intake of Ba (mg/kg body-weight /day)

Sample Name	LIBS (Male)	LIBS (Female)
Sarah	18.45 ± 2.43	20.38 ± 2.68
Bagoh	20.27 ± 2.67	22.40 ± 2.95
Bory	18.20 ± 2.39	20.10 ± 2.64
Hered	27.12 ± 3.57	29.96 ± 3.94
Bulfusyan	17.83 ± 2.34	19.70 ± 2.59

By dividing all EDI values of Barium in table 4.10 with its Rfd value, 0.2 mg/kg/day, risk criteria for Barium consumption can be summarized in table 4.11 and therefore the Barium risk can be evaluated and listed in table 4.12. Based on table 4.12, we can also see that consumption of all different fish samples has high Barium risk for both males and females. It is also true that female has higher risk to consume all fish samples. Of all fish samples, consumption of Hered fish induces the highest barium risk.

Table 4.11 Barium Risk Criteria

Ba Risk	EDI/Rfd
minimum	<=0.2
low	>0.2-1
moderate	>1-2
High	>2

Table 4.12 Barium Risk Consumption

Fish Samples	LIBS (Male)	Risk	LIBS (Female)	Risk
Sarah	92.27 ± 12.15	High	101.95 ± 13.43	High
Bagoh	101.37 ± 13.35	High	112.01 ± 14.76	High
Bory	91.00 ± 11.98	High	100.55 ± 13.24	High
Hered	135.61 ± 17.86	High	149.84 ± 19.74	High
Bulfusyan	89.15 ± 11.73	High	98.50 ± 12.97	High

4.5.1.2 Target hazard quotient (THQ)

$$THQ = \frac{(M_c \times IR \times 10^{-3} \times EF \times ED)}{(RfD \times BW \times ATn)} \quad (19)$$

Note that M_c is the metal concentration in ppm, IR is ingestion or consumption rate, using the same value as that in the calculation of EDI. EF is the exposure frequency (365 days/year), ED is the Exposure Duration, which is the life expectancy of the people of Saudi Arabia. In our case, at the average, Saudi Arabian male passes away at the age of 73.2 years old while female is at the age of 76 years old [4]. Rfd is the reference dose, BW is the average body weight, using the previous value, and ATn is the averaging time for non-carcinogen (365 days/year) multiplied by the exposure duration (ED).

THQ is the measure of non-carcinogenic risk. If $THQ < 1$ then there is no potential of non-carcinogenic risk. Otherwise, there is potential of non-carcinogenic risk. Based on data of males and females in Saudi Arabia, the results of THQ calculation can be summarized in table **4.13 - 4.15**

Based on table **4.13**, female is prone to have higher THQ of Fe. This is also due to their lower average bodyweight. We can also get information that Saudi Arabian female has the biggest potential of non-carcinogenic risk of iron if they consume Hered fish. Based on table **4.14** the biggest potential of non-carcinogenic Risk of Manganese can happen if a Saudi Arabian male or female consume Bulfusyan fish with the fact that female is prone to have bigger potential of non-carcinogenic risk than male. The last concerned THQ of the present heavy metal is that of Barium in table **4.15**. Based on the table, consumption of Hered Fish will result in the biggest potential of Non-carcinogenic risk of Barium for Females.

Table 4.13 Target Hazard Quotient (THQ) of Fe

Sample Name	LIBS (Male)	LIBS (Female)
Sarah	5.72E-06 ± 3.72E-07	6.33E-06 ± 4.12E-07
Bagoh	4.06E-06 ± 2.65E-07	4.49E-06 ± 2.93E-07
Bory	7.27E-06 ± 4.75E-07	8.03E-06 ± 5.25E-07
Hered	9.49E-06 ± 6.18E-07	10.5E-06 ± 6.83E-07
Bulfusyan	8.26E-06 ± 5.39E-07	9.13E-06 ± 5.95E-07

Table 4.14 Target Hazard Quotient (THQ) of Mn

Sample Name	LIBS (Male)	LIBS (Female)
Sarah	14.79E-05 ± 3.3768E-05	16.34E-05 ± 3.73E-05
Bagoh	5.50E-05 ± 1.25E-05	6.08E-05 ± 1.38E-05
Bory	7.24E-05 ± 1.65E-05	8.00E-05 ± 1.82E-05
Hered	16.55E-05 ± 8.0E-05	18.28E-05 ± 4.17E-05
Bulfusyan	103.497 E-05 ± 23.63E-05	114.35E-05 ± 26.11E-05

Table 4.15 Target Hazard Quotient (THQ) of Ba

Sample Name	LIBS (Male)	LIBS (Female)
Sarah	9.22E-05 ± 1.21E-05	10.19E-05 ± 1.34E-05
Bagoh	10.13E-05 ± 1.33E-05	11.20E-05 ± 1.48E-05
Bory	9.10E-05 ± 1.254E-05	10.05E-05 ± 1.32E-05
Hered	13.56E-05 ± 1.78E-05	14.98E-05 ± 1.97E-05
Bulfusyan	8.916E-05 ± 1.17E-05	9.85E-05 ± 1.29E-05

4.5.1.3 Hazardous index (HI)

$$HI = THQFe + THQMn + THQBa$$

HI is the total of THQ of the metallic elements in the fish samples. If $HI < 1$ then systematic effects are out of concern. Otherwise, the systematic effects are in concern [1].

By summing all THQ values in the three previous THQ tables, the results of HI calculation can be summarized in the following table:

Table 4.16 Hazardous Index

Sample Name	(Male)	(Female)
Sarah	24.58E-05 ± 4.63E-05	27.17E-05 ± 5.11E-05
Bagoh	16.05E-05 ± 2.62E-05	17.73E-05 ± 2.89E-05
Bory	17.06E-05 ± 2.896E-05	18.85E-05 ± 3.20E-05
Hered	31.06E-05 ± 5.63E-05	34.32E-05 ± 6.21E-05
Bulfusyan	113.24E-05 ± 24.85E-05	125.12E-05 ± 27.46E-05

Table 4.16 is the hazardous index of our fish samples. Based on the table, the fish that has the least value of HI is the Bagoh fish, while the highest HI is the Bulfusyan fish. The table shows that male and female have different HI values. Due to their lower average body weight, females are prone to have higher HI than males. Fortunately, the HI value of females are still less than 1. Overall, both male and female in Saudi Arabia have Hazardous Index value of less than 1. This means that the consumption of our fish samples will not give a systematic effect for Saudi Arabian people.

CHAPTER 5

CONCLUSION

The LIBS system for the analysis of various variety of fish present in the Arabian Gulf was developed. Prior to the LIBS data acquisition, the important LIBS parameters (time delay, laser energy, sample thickness, etc.) were optimized. The optimized set-up was successfully tested for detection of the main nutrients (elements) such as calcium, magnesium, potassium, heavy elements like iron, manganese, and barium and toxic element like mercury. Prior to the LIBS spectral analysis of the LIBS spectra, the plasma parameters – The number density and temperature of electron were previously studied. The quantitative analysis was done by preparing standard samples with known concentration to draw calibration curves. The concentration range of magnesium, calcium, iron, manganese and barium was $\{(685.67 \pm 44.16) - (2121.43 \pm 136.63)\}$ ppm, $\{(246.08 \pm 14.34) - (1620.32 \pm 94.41)\}$ ppm, $\{(10.26 \pm 0.67) - (23.96 \pm 1.56)\}$ ppm, $\{(27.79 \pm 6.34) - (522.26 \pm 119.25)\}$ ppm, and $\{(64.27 \pm 8.46) - (97.76 \pm 12.88)\}$ ppm.

The concentration of metals (Fe, Mn and Ba) was used to calculate health risk assessment parameters (EDI, THQ and HI). With respect to the EDI data, the fish consumption may cause Moderate to High risk to human health.

In general, based on THQ and HI data, considering only the three assessed heavy elements (Fe, Mn, Ba), the fish samples pose no potential of non-cancer risk and the systematic effect is out of concern. Therefore, we can *conclude* that our fish samples are considerably *safe for consumption with caution* of moderate to high risk of Fe and high risk of Mn and Ba.

For future works, the LIBS set-up should have permanently optimized condition for the optical and sample holder section, especially the distance between the sample surface and the fiber optics should be kept constant. In this optimized condition, we can just make standard pellet with the same thickness for all different samples for different purposes and interests. In this permanently optimized condition, we can also think about online LIBS system for governmental use of monitoring food and bio samples before they are sold to the public.

REFERENCES

- [1] USEPA (United States Environmental Protection Agency) (2011) USEPA Regional Screening Level (RSL) Summary Table: November 2011. <http://www.worldlifeexpectancy.com/saudi-arabia-life-expectancy>, 2014. [Online; last update: 20th January, 2014].
- [2] Average Body Weight of Men and Women. <https://www.worlddata.info/average-bodyheight.php>, 2018. [Online; accessed 4-July-2018].
- [3] Mn and ba maximum permissible limit. <https://www.lenntech.com/who-eu-water-standards.htm>, 2018. [Online; last update: 18th August, 2018].
- [4] World Health Rankings Live Longer Live Better. <http://www.worldlifeexpectancy.com/saudi-arabia-life-expectancy>, 2018. [Online; accessed 5-July-2018].
- [5] Homira Agah, Martine Leermakers, Marc Elskens, S Mohamad Rez Fatemi, and Willy Baeyens. Accumulation of trace metals in the muscle and liver tissues of five fish species from the persian gulf. *Environmental monitoring and assessment*, 157(1-4):499, 2009.
- [6] M Al-Busaidi, P Yesudhasan, S Al-Mughairi, WAK Al-Rahbi, KS Al-Harthy, NA Al-Mazrooei, and SH Al-Habsi. Toxic metals in commercial marine fish in oman with reference to national and international standards. *Chemosphere*, 85(1):67–73, 2011.
- [7] Abdul M Alhasmi, Mohammed A Gondal, Mohamed M Nasr, Sami Shafik, and Yusuf B Habibullah. Detection of toxic elements using laser-induced breakdown spectroscopy in smokersâ€™ and nonsmokersâ€™ teeth and investigation of periodontal parameters. *Applied optics*, 54(24):7342–7349, 2015.
- [8] Charly D Allemand. Spectroscopy of single-spike laser-generated plasmas. *Spectrochimica Acta Part B: Atomic Spectroscopy*, 27(5):185–204, 1972.

- [9] MA Almessiere, R Altuwiriqi, MA Gondal, RK AlDakheel, and HF Alotaibi. Qualitative and quantitative analysis of human nails to find correlation between nutrients and vitamin d deficiency using libs and icp-aes. *Talanta*, 185:61–70, 2018.
- [10] Amani S Alturqi and Lamia A Albedair. Evaluation of some heavy metals in certain fish, meat and meat products in saudi arabian markets. *The Egyptian Journal of Aquatic Research*, 38(1):45–49, 2012.
- [11] FC Alvira, T Flores Reyes, L Ponce Cabrera, L Moreira Osorio, Z Perez Baez, and G Vazquez Bautista. Qualitative evaluation of pb and cu in fish using laser-induced breakdown spectroscopy with multipulse excitation by ultracompact laser source. *Applied optics*, 54(14):4453–4457, 2015.
- [12] Carlos Aragon, Jose Antonio Aguilera, and Felix Penalba. Improvements in quantitative analysis of steel composition by laser-induced breakdown spectroscopy at atmospheric pressure using an infrared nd: Yag laser. *Applied spectroscopy*, 53(10):1259–1267, 1999.
- [13] George Asimellis, Nikolaos Michos, Ioanna Fasaki, and Michael Kompitsas. Platinum group metals bulk analysis in automobile catalyst recycling material by laser-induced breakdown spectroscopy. *Spectrochimica Acta Part B: Atomic Spectroscopy*, 63(11):1338–1343, 2008.
- [14] Lahib Balika, Cristian Focsa, Silviu Gurlui, Stéphane Pellerin, Nadia Pellerin, Daniel Pagnon, and Michel Dudeck. Laser-induced breakdown spectroscopy in a running hall effect thruster for space propulsion. *Spectrochimica Acta Part B: Atomic Spectroscopy*, 74:184–189, 2012.
- [15] Matthieu Baudelet, Laurent Guyon, Jin Yu, Jean-Pierre Wolf, Tanguy Amodeo, Emeric Fréjafon, and Patrick Laloi. Femtosecond time-resolved laser-induced breakdown spectroscopy for detection and identification of bacteria: A comparison to the nanosecond regime. *Journal of Applied Physics*, 99(8):084701, 2006.
- [16] JA Bolger. Semi-quantitative laser-induced breakdown spectroscopy for analysis of mineral drill core. *Applied Spectroscopy*, 54(2):181–189, 2000.

- [17] AH Bu-Olayan and MNV Subrahmanyam. Accumulation of copper, nickel, lead and zinc by snail, *lunella coronatus* and pearl oyster, *pinctada radiata* from the kuwait coast before and after the gulf war oil spill. *Science of the total environment*, 197(1-3):161–165, 1997.
- [18] LM Cabalin and JJ Laserna. Experimental determination of laser induced breakdown thresholds of metals under nanosecond q-switched laser operation. *Spectrochimica Acta Part B: Atomic Spectroscopy*, 53(5):723–730, 1998.
- [19] Simon Carter, Andy S Fisher, Phill S Goodall, Michael W Hinds, Steve Lancaster, and Sian Shore. Atomic spectrometry update. industrial analysis: metals, chemicals and advanced materials. *Journal of analytical atomic spectrometry*, 24(12):1599–1656, 2009.
- [20] Rosemarie C Chinni, David A Cremers, Leon J Radziemski, Melissa Bostian, and Claudia Navarro-Northrup. Detection of uranium using laser-induced breakdown spectroscopy. *Applied spectroscopy*, 63(11):1238–1250, 2009.
- [21] A Ciucci, Michela Corsi, Vincenzo Palleschi, S Rastelli, Antonio Salvetti, and Elisabetta Tognoni. New procedure for quantitative elemental analysis by laser-induced plasma spectroscopy. *Applied spectroscopy*, 53(8):960–964, 1999.
- [22] F Colao, R Fantoni, V Lazic, A Morone, A Santagata, and A Giardini. Libs used as a diagnostic tool during the laser cleaning of ancient marble from mediterranean areas. *Applied Physics A*, 79(2):213–219, 2004.
- [23] Nath Res Council. Recommended dietary allowances. *Food and Nutrition Board, Commission on Life Sciences, National Research Council. Washington: National Academic*, 1989.
- [24] David A Cremers and Leon J Radziemski. Basics of the libs plasma. *Handbook of Laser-Induced Breakdown Spectroscopy*, pages 23–52, 2006.
- [25] David A Cremers and Leon J Radziemski. Basics of the libs plasma. *Handbook of Laser-Induced Breakdown Spectroscopy, Second Edition*, pages 29–68, 2013.
- [26] David A Cremers, Fang-Yu Yueh, Jagdish P Singh, and Hansheng Zhang. *Laser-Induced Breakdown Spectroscopy, Elemental Analysis*. Wiley Online Library, 2006.

- [27] Gabriel Gustinelli Arantes de Carvalho, Lidiane Cristina Nunes, Paulino Florêncio de Souza, Francisco José Krug, Thasa Correia Alegre, and Dario Santos Jr. Évaluation of laser induced breakdown spectrometry for the determination of macro and micronutrients in pharmaceutical tablets. *Journal of analytical atomic spectrometry*, 25(6):803–809, 2010.
- [28] DL Death, AP Cunningham, and LJ Pollard. Multi-element analysis of iron ore pellets by laser-induced breakdown spectroscopy and principal components regression. *Spectrochimica Acta Part B: Atomic Spectroscopy*, 63(7):763–769, 2008.
- [29] Wolfgang Demtröder. Laser spectroscopy: Basic concepts and instrumentation(book). Berlin, Springer-Verlag(Springer Series in Chemical Physics., 5, 1981.
- [30] Wolfgang Demtröder. *Laser spectroscopy: basic concepts and instrumentation*. Springer Science & Business Media, 2013.
- [31] Sabry Mohamed El-Bahr and Ahmed Abdelghany. Heavy metal and trace element contents in edible muscle of three commercial fish species, and assessment of possible risks associated with their human consumption in saudi arabia. *Journal of Advanced Veterinary and Animal Research*, 2(3):271–278, 2015.
- [32] A El-Hussein, AK Kassem, H Ismail, and MA Harith. Exploiting libs as a spectrochemical analytical technique in diagnosis of some types of human malignancies. *Talanta*, 82(2):495–501, 2010.
- [33] Ozgur Emre, Halit Demir, Erkan Dogan, Ramazan Esen, Tugba Gur, Canan Demir, Edip Gonullu, Nedim Turan, and Mehmet Fatih Özbay. Plasma concentrations of some trace element and heavy metals in patients with metastatic colon cancer. *Journal of Cancer Therapy*, 4(6):1085, 2013.
- [34] Aaron S Eppler, David A Cremers, Donald D Hickmott, Monty J Ferris, and Aaron C Koskelo. Matrix effects in the detection of pb and ba in soils using laser-induced breakdown spectroscopy. *Applied Spectroscopy*, 50(9):1175–1181, 1996.

- [35] R Fantoni, L Caneve, F Colao, L Fornarini, V Lazic, and V Spizzichino. Methodologies for laboratory laser induced breakdown spectroscopy semi-quantitative and quantitative analysis—a review. *Spectrochimica Acta Part B: Atomic Spectroscopy*, 63(10):1097–1108, 2008.
- [36] Velmer A Fassel and Richard N Kniseley. Inductively coupled plasma. optical emission spectroscopy. *Analytical Chemistry*, 46(13):1110A–1120a, 1974.
- [37] Edilene C Ferreira, Eveline A Menezes, Wladiana O Matos, Débora MBP Milori, Ana Rita A Nogueira, and Ladislau Martin-Neto. Determination of ca in breakfast cereals by laser induced breakdown spectroscopy. *Food Control*, 21(10):1327–1330, 2010.
- [38] Quienly Godoi, Flavio O Leme, Lilian C Trevizan, Edenir R Pereira Filho, Iolanda A Rufini, Dario Santos, and Francisco J Krug. Laser-induced breakdown spectroscopy and chemometrics for classification of toys relying on toxic elements. *Spectrochimica Acta Part B: Atomic Spectroscopy*, 66(2):138–143, 2011.
- [39] MA Gondal, Umair Baig, MA Dastageer, and Mohsin Sarwar. Determination of elemental composition of coffee using uv-pulsed laser induced breakdown spectroscopy. In *AIP Conference Proceedings*, volume 1742, page 030007. AIP Publishing, 2016.
- [40] MA Gondal, A Dastageer, and ZH Yamani. Laser-induced photoacoustic detection of ozone at 266 nm using resonant cells of different configuration. *Journal of Environmental Science and Health, Part A*, 44(13):1457–1464, 2009.
- [41] MA Gondal, MA Dastageer, FF Al-Adel, AA Naqvi, and YB Habibullah. Detection of highly toxic elements (lead and chromium) in commercially available eyeliner (kohl) using laser induced break down spectroscopy. *Optics & Laser Technology*, 75:99–104, 2015.
- [42] MA Gondal, YB Habibullah, Umair Baig, and LE Oloore. Direct spectral analysis of tea samples using 266nm uv pulsed laser-induced breakdown spectroscopy and cross validation of libs results with icp-ms. *Talanta*, 152:341–352, 2016.
- [43] MA Gondal and T Hussain. Determination of poisonous metals in wastewater collected from paint manufacturing plant using laser-induced breakdown spectroscopy. *Talanta*, 71(1):73–80, 2007.

- [44] MA Gondal, T Hussain, and ZH Yamani. Optimization of the libs parameters for detection of trace metals in petroleum products. *Energy Sources, Part A*, 30(5):441–451, 2008.
- [45] MA Gondal, T Hussain, ZH Yamani, and MA Baig. Detection of heavy metals in arabian crude oil residue using laser induced breakdown spectroscopy. *Talanta*, 69(5):1072–1078, 2006.
- [46] MA Gondal, T Hussain, ZH Yamani, and MA Baig. On-line monitoring of remediation process of chromium polluted soil using libs. *Journal of Hazardous Materials*, 163(2-3):1265–1271, 2009.
- [47] MA Gondal, YW Maganda, MA Dastageer, FF Al-Adel, and A Naqvi. Study of temporal evolution of electron density and temperature for atmospheric plasma generated from fluid samples using laser induced breakdown spectroscopy. In *Electronics, Communications and Photonics Conference (SIEPC), 2013 Saudi International*, pages 1–4. IEEE, 2013.
- [48] MA Gondal, YW Maganda, MA Dastageer, FF Al Adel, AA Naqvi, and TF Qahtan. Detection of carcinogenic chromium in synthetic hair dyes using laser induced breakdown spectroscopy. *Applied optics*, 53(8):1636–1643, 2014.
- [49] MA Gondal, ZS Seddigi, MM Nasr, and B Gondal. Spectroscopic detection of health hazardous contaminants in lipstick using laser induced breakdown spectroscopy. *Journal of Hazardous Materials*, 175(1-3):726–732, 2010.
- [50] Mohammad A Gondal, Mohamed A Shemis, Ahmed AI Khalil, Mohamed M Nasr, and Bilal Gondal. Laser produced plasma diagnosis of carcinogenic heavy metals in gallstones. *Journal of Analytical Atomic Spectrometry*, 31(2):506–514, 2016.
- [51] Mohammed A Gondal, Yusuf B Habibullah, Luqman E Oloore, and Mohammed A Iqbal. Determination of carcinogenic fluorine in cigarettes using pulsed uv laser-induced breakdown spectroscopy. *Applied optics*, 54(17):5560–5567, 2015.
- [52] Mohammed A Gondal, Talib Hussain, Zulfiqar Ahmed, and Ahmed H Bakry. Detection of contaminants in ore samples using laser-induced breakdown spectroscopy. *Journal of Environmental Science and Health Part A*, 42(7):879–887, 2007.

- [53] Mohammed A Gondal, Mohamed A Shemis, Bilal Gondal, and Ahmed AI Khalil. Gallbladder stones analysis using pulsed uv laser induced breakdown spectroscopy. *J Med Bioeng*, 5(2), 2016.
- [54] Mohammed A Gondal and Mohammad N Siddiqui. Identification of different kinds of plastics using laser-induced breakdown spectroscopy for waste management. *Journal of Environmental Science and Health Part A*, 42(13):1989–1997, 2007.
- [55] Mohammed A Gondal, Mohammad N Siddiqui, and Mohamed M Nasr. Detection of trace metals in asphaltene using an advanced laser-induced breakdown spectroscopy (libs) technique. *Energy & Fuels*, 24(2):1099–1105, 2009.
- [56] R Gordon Gould et al. The laser, light amplification by stimulated emission of radiation. In *The Ann Arbor conference on optical pumping, the University of Michigan*, volume 15, page 128, 1959.
- [57] SS Harilal, CV Bindhu, VPN Nampoory, and CPG Vallabhan. Temporal and spatial behavior of electron density and temperature in a laser-produced plasma from $\text{Yb}_2\text{Cu}_3\text{O}_7$. *Applied spectroscopy*, 52(3):449–455, 1998.
- [58] Russell S Harmon, Jeremiah Remus, Nancy J McMillan, Catherine McManus, Leslie Collins, Jennifer L Gottfried Jr, Frank C DeLucia, and Andrzej W Miziolek. Libs analysis of geomaterials: geochemical fingerprinting for the rapid analysis and discrimination of minerals. *Applied Geochemistry*, 24(6):1125–1141, 2009.
- [59] T Hussain and MA Gondal. Monitoring and assessment of toxic metals in gulf war oil spill contaminated soil using laser-induced breakdown spectroscopy. *Environmental monitoring and assessment*, 136(1-3):391–399, 2008.
- [60] AE Hussein, PK Diwakar, SS Harilal, and A Hassanein. The role of laser wavelength on plasma generation and expansion of ablation plumes in air. *Journal of Applied Physics*, 113(14):143305, 2013.
- [61] Zen-Wen Hwang, Ye-Yung Teng, Kuang-Pang Li, and Joseph Sneddon. Interaction of a laser beam with metals. part i: quantitative studies of plasma emission. *Applied spectroscopy*, 45(3):435–441, 1991.

- [62] Sreenivasa Rao Jarapala, Bhaskarachary Kandlakunta, and Longvah Thingnganing. Evaluation of trace metal content by icp-ms using closed vessel microwave digestion in fresh water fish. *Journal of environmental and public health*, 2014, 2014.
- [63] Wu Jinquan, Zhang Wenyan, and S Xiuqin. Simulated body fluid by laser-induced breakdown spectroscopy. *Chinese Journal of Lasers*, 35(3):445, 2008.
- [64] Ahmed Asaad I Khalil, Mohammed A Gondal, and Mohamed A Dastageer. Detection of trace elements in nondegradable organic spent clay waste using optimized dual-pulsed laser induced breakdown spectrometer. *Applied optics*, 53(8):1709–1717, 2014.
- [65] Ahmed Asaad I Khalil, Mohammed A Gondal, Mohamed Shemis, and Irfan S Khan. Detection of carcinogenic metals in kidney stones using ultraviolet laser-induced breakdown spectroscopy. *Applied optics*, 54(8):2123–2131, 2015.
- [66] DE Kim, KJ Yoo, HK Park, KJ Oh, and DW Kim. Quantitative analysis of aluminum impurities in zinc alloy by laser-induced breakdown spectroscopy. *Applied Spectroscopy*, 51(1):22–29, 1997.
- [67] Andrew K Knight, Nancy L Scherbarth, David A Cremers, and Monty J Ferris. Characterization of laser-induced breakdown spectroscopy (libs) for application to space exploration. *Applied Spectroscopy*, 54(3):331–340, 2000.
- [68] N Konjevic, A Lesage, Jeffrey R Fuhr, and Wolfgang L Wiese. Éxperimental stark widths and shifts for spectral lines of neutral and ionized atoms (a critical review of selected data for the period 1989 through 2000). *Journal of Physical and Chemical Reference Data*, 31(3):819–927, 2002.
- [69] Rohit Kumar, Awadhesh K Rai, Devanathan Alamelu, and Suresh K Aggarwal. Monitoring of toxic elements present in sludge of industrial waste using cf-libs. *Environmental monitoring and assessment*, 185(1):171–180, 2013.
- [70] Mikio Kuzuya, Hitoshi Matsumoto, Hideaki Takechi, and Osamu Mikami. Effect of laser energy and atmosphere on the emission characteristics of laser-induced plasmas. *Applied spectroscopy*, 47(10):1659–1664, 1993.

- [71] Nina L Lanza, Roger C Wiens, Samuel M Clegg, Ann M Ollila, Seth D Humphries, Horton E Newsom, and James E Barefield. Calibrating the chemcam laser-induced breakdown spectroscopy instrument for carbonate minerals on mars. *Applied Optics*, 49(13):C211–C217, 2010.
- [72] Stéphane Laville, Mohamad Sabsabi, and François R Doucet. Multi-elemental analysis of solidified mineral melt samples by laser-induced breakdown spectroscopy coupled with a linear multivariate calibration. *Spectrochimica Acta Part B: Atomic Spectroscopy*, 62(12):1557–1566, 2007.
- [73] V Lazic, A Trujillo-Vazquez, H Sobral, C Márquez, A Palucci, M Ciaffi, and M Pistilli. Corrections for variable plasma parameters in laser induced breakdown spectroscopy: Application on archeological samples. *Spectrochimica Acta Part B: Atomic Spectroscopy*, 122:103–113, 2016.
- [74] B Le Drogoff, J Margot, M Chaker, M Sabsabi, O Barthelemy, TW Johnston, S Laville, F Vidal, and Y Von Kaenel. Temporal characterization of femtosecond laser pulses induced plasma for spectrochemical analysis of aluminum alloys. *Spectrochimica acta part B: Atomic spectroscopy*, 56(6):987–1002, 2001.
- [75] WQ Lei, J El Haddad, V Motto-Ros, N Gilon-Delepine, Alice Stankova, QL Ma, XS Bai, LJ Zheng, HP Zeng, and J Yu. Comparative measurements of mineral elements in milk powders with laser-induced breakdown spectroscopy and inductively coupled plasma atomic emission spectroscopy. *Analytical and bioanalytical chemistry*, 400(10):3303–3313, 2011.
- [76] DC Little, N Kundu, M Mukherjee, and BK Barman. Marketing of fish in peri-urban kolkata. institute of aquaculture, university of stirling. <http://www.dfd.stir.ac.uk/dfd/nrsp/kolkata.htm>, 2002.
- [77] TR Loree and LJ Radziemski. Laser-induced breakdown spectroscopy: time-integrated applications. *Plasma Chemistry and Plasma Processing*, 1(3):271–279, 1981.
- [78] Yasin Wandhami Maganda. Development of a laser induced breakdown spectrometer for detection of toxic elements in cosmetic products. Master’s thesis, King Fahd University of Petroleum and Minerals, Saudi Arabia, 2013.

- [79] Shahid Mahboob, HF Alkahem Al-Balawi, F Al-Misned, S Al-Quraishy, and Z Ahmad. Tissue metal distribution and risk assessment for important fish species from Saudi Arabia. *Bulletin of environmental contamination and toxicology*, 92(1):61–66, 2014.
- [80] A Mansoori, B Roshanzadeh, M Khalaji, and SH Tavassoli. Quantitative analysis of cement powder by laser induced breakdown spectroscopy. *Optics and Lasers in Engineering*, 49(3):318–323, 2011.
- [81] AO Mehder, Mohammed A Gondal, Mohamed A Dastageer, Yusuf B Habibullah, Mohammed A Iqbal, Luqman E Oloore, and Bilal Gondal. Direct spectral analysis and determination of high content of carcinogenic bromine in bread using uv pulsed laser induced breakdown spectroscopy. *Journal of Environmental Science and Health, Part B*, 51(6):358–365, 2016.
- [82] AO Mehder, YB Habibullah, MA Gondal, and Umair Baig. Qualitative and quantitative spectro-chemical analysis of dates using uv-pulsed laser induced breakdown spectroscopy and inductively coupled plasma mass spectrometry. *Talanta*, 155:124–132, 2016.
- [83] Andrzej W Miziolek, Vincenzo Palleschi, and Israel Schechter. *Laser induced breakdown spectroscopy*. Cambridge University Press, 2006.
- [84] Lieselotte Moenke-Blackenburg and Carmen W Huie. Laser microanalysis, on-line process analyzers, and electrophoresis. *Analytical Chemistry*, 61(24):1376A–1379A, 1989.
- [85] MM Nasr, MA Gondal, MM Ahmed, MM Yousif, and NA Al-Muslet. Direct spectral analysis of different gum arabic samples using laser induced breakdown spectroscopy. In *AIP Conference Proceedings*, volume 1976, page 020025. AIP Publishing, 2018.
- [86] O Aied Nassef, Harby E Ahmed, and MA Harith. Surface and stratigraphic elemental analysis of an ancient Egyptian cartonnage using laser-induced breakdown spectroscopy (LIBS). *Analytical Methods*, 8(39):7096–7106, 2016.
- [87] Austin Nevin, Giuseppe Spoto, and Demetrios Anglos. Laser spectroscopies for elemental and molecular analysis in art and archaeology. *Applied Physics A*, 106(2):339–361, 2012.

- [88] Lidiane Cristina Nunes, Gilmore Antônia da Silva, Lilian Cristina Trevizan, Dario Santos Júnior, Ronei Jesus Poppi, and Francisco José Krug. Simultaneous optimization by neuro-genetic approach for analysis of plant materials by laser induced breakdown spectroscopy. *Spectrochimica Acta Part B: Atomic Spectroscopy*, 64(6):565–572, 2009.
- [89] Taoreed O Owolabi and Mohammed A Gondal. Development of hybrid extreme learning machine based chemo-metrics for precise quantitative analysis of libs spectra using internal reference pre-processing method. *Analytica Chimica Acta*, 2018.
- [90] Taoreed Olakunle Owolabi and Mohammed Gondal. Novel techniques for enhancing the performance of support vector regression chemo-metric in quantitative analysis of libs spectra. *Journal of Analytical Atomic Spectrometry*, 2017.
- [91] N Ozbek and S Akman. Method development for the determination of fluorine in water samples via molecular absorption of caf using a high-resolution continuum source electrothermal atomic absorption spectrophotometer. In *E3S Web of Conferences*, volume 1. EDP Sciences, 2013.
- [92] Shiwani Pandhija, NK Rai, Awadhesh K Rai, and Surya N Thakur. Contaminant concentration in environmental samples using libs and cf-libs. *Applied Physics B*, 98(1):231–241, 2010.
- [93] U Panne, C Haisch, M Clara, and R Niessner. Analysis of glass and glass melts during the vitrification process of fly and bottom ashes by laser-induced plasma spectroscopy. part i: Normalization and plasma diagnostics. *Spectrochimica Acta Part B: Atomic Spectroscopy*, 53(14):1957–1968, 1998.
- [94] EH Piepmeier. Laser ablation for atomic spectroscopy, 1986.
- [95] Jozef Rakovsky, Olivier Musset, JeanFrancois Buoncristiani, Vincent Bichet, Fabrice Monna, Pascal Neige, and Pavel Veis. Testing a portable laser-induced breakdown spectroscopy system on geological samples. *Spectrochimica Acta Part B: Atomic Spectroscopy*, 74:57–65, 2012.

- [96] I Rehan, MA Gondal, and K Rehan. Determination of lead content in drilling fueled soil using laser induced spectral analysis and its cross validation using icp/oes method. *Talanta*, 182:443–449, 2018.
- [97] I Rehan, MA Gondal, and K Rehan. Optimized laser-induced breakdown spectroscopy for determination of xenobiotic silver in monosodium glutamate and its verification using icp-aes. *Applied optics*, 57(12):3191–3197, 2018.
- [98] O Samek, DCS Beddows, HH Telle, GW Morris, M Liska, and J Kaiser. Quantitative analysis of trace metal accumulation in teeth using laser-induced breakdown spectroscopy. *Applied Physics A*, 69(1):S179–S182, 1999.
- [99] Jean E Sansonetti and William Clyde Martin. Handbook of basic atomic spectroscopic data. *Journal of Physical and Chemical Reference Data*, 34(4):1559–2259, 2005.
- [100] Arnab Sarkar, Suresh K Aggarwal, and D Alamelu. Laser induced breakdown spectroscopy for rapid identification of different types of paper for forensic application. *Analytical Methods*, 2(1):32–36, 2010.
- [101] Susanne Schröder, SG Pavlov, I Rauschenbach, EK Jessberger, and H-W Hübers. Detection and identification of salts and frozen salt solutions combining laser-induced breakdown spectroscopy and multivariate analysis methods: A study for future martian exploration. *Icarus*, 223(1):61–73, 2013.
- [102] Vivek K Singh, Anjali Gupta, Omisha Gupta, Vinay Kumar, and Mohammad A Gondal. Spectroscopic evaluation of cyperus rotundus rhizomes using wd-xrf, libs, ftir and uv-vis spectroscopy. *Materials Focus*, 6(1):7–14, 2017.
- [103] P Sivakumar, A Fernández-Bravo, L Taleh, JF Biddle, and N Melikechi. Detection and classification of live and dead escherichia coli by laser-induced breakdown spectroscopy. *Astrobiology*, 15(2):144–153, 2015.
- [104] Andrew W Speedy. Global production and consumption of animal source foods. *The Journal of nutrition*, 133(11):4048S–4053S, 2003.
- [105] Birute Staniškiene, Paulius Matusevicius, and Alvidas Urbanavicius. Distribution of heavy metals in muscles of fish: concentrations and change tendencies. *Environmental Research, Engineering and Management*, 48(2):35–41, 2009.

- [106] Xiong Wan and Peng Wang. Analysis of heavy metals in organisms based on an optimized quantitative libs. *Optik-International Journal for Light and Electron Optics*, 126(19):1930–1934, 2015.
- [107] Richard Wisbrun, Israel Schechter, Reinhard Niessner, Hartmut Schroeder, and Karl L Kompa. Detector for trace elemental analysis of solid environmental samples by laser plasma spectroscopy. *Analytical Chemistry*, 66(18):2964–2975, 1994.
- [108] Steven H Wise and Jose R Almirall. Chemical taggant detection and analysis by laser-induced breakdown spectroscopy. *Applied optics*, 47(31):G15–G20, 2008.
- [109] Karen Y Yamamoto, David A Cremers, Monty J Ferris, and Leeann E Foster. Detection of metals in the environment using a portable laser-induced breakdown spectroscopy instrument. *Applied Spectroscopy*, 50(2):222–233, 1996.
- [110] Mingyin Yao, Lin Huang, Jianhong Zheng, Shiquan Fan, and Muhua Liu. Assessment of feasibility in determining of cr in gannan navel orange treated in controlled conditions by laser induced breakdown spectroscopy. *Optics & Laser Technology*, 52:70–74, 2013.

Vitae

Name :Lutfi Mulyadi Surachman |
Nationality :Indonesia |
Date of Birth :4/18/1987|
Email :lutfi.mulyadi@gmail.com|
Address :Jl Cihaurbeuti No 38 RT 04 RW 02|
Academic Background :BSc. In Physics ITB |

List of publications :

1. Lutfi Mulyadi, M.A. Gondal, M.A. Dastageer, Fida El-Adel, Owolabi Taoreed, and Abul Lais. Development of laser-induced breakdown spectroscopy for the analysis of fish samples from the Arabian Gulf, Applied Optics (2018), (pre-submission).